Università degli Studi di Ferrara

DOTTORATO DI RICERCA IN SCIENZE DELLA TERRA

COORDINATORE PROF. LUIGI BECCALUVA

GEOCHEMICAL AND ISOTOPIC COMPOSITION OF NATURAL WATERS IN THE CENTRAL MAIN ETHIOPIAN RIFT: EMPHASIS ON THE STUDY OF SOURCE AND GENESIS OF FLUORIDE

DOTTORANDO
DOTT. GODEBO TEWODROS RANGO

TUTORE
PROF. LUIGI BECCALUVA

XXI° CICLO

ANNI 2006 - 2008

Università degli Studi di Ferrara

DOTTORATO DI RICERCA IN
"Scienza della Terra"

CICLO: **(XXI)**

COORDINATORE: **Prof. Luigi Beccaluva**

Geochemical and Isotopic Composition of Natural Waters in the Central Main Ethiopian Rift: emphasis on the study of source and genesis of fluoride

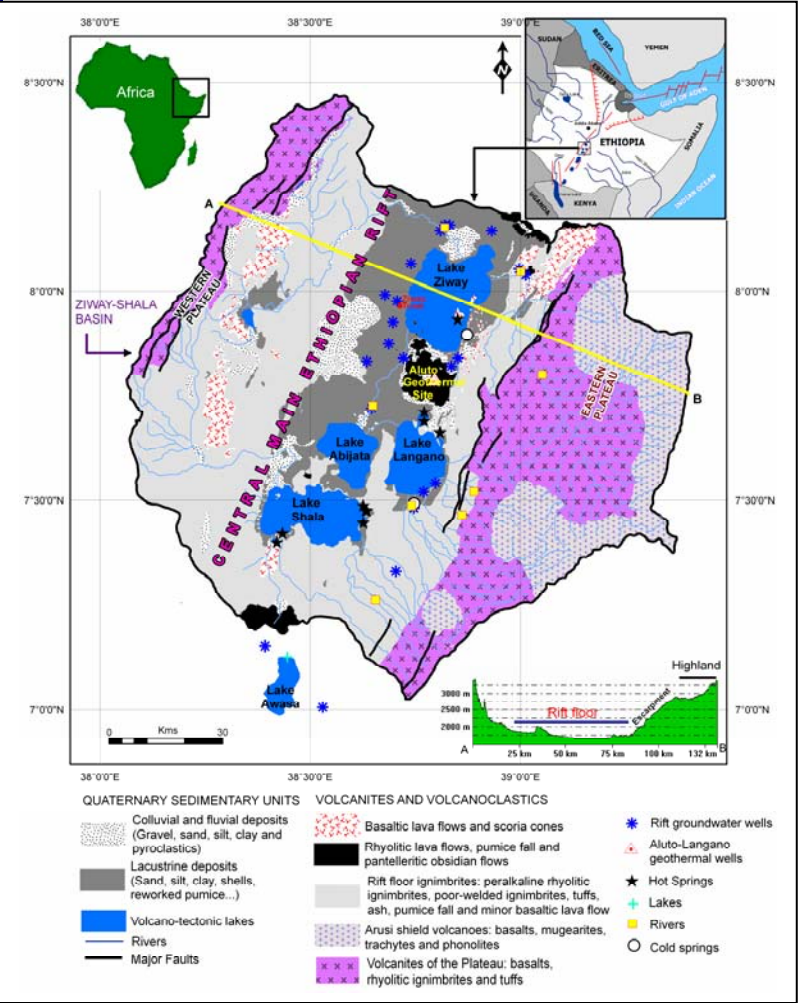

Settore Scientifico Disciplinare
GEO/07

Dottorando
Dott. Godebo Tewodros Rango

_____
(firma)

Tutore
Prof. Luigi Beccaluva

_____
(firma)

Co-Tutore

Dr. Gianluca Bianchini

_____*(firma)*_____

Dr. Tenalem Ayenew

_____*(firma)*_____

Anni 200**6**/200**8**

LIST OF CONTENTS……PAGES

ACKNOWLEDGEMENTS

First and foremost, I would like to thank the University of Ferrara for initiating research collaboration with Addis Ababa University, Ethiopia, through the proposition of this PhD program. The financial grant from the University of Ferrara is gratefully acknowledged.

I am greatly indebted to my primary supervisor, Director of the Doctorate program, Prof. Luigi Beccaluva, for significantly supporting and facilitating this research activity. I sincerely thank my co-supervisor, Dr. Gianluca Bianchini, University of Kingston, England, who was most available and responsible in supporting this research through close consultations and for providing assistance and alternative views in my perspective which significantly improved the quality of the research outcome.

I would also like to thank Prof. Paolo Billi, for being the main link between Addis Ababa and the University of Ferrara and for making this PhD opportunity possible. I am thankful for his valuable assistance in academics as well as his willingness to support other aspects of my life.

I am also thankful for Prof. Riccardo Petrini and Dr. Barabara Stenni, University of Trieste, Italy, for providing analytical facilities for isotope analysis and for their valuable consultations as well as Dr. Renzo Tassinari, University of Ferrara, Italy, for kindly carrying out all the necessary analytical analyses (AAS, ICP-MS, and XRF).

I would like to thank Dr. Dereje Ayalew, Dr. Mohammed Umer and Dr. Bekele Abebe from Addis Ababa University, Ethiopia, for being responsible and having the confidence in me so as to choose to involve me in this PhD program.

I am grateful to Dr. Daniel Mege, University of Nantes, France, for being a great scientific colleague, and for his support to me and my family.

I thank to Nicolo Colombani and Micol Mastrocicco for setting up the column experiment and for analytical analyses (IC) as well as their valuable scientific consultations.

I am thankful to Sathiyaseelan Theneshkumar, Mohammed Al-Dhoun, and Omar Mabrouk for being close friends and sharing sometime during my PhD experience.

I would like to mention and sincerely thank my good friends Eeelco Varinga, Octavian Niculita for their support and encouragement and Laetitia Le Deit for her thoughtfulness to me.

I would like to thank all the staff members (Claudio, Costanza, Barabara, Elena, Mattia, Yan Tao, Massimo and Alexandro) in the department of Earth sciences, Ferrara for the support that helped to make the transition to life in Ferrara an easy one.

My deepest heartfelt gratitude goes to my family who are the source of my strength and inspiration which makes me work hard and do my best. They will always be one of the main reasons to keep me on the right track in difficult times. I thank my father who first directed and supported my education life. This may be one of the most valuable moments to thank my mother, for her unconditional love, consistent care and support since my childhood.

I also thank to my close relatives, all friends and colleagues who have accompanied and assisted me all along. I am very much thankful.

Tewodros Rango Godebo
University of Ferrara
March, 2009

Dedicated to my mother

Askale Enderias

LIST OF FIGURES……..... PAGES

LIST OF TABLES…….....PAGES

LIST OF APPENDICES……PAGES

ABBREVIATIONS

Abbreviation	Meaning
AAS	Atomic Absorption Spectroscopy
ADE	Advection Dispersion Equation
CRM	Certified Reference Material
$\delta^{2}H$ or Delta ^{2}H	Isotope ratio of hydrogen
$\delta^{18}O$ or Delta ^{18}O	Isotope ratio of oxygen
EU	European Union
EC	Electrical Conductivity
FAO	Food and Agriculture Organization
GMWL	Global Meteoric Water Line
GIS	Geographical Information System
GPS	Global Positioning System
IC	Ionic Chromatography
ICP-MS	Inductively Coupled Plasma-Mass Spectrometry
ITCZ	Intertropical Convergence Zone
LMWL	Local Meteoric Water Line
MER	Main Ethiopian Rift
MINTEQA2	a geochemical modeling software program
MODFLOW	Modular Three-Dimensional Finite-Difference Groundwater Flow Model
MT3DMS	Modular Transport Three Dimensional Model Simulator
PHREEQC	PH (pH), RE (redox), EQ (equilibrium), C (program written in C)
SDZFB	Silti Debre Zeyt Fault Zone
SEM	Scanning Electron Microscope
SI	Saturation Index
$^{87}Sr/^{86}Sr$	Strontium isotope ratio
TAS	Total Alkali-versus-Silica
TDS	Total Dissolved Solids
USGS	United States Geological Survey
UNDP	United Nations Development Programme
USEPA	United States Environmental Protection Agency

VSMOW	Vienna Standard Mean Ocean Water
WHO	World Health Organization
WFB	Wonji Fault Belt
WATEQ4F	a geochemical modeling software program
XRD	X-ray Diffraction
XRF	X-ray fluorescence

ABSTRACT

In the Main Ethiopian Rift (MER), the supply of drinking water principally relies on groundwater wells, springs (including some hot springs), and rivers, and is characterized by a significant problem of fluoride (F^-) contamination. New analyses reveal that the F^- geochemical anomaly is sometimes associated with hazardous content of other potentially toxic elements such as As, B, Mo, U, Al, Fe, and Mn. The F^- content exceeds the permissible limit for drinking prescribed by the World Health Organization (WHO; 1.5 mg/L) in many important wells (up to 20 mg/L), with even more extreme F concentration in hot springs and alkaline lakes (up to 97 mg/L and 384 mg/L respectively) and is causing prevalent endemic fluorosis disease in the region.

87 % of the groundwater wells, 38 % of rivers and 100 % of hot springs and lakes show F^- content above 1.5 mg/L. The groundwater and surface water from the highlands, typically characterized by low Total Dissolved Solids (TDS) and Ca^{2+} (Mg^{2+})-HCO_3^- hydrochemical facies, do not show high F^- content. The subsequent interaction of these waters with the various rocks of the rift valley induces a general increase of the TDS and a variation of the chemical signature towards Na^+-HCO_3^- compositions, with a parallel enrichment of F^-. The interacting matrixes are mainly rhyolites consisting of volcanic glass and only rare F-bearing accessory minerals (such as alkali amphibole).

Comparing the abundance and the composition of the glassy groundmass with other mineral phases, it appears that the former stores most of the total F^- budget. This glassy material is extremely reactive, and its weathering products (i.e. fluvio/volcano-lacustrine sediments) further concentrate the fluoride. The interaction of these "weathered/reworked" volcanic products with water and carbon dioxide at high pH causes the release of fluoride into the interacting water. This mainly occurs by a process of base-exchange softening with the neo-formed clay minerals (i.e. Ca-Mg uptake by the aquifer matrix, with release of Na^+ into the groundwater). This is plausibly the main enrichment mechanism that explains the high F^- content of the local groundwater, as evidenced by positive correlation between F^-, pH, and Na^+, and inverse correlation between F^- and Ca^{2+} (Mg^{2+}). Saturation indices (SI) were calculated (using PHREEQC-2) for the different water groups, highlighting that the studied waters are undersaturated in fluorite. In these conditions, fluoride can not precipitate as CaF_2, and so F^- mobilizes freely without forming other complexes.

On the other hand, 35 % of the 23 investigated groundwater wells and 70 % of the 12 hot springs (and deep geothermal wells) show Arsenic concentration above the recommended limit of 10µg/L (WHO 2006). The average concentration of Arsenic is 0.9µg/L in rivers, 39µg/L in hot springs, 236µg/L in deep geothermal wells, 21.4µg/L in groundwater wells, 77µg/L in lakes, whereas maximum concentrations reach up to 3µg/L, 156µg/L, 278µg/L, 157µg/L and 405 µg/L respectively. Arsenic in groundwater wells shows positive correlations with Na^+ (R^2=0.63) and HCO_3^- (R^2=0.70) as well as with other trace elements such as Mo (R^2=0.79), U (R^2=0.70), V (R^2=0.68) whereas no correlations are observed with Fe and Mn. PHREEQC speciation modelling indicates that Fe and Al oxides and hydroxides are stable in the water systems, suggesting that Fe and Al mineral phases are potential adsorbents and thus influence the mobility of As. The oxidizing, high pH condition combined with Na^+-HCO_3^- hydrochemical facies (competing effect of HCO_3^- for adsorption sites) of the MER waters play an important role in the mobilization of arsenic.

Chemical analyses of leachates from MER rhyolitic rocks and their weathered and reworked fluvio-lacustrine sediments were performed in order to evaluate their contribution as a source of the mentioned geochemical anomalies. The leachates were obtained from a one-year leaching experiment on powdered rocks and sediments mixed with distilled water (10g:50ml). The sediment leachates contain as much as 7.6 mg/L of F^-, 220 µg/L of As, 181 µg/L of Mo, 64 µg/L of U and 254 µg/L of V suggesting that the local sediments represent the main source and reservoir of toxic elements. Laboratory column experiment was also conducted in volcanic ash sample using synthetic rain water flushing, and the result showed that significant amount of F^- were leached out over the duration of the experiments.

This showed that these elements were originally present in the glassy portion of the MER rhyolitic rocks, were progressively concentrated in weathered and redeposited products. It further confirms that the pyroclastic materials are the major source and reservoir of many of the chemical elements (e.g. F^-, As). Therefore, together with the renowned F^- problem, the possible presence of geochemical anomalies in As, B, Mo, V, U, Al, Fe, and Mn have to be taken into consideration in water quality issues and future works has to investigate their possible health impact on the population of MER and other sectors of the east African rift.

The stable $\delta^{18}O$, δD and radiogenic ($^{87}Sr/^{86}Sr$) isotopic composition of waters and representative volcanic rocks (Ignimbrite and basalt) were carried out during this study. Different ranges of isotopic values were recorded for different water groups: 10 hot spring samples show $\delta^{18}O$ value with in the

range of (-3.36‰ − 3.69‰) and δD (-15.85‰ − 24.23‰) (VSMOW), 12 groundwater wells $\delta^{18}O$ (-3.99‰ − 5.14‰) and δD (-19.69‰ − 32.27‰) in contrast to the 5 Lakes $\delta^{18}O$ (3.98‰ − 7.92‰) and δD (26.19‰ − 45.71‰). The 2 deep geothermal wells and 1 of the 2 river samples are depleted in stable isotopic values. $^{87}Sr/^{86}Sr$ values range from 0.7045 to 0.7076 in the hot springs, and the two deep geothermal wells have 0.7043 and 0.7054 values. These signatures are typical of water interacted with mantle derived materials (with a minor crustal contamination), similar to the rocks widely covering the study area. The Sr isotope values of the basalt and ignimbrite samples are 0.7063 and 0.7071 respectively. Generally, the result shows that there exists a complex surface water and groundwater interactions that is reflected on a diversity of the stable and Sr isotopic signature in waters.

The preliminary results of the study has showed that there is a need for future extended works on the geochemistry of solid samples (rocks, sediments and soils) as well as in waters that investigate all the spectrum of chemical elements that are potentially detrimental to human health and environment. Furthermore, from water resource point of view, the following works must focus on a comprehensive study of various isotopes and geochemical data to constrain groundwater age dating, water-rock interaction and flow path and thus help to model and systematize the hydrologic cycles in the basin.

Key words: Aqueous geochemistry, major and trace elements, toxic elements, leaching experiment, $\delta^{18}O$, δD and $^{87}Sr/^{86}Sr$ isotopes and MER (Main Ethiopian Rift).

RIASSUNTO

Nella "Main Ethiopian Rift" (MER) l'approvigionamento idropotabile avviene sfruttando principalmente acqua di falda e subordinatamente attraverso acque delle sorgenti (alcune di queste termali) e acque dei fiumi. Tali acque sono spesso caratterizzate da una significativa contaminazione da fluoro (F^-). Le analisi presentate in questa tesi rivelano che tale anomalia geochimica è talvolta associata con alte concentrazioni di altri elementi potenzialmente tossici come As, B, Mo, U, Al, Fe e Mn.

Il contenuto di F^- in queste acque spesso eccede la concentrazione massima ammissibile (1.5 mg/L) prescritta dall'organizzazione mondiale delle sanità (WHO) in molti importanti pozzi della zona dove talvolta si osservano sino a 20 mg/L, e concentrazioni ancora più estreme si rinvengono nelle acque delle sorgenti termali (sino a 97 mg/L) e nelle acque dei laghi (sino a 384 mg/L), causando fluorosi come malattia endemica nelle popolazioni locali.

87% delle acque dei pozzi, 38% delle acque dei fiumi e 100% delle acque termali e dei laghi sono contraddistinte da tale problema avendo concentrazione in F^- superiore ad 1.5 mg/L.

Le acque superficiali e sotterranee degli adiacenti altopiani, tipicamente caratterizzate basse concentrazioni di sali disciolti (TDS) e da una facies idrochimica carbonato-calcica non mostrano invece tali arricchimenti in F^-. La successiva interazione di tali acque che provengono dagli altopiani con le varie litologie che si rinvengono nella rift valley induce un generale incremento della TDS, una variazione della facies idrochimica verso composizioni carbonato-sodiche, e un arricchimento parallelo in F^-. Le principali litologie che si rinvengono in tali acquiferi della rift valley sono rocce vulcaniche di natura riolitica principalmente costituite da vetro e solo subordinatamente da fasi accessorie contenenti fluoro (es.: anfibolo). Ne deriva che il vetro vulcanico sembra essere la fase che contiene quasi la totalità del fluoro. Tale fase vetrosa è molto reattiva durante i processi di weathering, e i relativi prodotti di alterazione, ri-depositati come sedimenti fluviali e lacustri, tendono a concentrare ulteriormente il fluoro. Successivamente l'interazione fra questi depositi e le acque di falda in presenza di CO_2, e ad alti pH, causa il rilascio del F^-. Avvengono quindi dei processi di scambio fra le acque e i minerali argillosi di neo-formazione presenti nei depositi fluvio-lacustri che acquisiscono Ca^{2+} e Mg^{2+} rilasciando Na^+. Tali processi portano ad un parallelo arricchimento in F^-, come evidenziato dalla correlazione positiva fra F^-, Na^+, e pH, e dalla correlazione inversa fra F^- e Ca^{2+} (Mg^{2+}). Il calcolo degli indici di saturazione (SI) calcolati con PHREEQC-2 mostra inoltre sottosaturazione rispetto alla fluorite che non precipitando consente la permanenza del F^- libero in soluzione.

La presenza di As sembra essere un ulteriore problema che induce seria preoccupazione in quanto 35% dei pozzi e 70% delle sorgenti termali sono caratterizzati da acque con contenuti che eccedono la concentrazione massima ammissibile delineata dalla WHO (10 μg/L). In particolare, la concentrazione di As è 0.9 μg/L nelle acque dei fiumi, 39μg/L nelle acque delle sorgenti termali, 236 μg/L nelle acque di alcuni pozzi geotermici, 21.4 μg/L nelle acque dei pozzi ad uso idropotabile, 77μg/L nelle acque dei laghi, con concentrazioni massime che raggiungono 3 μg/L, 156 μg/L, 278 μg/L, 157 μg/L e 405 μg/L, rispettivamente. As esibisce correlazioni positive con Na^+ (R^2=0,63) e con HCO_3^- (R^2=0,70) e con altri elementi in traccia come Mo (R^2=0.79), U (R^2=0.70), V (R^2=0.68). ma non con elementi quali Fe e Mn. Le condizioni ossidanti, la presenza di alti pH e la generale facies idrochimica carbonato-sodica giocano evidentemente un significativo ruolo alla mobilizzazione dell'arsenico.

Sono stati effettuati tests di lisciviazione sui principali litotipi che caratterizzano gli acquiferi oggetto di studio al fine di evidenziare il loro ruolo e il possibile contributo alla genesi dell'anomalia in fluoro riscontrata nelle acque. Tali tests sono stati ottenuti mettendo 10 g di polvere di ogni campione a contatto con acqua distillata (50 ml) per un periodo di 1 anno. Fra i vari campioni investigati, le soluzioni ottenute lisciviando i depositi fluvio-lacustri contengono sino a 7.6 mg/L di F^-, 220 μg/L di As, 181 μg/L di Mo, 64 μg/L di U e 254 μg/L di V, suggerendo che tali litotipi rappresentano la principale sorgente di elementi potenzialmente tossici. Esperimenti simili sono stati inoltre effettuati per tempi più brevi su "colonne" opportunamente riempite con litotipi rappresentativi, campionando nel tempo l'acqua che vi fuoriusciva.

Riassumendo, si suggerisce che tali elementi tossici originariamente presenti nella fase vetrosa che costituisce le rocce riolitiche estremamente diffuse nella MER siano progressivamente concentrati nelle coltri di alterazione o nei sedimenti da queste prodottisi. Si suggerisce inoltre che oltre al conosciuto problema della contaminazione da F^- anche altre anomalie geochimiche relative ad elementi come As, B, Mo, U, Al, Fe e Mn dovrebbero essere prese in serie considerazione in quanto possono indurre un ulteriore impatto sanitario alla popolazione della MER e di altri settori del rift east-africano.

In tale tesi vengono vengono inoltre riportati dati degli isotopi stabili dell'ossigeno e dell'idrogeno ($\delta^{18}O$, δD) effettuati sulle acque oggetto di studio e dati degli isotopi radiogenici dello stronzio ($^{87}Sr/^{86}Sr$) effettuati sia sulle acque che sui litotipi più rappresentativi. Le acque delle sorgenti termali mostrano $\delta^{18}O$ fra − 3.36 e -3.69 e δD fra -15.85 e -24.23; le acque dei pozzi mostrano $\delta^{18}O$ fra − 3.99 e -5.14 e δD fra -19.69 e -32.27; in contrasto le acque dei laghi mostrano $\delta^{18}O$ fra 3.98 e -7.92 e δD fra 26.19 e -45.71.

$^{87}Sr/^{86}Sr$ varia fra 0.7045 e 0.7076 nelle acque delle sorgenti termali, e fra 0.7043 e 0.7054 nelle acque di pozzi profondi di natura geotermica. Tale segnatura isotopica è comparabile con quella che si è rinvenuta nelle rocce affioranti nell'area, in quanto l'analisi di roccia basaltica e di una roccia ignimbritica ha fornito valori di 0.7063 e 0.7071 rispettivamente. Tali analisi isotopiche contribuiranno ad una miglior interpretazione della situazione idrogeologica caratterizzata da un complessa interazione fra acque superficiali ed acque sotterranee.

Più in generale si sottolinea l'esigenza di ulteriori studi che coinvolgano oltre alle acque anche la geochimica delle matrici solide che tengano in considerazione un ampio spettro di elementi potenzialmente tossici, nonché di ulteriori studi isotopici che potrebbero fornire informazioni sulle direzioni dei flussi sotterranei, sulle litologie con le quali le acque interagiscono e sui tempi di circolazione di dette acque nei relativi acquiferi.

Parole chiavi: Geochemica delle acque, elementi maggiori e in traccia, test di estrazione, isotopi dell'ossigeno, dell'idrogeno, dello stronzio e MER (Main Ethiopian Rift).

1. General introduction

In the MER system, groundwater resources from wells and springs as well as from rivers are a very important supply of drinking water for millions of people living in the area. The MER is part of the East African Rift, located within the central part of the Ethiopia Rift system and characterized by semi-arid to arid climate conditions where water scarcity is often associated with water quality problems. The natural waters of this region are characterized by geochemical anomalies of high fluoride concentration (Kilham and Hecky, 1973; Chernet, 1982; Calderoni et al., 1993; Gizaw, 1996; Darling et al., 1996) often exceeding the 1.5 mg/L tolerance limit for drinking water (WHO, 2006). Above this threshold, the high fluoride concentration causes dental fluorosis (above 1.5mg/L), skeletal fluorosis (above 4 mg/L) and crippling fluorosis (above 10 mg/L; Dissanayaka, 1991). The local population is affected by diseases such as mottled teeth and skeletal fluorosis (Tekle-Haimanot et al., 1987, Kloos and Tekle-Haimanot, 1999) which are linked to the high fluoride concentration observed in the rift's waters (**Figure 1**)

Figure 1.1: Dental fluorosis in the main Ethiopian rift (photo: January 2007)

In the past few decades, many geochemical studies have addressed the fluoride problem in order to elucidate its origin (Chernet and Travi, 1993; Gizaw, 1996; Yirgu et al., 1999; Chernet et al., 2001; Ayenew, 2005; Rango et al., 2008) and to investigate the associated health problems (Lester, 1974; Olsson, 1979; Tekle-Haimanot et al., 1987; Tekle-Haimanot, 1990; Shiferaw and Teklehaimanot, 1999; Kloos and Tekle-Haimanot, 1999). Although the health related impact of fluorine is well known, the

hydrogeochemistry of fluorine, with respect to the controlling phases (minerals and/or amorphous), and the processes that induce its enrichment are not extensively studied in the Ethiopian rift system. Similarly, geochemical studies on trace elements are also not yet well investigated in the region.

A proper water quality assessment requires the investigation of a more complete spectrum of potentially toxic elements in order to foresee possible negative health effects in the short or long term. Such kind of studies are extremely important especially in active volcanic areas which are characterized by extremely reactive lithotypes (that can release their chemical budget into the interacting water) and by persisting geothermal manifestations (possibly including juvenile fluids) that can pollute the shallow aquifers. This is the case of the Main Ethiopian rift (MER), where the presence of felsic-volcanic rocks (ashes, tuffs, rhyolitic ignimbrites) and their weathered and re-deposited fluvio-volcano lacustrine sediments, as well as the presence of active geothermal activities, could contribute to the existence of multiple geochemical anomalies with detrimental effects on human health.

This study mainly deals with the natural occurrence of these trace elements, particularly fluoride and arsenic. Occurrence (Kilham and Hecky, 1973; Calderoni et al., 1993; Ashely and Burley, 1994; Gizaw, 1996; Darling et al., 1996) and health problems related to the first element are well known in East Africa (Smith et al., 1953; Grech, 1966; Ocherse, 1953; Moller et al., 1970), whereas geochemistry and related health risks of the latter (together with other associated trace elements) have not yet been documented or are poorly understood. This study highlights the presence of these toxic elements in the MER waters, and discusses their origin, distribution and speciation.

The determination of potentially harmful inorganic substance concentrations in natural water and in the aquifer lithologies is essential. Leaching procedures on the latter are also important as they provide an estimate of the bioavailable elemental budget. The results will provide information on the potential inorganic trace element contaminants harmful to humans and the environment. In addition, fundamental data for further detailed geochemical studies concerning sources, occurrences and speciation of toxic trace elements in the hydrological cycle will be provided. Policy makers could then use this information for planning strategies for water exploitation and consumption.

The other aspect addressed in this study is the isotopic composition of natural waters δD, $\delta^{18}O$ and strontium isotope ($^{87}Sr/^{86}Sr$) in order to understand surface water and groundwater circulation and their interactions and water-rock interactions in the region.

Therefore, the objectives of this study can be summarized into three parts:

- The principal objective of the study is to gain a better knowledge and understanding of fluoride problem with respect to its sources, genesis and distribution in order to support water quality management issues in the central sector of Main Ethiopian Rift (MER) floor.

  In this framework we performed an integrated study of both waters and coexisting representative solid aquifer matrixes in the Ziway-Shala lakes basin of the central MER, in order to unravel the water-rock/sediment interactions that ultimately lead to the peculiar geochemical features of the Ethiopian rift waters. Therefore, the hydrochemical investigation was coupled with the mineralogical/geochemical characterization of the lithologies outcropping in the area. Moreover, laboratory leaching tests (batch and column) were also carried out to evaluate the potential release of fluoride from the various rock/sediment types. These approaches serve to understand the lithologic sources and the enrichment mechanisms controlling the anomalous fluoride content in the waters.

- The second objective is to perform a more general water quality assessment in order to identify other potentially toxic trace elements and to make a future plan for detail geochemical investigations in solid phases and natural waters of the region, and

- The third objective is to investigate the origin of waters, water/rock interactions and mixings processes (among surface waters and groundwaters) in the basin using stable isotopes δD, $\delta^{18}O$ and radiogenic isotopes ($^{87}Sr/^{86}Sr$) in waters and lithotypes.

2. Description of the central Main Ethiopian Rift (MER)

2.1. Morphology and hydrology

The Ethiopian rift system represents the northern half of the East African Rift that consists of three zones with distinct volcanic assemblages and tectonic features. These are the Afar Rift system to the north, the Main Ethiopian Rift (MER) valley at the central and the south western part. The central sector is more than 200 km long and about 75 km wide. The afar rift forms a triangular depression formed by triple tectonic interactions of the Red Sea and Gulf of Aden oceanic rifts with the continental MER.

Rift extension in the MER is generally NW-SE (Mohr and Wood, 1976; Korme et al., 1997) and it is strongly affected by NNE-SSW oriented active normal faults of the Wonji Fault Belt (WFB) on the east and the Silti−Debre Zeyt Fault Zone (SDZFZ) on the west, with a large displacement of about 1500−2000 m between the rift floor and the plateau (Mohr 1962, Di Paola, 1972; Woldegabriel et al., 1990) (**Figure 2.1).**

From geomorphological point of view Ziway-Shala basin divided into three zones: the rift, the transitional escarpment and the highlands. The rift zone is characterized by an average altitude of 1600 m above sea level (m.a.s.l), is bordered by the Ethiopian plateau to the east and west, having an average altitude of 2500 m.a.s.l) (cross-section AB, **Figure 2.1**).

In the basin the lowest elevation is at Lake Shala (1550 m.a.s.l). The large Pliocene trachytic shield volcanoes of Mount Chilalo (4006 m), Mount Badda (4170 m), Mount Kubsa (3760 m) overlook the Ziway−Shala basin from the east. Several dormant silicic caldera volcanoes rise above the rift floor: Mount Bora (2293 m), the Alutu Caldera (2328 m), the O'a Caldera (1960 m), and the Corbetti Caldera (2320 m) **(Figure 2.1**). Quaternary calderas of Aluto, Gademotta and Shala are present in the basin. South west of Ziway−Shala basin, Awasa caldera forms a closed basin.

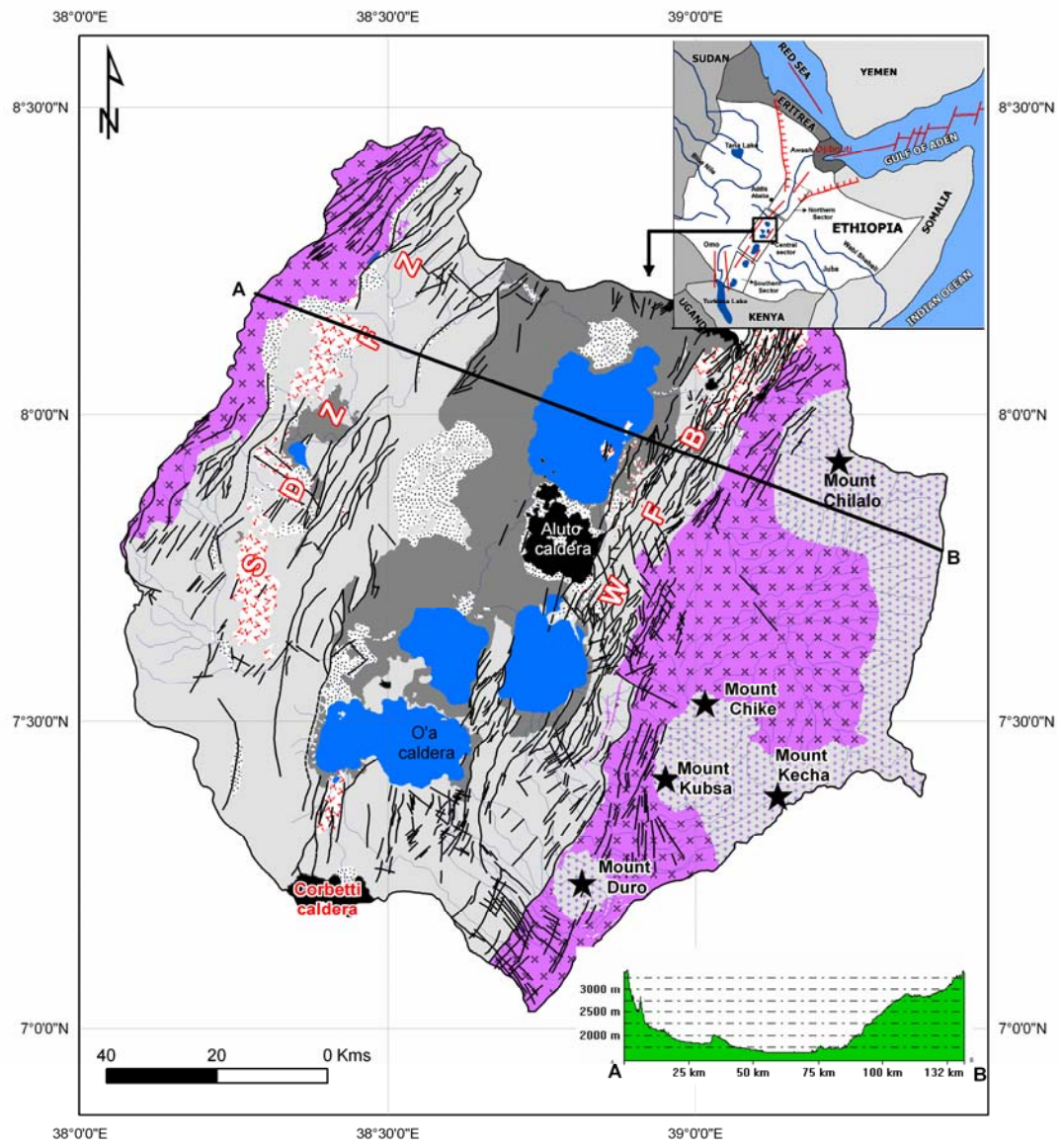

Figure 2.1: Tectonic map of the central MER in Ziway-Shala basin.

The Ziway−Shala basin (7−8º30`N lat.; 38º−39º30`E long.) of the central MER comprises a rift-bounded chain of lakes (Ziway-Langano-Abijata-Shala), chemically characterized by fresh (e.g Lake Ziway) to alkaline lakes (e.g Lake Shala and Abijata). These lakes are hydrologically closed. The three northernmost lakes, Ziway, Langano, and Abijata are connected by a surface network. Lake Ziway drains into Abijata via the Bulbula River and Lake Langano overflows seasonally into Abijata via the Horakelo River, whereas the Lake Shala, the deepest lake (266m) in Ethiopia lies on a caldera and forms a separate basin. The shallowest and most northerly, Lake Ziway receives surface inflows from the west

by Meki and from southeast by Ketar Rivers that draining the western and eastern highlands of the basin. Lake Langano is fed by small streams from southeast. Lake Shala receives water from Gidu River from the west and Adabat River from the southeast. It partly fed by groundwater seepage from the other lakes (Street, 1979; Chernet, 1982). Lake Chitu is a small crater lake southeast of Lake Shala. Lake Awasa found south of Ziway-Shala basin, where its main tributary is Tikur Wuha River which drains swampy Lake Shallo. Ziway-Shala basin is bordered by Lake Awasa basin to the south, the Bilate River basin to the west, the Awash River basin to the north and the Wabishebelle River basin to the east.

Photos below are taken from Lake Langano and Lake Chitu **(Figure 2.2 and Figure 2.3)**.

Figure 2.2: Partial view of Lake Langano (photo: January 2007)

Figure 2.3: Partial view of Chitu Crater Lake with flamingos (photo: January 2007)

Each of the three lakes (Ziway-Langano-Abijata) has an elongate shape parallel to the main trend of the MER and can be defined as tectonically controlled lakes. Due to differences in the geomorphological setting they vary in depth, shape and size **(Table 1.1)**.

Lakes	Altitude (m.a.s.l)	Surface area (km^2)	Catchement area (km^2)	Maximum depth (m)	Mean depth (m)	Volume ($10^6 m^3$)	Salinity (g/L)
Ziway	1636	440	7380	8.9	2.5	1466	0.349
Langano	1585	230	2000	47.9	17	3800	1.88
Abijata	1580	180	10740	14.2	7.6	957	16.2
Shala	1550	370	2300	266	8.6	37000	21.5

Table 2.1: Basic hydrological data of the lakes (Wood and Talling, 1988; Chernet, 1982 and Ayenew, 1998)

2.2. Geothermal activities

The Ethiopian rift system is an area known for its significant geothermal resources. These resources are found scattered throughout the Main Ethiopian Rift valley and in the Afar Depression.

It is characterized by circulation of geothermal fluids which are manifested as geothermal wells, hot springs, fumerols and geysers. This could be due to the persistence of magma at shallow depth, generating heat that induces geothermal and fumarolic activities (e.g. at Aluto-Langano volcanic center; **Figure 2.4**) and high temperature thermal fluids outpouring as springs bordering the lakes (Langano, Shala and Chitu). Hydrothermal fields exist on the Tulu Gudu Island of Lake Ziway, along the northern and eastern shores of Lake Langano (North Bay and Edo Laki Island, Bole, and O-itu Bay) and on the east, southeast and southwest shores of Lake Shala (UNDP, 1973; Chernet, 1982) and hot springs bordering Lake Chitu (**Figure 2.5**).

Figure 2.4: Deep (>2 kms) geothermal well at Aluto-Langano geothermal field (photo: January 2007)

Figure 2.5: Hot spring close to Lake Chitu with the local community taking water for domestic use (photo: January 2007)

2.3. Climate and vegetation

The modern climate of the Ziway−Shala region is mainly characterized by alternating wet and dry seasons following the annual movements of the Intertropical Convergence Zone (ITCZ) which separates the air streams of the northeast and southeast monsoons (Nicholson, 1996). Different climatic conditions characterize the highlands, the escarpment and the rift valley. Annual rainfall ranges from around 650 mm in the rift valley to 1100 mm in the highlands (Ayenew, 1998). Mean annual temperature is less than 15ºC in the highlands and more than 20ºC in the lowlands and evaporation ranges from more than 2500 mm on the rift floor to less than 1000 mm in the highlands (Le Turdu et al., 1999). Highland areas west of Butajira and east of Asela and Shashemene are humid to dry sub-humid. Because evaporation

exceeds rainfall, the rift valley suffers water deficit, as a result surface water and groundwater resources can be constrained.

The vegetation types ranges from tropical woodland to bushed grassland on the rift floor. Rift shoulders are characterized by bushed grassland, then remnants of dry, montane forest and, from 3200 to 3500 m, ericaceous scrub and Afroalpine moorland (Makin et al., 1975).

2.4. Soils

Generally, the soils of the Ethiopian Rift Valley divided into thirteen major soil mapping units and a further six sub-units based on the FAO/UNESCO soil classification. The major soil units in terms of area covered are: Vertisols (19.2%), Cambisols (17.9%), Fluvisols (16.2%), Regosols (15.8%), Lithosols (9.5%), Andosols (7.1%) and Acrisols (6.1%) (King and Birchall., 1975; FAO/UNESCO, 1977).

The soils of the Rift Valley are largely derived from recent volcanic rocks and, by comparison with many areas of east Africa; their base status is generally good. The main parent materials of the Rift Valley soils are: basalt, ignimbrites, lava, gneiss, volcanic ash, alluvium and pumice. Some of the soil problems include, low phosphorus levels, micronutrient imbalances and in some cases poor physical structure (Makin et al., 1975). Fertile volcanic soils prevail in wide areas of the highlands, where mean annual rainfall exceeds 800 mm (Ethiopian Mapping Authority, 1988).

2.5. Settlements and water supply

The rift and the bordering highlands in the study area is one of the most populated regions of the country. The main towns in the basin are Ziway, Meki, Awassa, Shashemene, Arsi-Negele, Butajira, Silte, Bekoji, Asela and Kofele. People live also in scattered villages across the basin. The water supply source in the region is mainly from groundwater wells (dug wells and boreholes), unprotected springs (cold springs and sometimes hot springs) and rivers (**Figure 2.6**). Majority of the population depend on agriculture. Irrigation is practiced by diverting rivers and abstracting from Lake Ziway.

Figure 2.6: Community water supply well from the study area (photo: January 2007)

2.6. Significance of the Ethiopian rift system

The Ethiopian rift system has a great geological significance to study the processes and evolution of volcanism and rifting. It is also abundant in natural resources such as fertile volcanic soils, industrial minerals, geothermal energy, surface and groundwater and scenic landscape formed by volcanic and tectonic processes. The presence of lakes (such as Ziway and Langano) and hot springs throughout the rift are known as touristic destinations for foreigners and local populations. Moreover, the rift sedimentary basins are rich in paleoanthropological, paleontological, and archeological heritages for understanding human origin and evolution and use of tools (Woldegabriel et al., 2000). The MER especially the central section is a well-known reference area for palaeoclimatical studies (Street, 1979; Chalié and Gasse, 2002). Despite the great benefit provided by volcanic products and tectonic features, natural hazards and risks associated to volcanoes and tectonics pose potentially destructive threats to the society and environment. As a matter of this fact, the surface and groundwater resources of the rift are contaminated by some toxic elements (such as widely recognized Fluorine).

2.7. Geological settings

The present day geologic and geomorphic features of the region are built by Cenozoic volcano-tectonic and sedimentation processes. Geographic distribution and compositional diversity among the rock units of the Ethiopian volcanic province indicate that there has been a relationship between magma composition and rifting (woldegabriel and Aronson, 1986; Hart et al., 1989). The initial phase of development of the MER is attributed to the influence of a mantle plume beneath the Ethiopian Plateau resulting in widespread flood-basalt volcanism and plateau uplift with two main episodes dated at 45−30 Ma and 18−14 Ma (Davidson and Rex, 1980; Mohr, 1983; Hart et al., 1989; WoldeGabriel et al., 1991; Ebinger et al., 1993; Hofmann et al., 1997). In the southern and central sectors of the MER, volcanism started as early as in Eocene time with important basaltic eruptions, associated with an early stage of rifting characterized by uplift and faulting (WoldeGabriel et al., 1990, 1991; Ebinger et al., 1993). From Late Oligocene to Early Miocene times, the first major phase of rifting within the MER resulted in a series of asymmetric half-grabens with alternating polarity. By mid-Late Miocene time, the eastern and western faulted margins of the MER had formed (Davidson and Rex, 1980; WoldeGabriel et al., 1990)

The most important volcano−tectonic event in the central sector of the MER occurred in Early Pliocene, with the eruption of voluminous flows of rhyolitic ignimbrites and the collapse of very large calderas (Di Paola, 1972; Woldegabriel et al., 1990). From early Pleistocene to the present, tectonic and volcanic activity was concentrated along the Wonji Fault Belt (WFB) to the east, and along the Silti Debre Zeit Fault Zone (SDZFZ) to the west (Mohr, 1962; Di Paola, 1972).

The MER divides the volcanic province of Ethiopia into northwestern and southeastern plateau during the Miocene. Despite the occurance of widespread faulting, subsidence and uplifting related to the formation of the MER, the pre-rift geology is barely exposed along the rift system (Woldegabriel et al., 2002). The boundary faults expose crystalline basement rocks beneath tertiary volcanic rocks in the southern sector of the MER, whereas in the central and the northern sectors, the rift margins are tertiary mafic and silicic rocks. Pre-Tertiary crystalline basement and Mesozoic sedimentary rocks that are unconformably overlain by Oligocene to Pliocene basalt flows and silicic tephra are exposed in the western margin of the central sector at the Gurage Mountains (Woldegabriel et al., 1990).

As in many parts of the Afro-Arabian rift system, the Ethiopian volcanic terrain was constructed by several episodes of eruptions representing diverse volcanic sequences. The volcanic products in places

were fissural basaltic lava flows, stacked one over the other, alternating with volcanoclastic deposits derived from tuff, ignimbrite and volcanic ash.

In the rift recent continental type volcanism has developed, giving rise to lage silicic rocks from predominantly central type eruptions partly accompanied by fissural basaltic lava flows. The oldest flows are rarely exposed beneath thick younger flows, and the individual flows are only local (Barberi et al., 1975; Zanetti et al., 1978; Berhe et al., 1987). The basalts are now concealed by a cover of silicic stratoid volcanics (Di Paola, 1972). Subsequent volcanic activitity has been largely confined to the active Wenji Fault Belt running parallel to the rift axes (Mohr, 1967).

The highlands are dominantly covered with basic volcanic rocks mainly of tertiary age. The oldest volcanic rocks (Plateau Trap Series or Volcanites of Plateau; **Figure 2.7**, Unit 1) are exposed in the western and eastern elevated areas. The western escarpment consists of about 1000 m of basaltic lava flows, with inter-bedded ignimbritic horizons, overlain by massive rhyolites, tuffs and basalts (Di Paola, 1972; Merla et al., 1979; Woldegabriel et al., 1990). Radiometric ages range from 40 to 25 Ma in the basalts and from 37 to 27 Ma in the rhyolites (Merla et al., 1979; Woldegabriel et al., 1990). Middle Miocene to Pliocene (15−3 Ma) basalt flows, rhyolites and tuffs unconformably cap the early Tertiary volcanic units (Merla et al., 1979; Woldegabriel et al., 1990). The eastern plateau is characterized by shield volcanoes of Pliocene to early Pleistocene (4.6−1.6 Ma) consisting of mainly trachytes with subordinate basalts, mugearites and phonolites (Di Paola, 1972) (Arusi Shield Volcanoes; **Figure 2.7**, Unit 2).

In the central sector of the MER, the outcropping lithologies consist of plio-pleistocene volcanites (pyroclastic products of felsic composition and subordinate basaltic lava flows) and sediments (Benvenuti et al., 2002); and the sediments in large consists of lacustrine deposits (**Figure 2.7**, Unit 3) and volcano-clastic and fluvial sediments (**Figure 2.7**, Unit 4). They are characterized by upper quaternary fluvio-volcano lacustrine facies, and colluvial deposits that represent weathered/remobilized volcanic rocks and silicic tephra. **Figure 2.8** shows fluvio-lacustrine sediments outcrop, east of Lake Shala. The sediments occupy the rift floor where in the past it was covered by a wide lake. The four present day lakes had once been a single fresh water lake (Nilsson, 1940).

In particular, most of the MER rift floor is covered by silicic pyroclastic materials (rift floor ignimbrites; **Figure 2.7**, Unit 5), Early to Middle Pliocene (4.2−3 Ma, Woldegabriel et al., 1990) mainly consisting of peralkaline rhyolitic ignimbrites, interlayered with basalts and tuffs, associated with layered and

unwelded pumices (Di Paola, 1972; Woldegabriel et al., 1990). Ashes are frequently found inter-bedded with ignimbrites and pumice layers.

Some outcrops of alkaline and peralkaline rhyolitic lava flows and domes associated with pumice and ash (with in unit 3) represent the late silicic volcanic events (Di Paola, 1972). These lavas were erupted from Late Pliocene to Middle Pleistocene and, in some places; crop out as remnants of large calderas. The Gademota Ridge, dated 1.30−1.27Ma (Laury and Albritton, 1975; Mohr et al., 1980; Woldegabriel et al., 1990) is one such remnant. It rises in an arc structure, 25−30 km in diameter, up to 400 m above the plain west of Lake Ziway.

A more recent volcanic unit, (basaltic lava flows; **Figure 2.7,** Unit 6), crops out along the SDZFZ and the WFB (Di Paola, 1972; Kazmin et al., 1980); it is made up of basaltic lava flows, associated with hyaloclastites and scoria cones. It is very recent with a radiometric age of 0.13 Ma (Woldegabriel et al., 1990).

Young volcanoes and calderas, such as the Alutu volcano, and Corbetti calderas, are made up of rhyolitic lava flows, unwelded pumice flows, pumice falls and ashes (rhyolite lava flow; **Figure 2.7,** Unit 7). Obsidian flows represent the final product of the volcanic activity (Di Paola, 1972; Mohr et al., 1980). **Figure 2.9** shows pumice falls at NE of Lake Ziway.

These recent volcanoes started to be active from the Middle Pleistocene (about 0.25 Ma, Di Paola, 1972; Mohr et al., 1980; Woldegabriel et al., 1990) with intermittent Late Holocene activity; obsidian flows and pumices were dated 2000 yBP (Gianelli and Teklemariam, 1993) and very recent ash deposits 1500 and 230 y BP (Haynes and Haas, 1974). Many of these volcanoes are presently in a fumarolic stage (Di Paola, 1972).

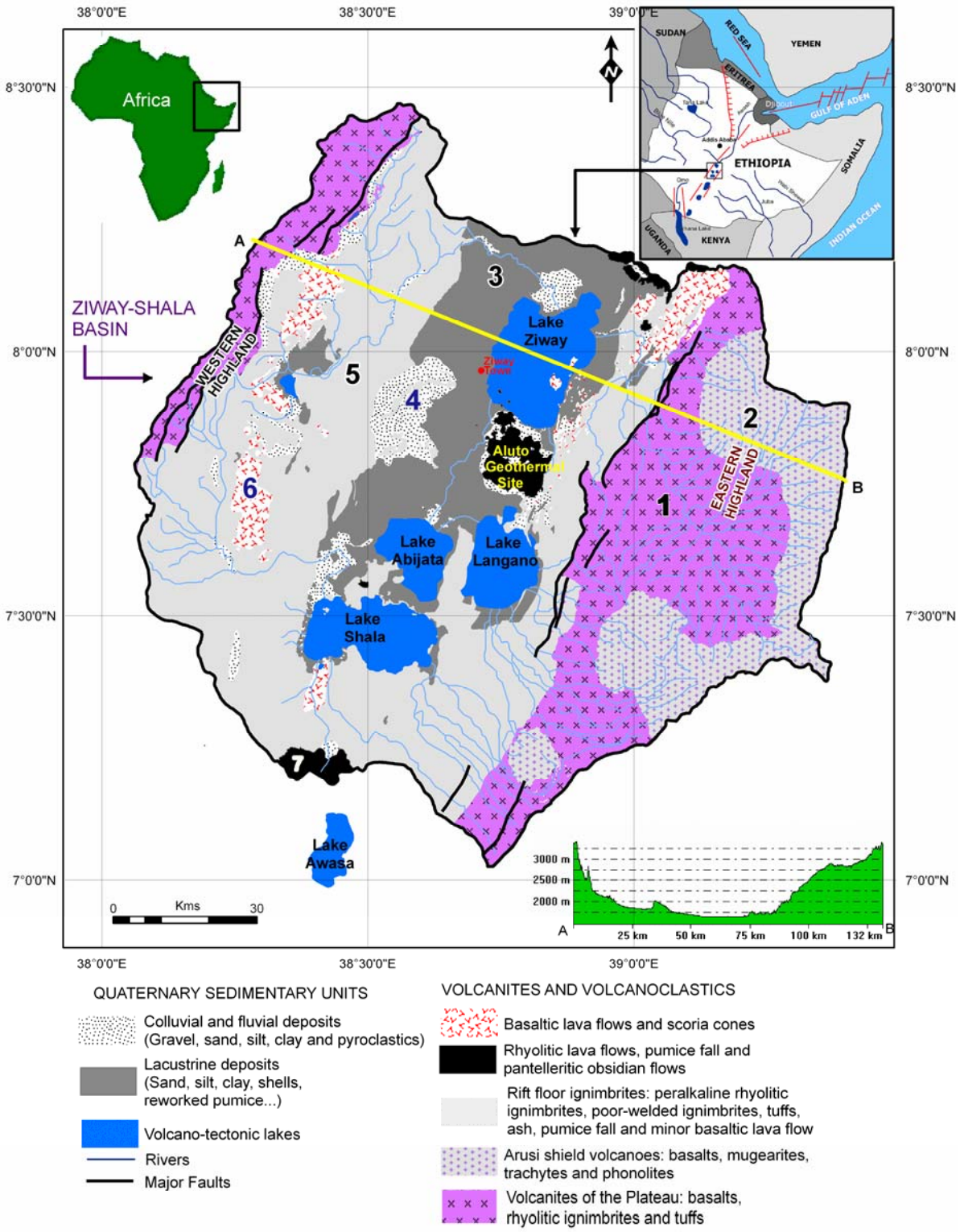

Figure 2.7: Simplified geologic map of the study area (Ziway-shala lakes basin) modified from (Dainelli et al., 2001).

Figure 2.8: Fluvio-lacustrine sediment, east of Lake Shala (photo: January 2007)

Figure 2.9: Pumice deposit, northeast of Lake Ziway (photo: January 2007)

3. Geochemistry of rocks and sediments from the central MER

3.1. Rock/sediment sampling and analytical techniques

Representative rock and sediment samples were collected during the field campaign. Rock samples were preliminary characterized by studying thin-sections at the transmitted light microscope. Whole-rock analysis of selected samples were performed by X-ray fluorescence spectrometry (XRF) on pressed powder pellets using wavelength-dispersive automated ARL Advant'X spectrometer at the Department of Earth Sciences of the University of Ferrara. Accuracy and precision, based on the analysis of certified international standards, are estimated as better than 3% for Si, Ti, Fe, Ca and K, and 7% for Mg, Al, Mn, Na, and 10% for trace elements at ppm level. Representative samples that reflect the main lithotypes were subsequently selected for leaching experiments.

In these experiments, powdered samples were mixed with distilled water having a pH of about 5.5, at a ratio of 1 to 5 (10g/50ml; room temperature), and shaken for 12 months at a frequency of 100 rev/min. The experiment was carried out in closed system, i.e. utilizing closed plastic bottles which did not allow interaction with atmospheric gases (such as CO_2). The test simulates the potential extractability (leachability) of soluble components during water-rock/sediment interaction processes. Analysis of major and trace elements on leachates were done, with the above mentioned analytical techniques, after separation from the residue and filtering through (0.45µm membrane filters).

In situ analyses of the constituent phases (minerals and volcanic glasses) were carried out with a Cameca SX 50 microprobe (CNR-IGG Institute of Padova) using natural silicates and oxides as standards.

3.2. Chemical and mineralogical composition of rocks

Bulk rock XRF analyses of the aquifer solid matrixes are reported in **Table 3.1**. The results is reported in an alkali-silica classification diagram (**Figure 3.1**), indicate that the prevalent volcanic rocks are rhyolites (i.e. felsic magmas) and the fluvio-volcano lacustrine sediments represent the weathered - redeposited products of the above mentioned volcanic rocks (**Table 3.1**). These rocks are also further characterized by their high oxides of SiO_2 and incompatible elements like Zr, Ce, La, Nb, Y, Rb and lower concentration of compatible elements Co, Ni, Cr, V, and Sc.

	TW9	TW11	Ted3	Ted4	Ted5	Ted25	Ted47	Ted48	Ted51	Ted52	Ted53	Ted6	Ted21
	Rhyolites										Basalt	Sediments	
SiO_2	74.21	67.04	73.03	71.34	72.12	75.81	73.46	69.81	71.86	74.68	50.63	71.78	64.63
TiO_2	0.33	0.45	0.34	0.36	0.40	0.27	0.68	0.60	0.36	0.38	2.49	0.37	0.64
Al_2O_3	9.96	16.02	10.38	9.33	9.73	9.32	9.40	11.10	9.35	9.87	16.67	8.75	8.23
Fe_2O_3	5.02	4.68	5.61	5.93	5.74	4.62	5.06	6.31	5.48	5.26	12.13	6.66	5.09
MnO	0.23	0.18	0.20	0.20	0.21	0.21	0.11	0.20	0.21	0.20	0.17	0.23	0.19
MgO	0.01	0.13	0.01	0.14	0.18	0.00	1.33	0.51	0.23	0.05	3.44	0.12	3.88
CaO	0.26	0.60	0.24	0.24	0.36	0.19	0.99	0.72	0.86	0.27	9.05	0.29	4.53
Na_2O	5.78	4.47	5.63	2.89	4.58	5.26	0.97	3.67	4.36	4.88	3.70	2.87	1.88
K_2O	4.04	4.37	4.38	4.67	4.33	4.09	2.31	4.12	4.00	4.17	1.33	4.28	2.58
P_2O_5	0.00	0.03	nd	nd	0.02	nd	0.02	0.14	nd	nd	0.41	nd	0.07
LOI	0.15	2.04	0.18	0.34	2.34	0.23	5.67	2.83	3.29	0.24	0.00	4.64	8.26
Ba	202	799	49	50	139	100	167	627	79	72	438	39	211
Ce	278	108	267	256	192	696	120	187	243	263	nd	283	124
Co	nd	nd	nd	nd	nd	nd	3.4	0.6	nd	nd	33	nd	2.1
Cr	nd	1.0	nd	nd	nd	nd	28	nd	nd	nd	36	nd	14
La	133	166	168	159	150	238	130	197	143	136	88	166	110
Nb	166	123	143	130	115	225	82	113	118	135	29	132	90
Ni	nd	nd	3.7	6.2	3.9	5.9	21	7.9	2.0	nd	12	4.1	14
Pb	5	0.3	18	17	18	24	17	12	17	20	5.3	19	12
Rb	91	68	125	141	119	122	86	85	115	127	25	119	84
Sr	nd	112	0.7	3.9	16	1.9	103	38	14	3.4	473	5.4	250
Th	19	15	19	24	19	21	18	16	18	19	4.1	20	14
V	2.1	17	4.9	6.7	7.0	5.2	30	19	7.8	3.9	319	7.1	45
Y	98	83	101	88	87	174	60	117	84	73	34	94	58
Zn	251	166	225	212	219	395	166	244	219	242	99	234	162
Zr	1076	812	1031	1000	910	1728	749	1016	942	1047	210	1023	709
Cu	nd	0.8	3.5	3.6	3.6	2.0	16	4.6	3.7	4.0	68	2.6	8.1
Ga	21	22	26	31	28	28	28	36	32	26	21	31	31
Nd	93	181	24	36	33	387	nd	148	28	nd	nd	80	nd
S	nd	nd	nd	nd	nd	nd	nd	nd	nd	nd	nd	nd	nd
Sc	nd	8.4	4.7	5.5	6.7	5.2	11	8.2	5.1	5.1	29	4.3	11

Table 3.1: Bulk rock XRF analyses of the MER rocks and sediments

Ted29	Ted38	Ted39	Ted45	TW14	TW15	TW22	TW29	TW30	TW31	TW34	TW39	TW43
Sediments												
49.66	55.42	67.45	70.33	67.64	57.78	61.30	70.35	67.68	72.06	71.14	71.25	56.01
0.33	0.58	0.39	0.36	0.46	0.46	0.59	0.65	0.61	0.60	0.40	0.40	0.20
1.76	9.57	8.75	8.52	9.55	8.97	7.96	10.46	12.00	10.74	9.08	9.40	7.28
1.01	6.68	5.32	8.05	5.29	6.63	4.80	6.09	7.33	5.66	6.35	6.53	5.35
0.05	0.21	0.21	0.24	0.22	0.26	0.21	0.19	0.34	0.28	0.47	0.25	0.26
24.68	3.04	1.14	0.41	1.36	2.53	5.34	0.77	0.47	0.31	0.32	0.13	0.47
3.36	10.34	4.19	0.24	4.17	8.17	5.92	0.96	0.38	0.27	0.41	0.33	0.35
3.81	1.84	3.16	3.88	2.54	2.98	1.36	4.02	3.95	5.41	3.62	2.66	4.82
0.62	3.15	2.84	4.68	3.12	3.38	2.27	4.20	4.13	4.16	4.31	4.29	2.47
0.05	0.04	0.07	nd	0.08	0.04	0.07	0.16	0.03	0.02	0.02	0.01	0.01
14.67	9.12	6.46	3.29	5.58	8.80	10.18	2.15	3.08	0.48	3.89	4.76	22.78
85	260	253	46	289	380	207	596	360	271	70	45	349
nd	30	258	233	200	155	148	197	227	198	222	243	153
3.3	3.7	2.4	nd	nd	nd	nd	nd	nd	nd	nd	nd	nd
nd	14	8.6	nd	12	10	17	1.9	1.1	nd	nd	1.3	nd
7.9	128	152	167	109	109	82	103	141	133	131	137	113
nd	96	139	131	123	103	72	101	153	149	169	124	nd
6.2	10	11	2.4	0.9	nd	4.9	nd	nd	nd	nd	0.9	2.9
2.9	13	13	15	5.3	1.7	0.4	4.7	2.2	4.8	6.1	7.4	1.7
10	87	81	132	83	67	68	86	84	77	109	106	14
791	261	116	5.9	113	256	278	47	12	4.3	15	5.3	31
3.6	11	14	16	14	10	12	14	15	17	19	17	29
249	33	33	6.8	27	20	52	26	10	6.7	5.2	6.2	4.6
5.4	67	81	101	73	65	51	87	94	78	97	89	nd
17	133	238	240	175	152	134	216	233	228	230	216	126
1.2	662	944	1055	849	666	601	931	872	848	1131	988	337
14	8.2	7.5	3.4	2.1	2.3	6.7	1.8	nd	nd	0.7	nd	nd
0.2	32.8	29	35	21	25	18	26	28	24	29	25	47
97	nd	44	62	86	80	63	88	107	99	93	106	120
953	nd	nd	nd	nd	nd	145	nd	nd	nd	nd	nd	nd
8.9	9.9	10	5.8	5.8	4.9	10	4.4	11	9.7	1.0	0.2	0.4

Table 3.1: continued from the previous page

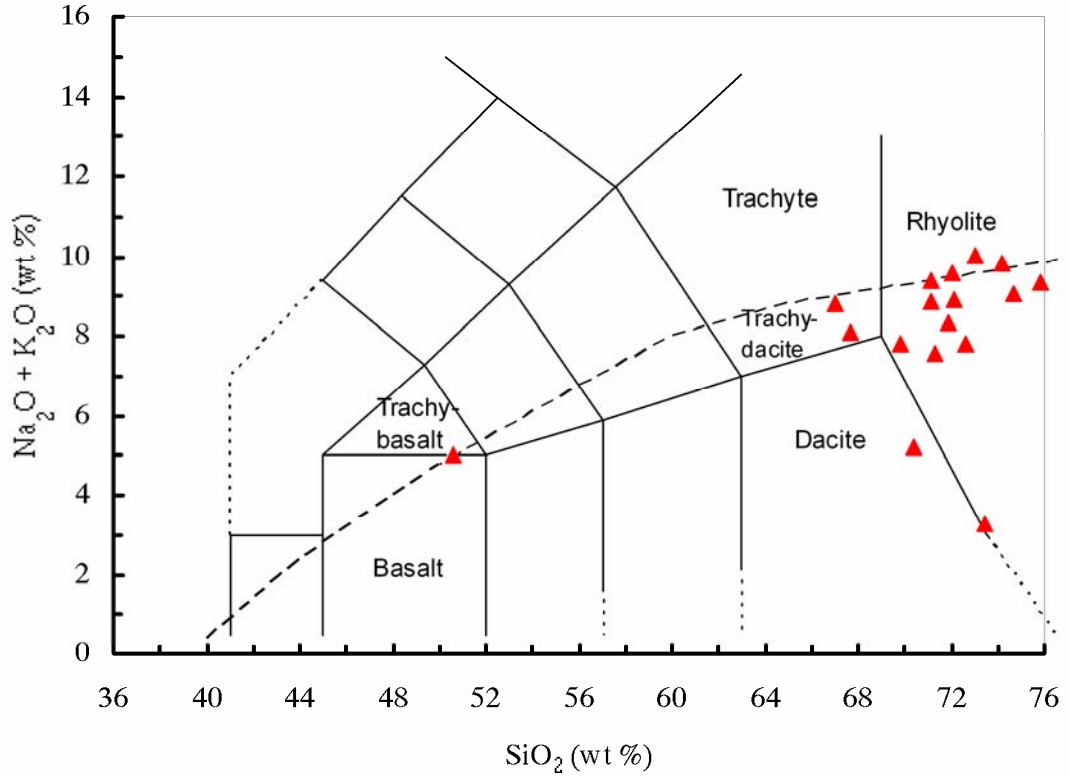

Figure 3.1: TAS diagram of volcanic rocks from the central MER.

The petrographic investigation of representative thin sections shows that they are characterized by a few crystals of quartz, alkali-feldspar, orthopyroxene and amphibole within a prevalent glassy groundmass. Potential F-bearing minerals such as fluorite and apatite have not been observed.

Microprobe analyses have been carried out on the main mineral phases and on the glassy matrix (**Table 3.2**). The results revealed that the concentration of F is as high as 180 ppm in the glassy groundmass and up to 260 ppm in accessory phases such as alkali amphibole (riebeckite composition) **(Table 3.3)**. Therefore, considering the modal proportions of the investigated rocks (hydrous mineral phases are extremely rare); we assume that most of the fluorine budget is concentrated in the glassy matrix.

This glassy matrix is reactive and easily affected by weathering processes that induce the neo-formation of clay minerals that can potentially trap fluorine (as F^- can replace OH^- in phyllosilicates).

This implies that the weathering products of these volcanic rocks, i.e. the clay-rich fluvio/volcano lacustrine sediments, are enriched in F^- with respect to the original mother rocks. Coherently, the higher concentrations of F in groundwater have been recorded in those wells drilled on the fluvio/volcano lacustrine sediments.

Label	TW30 (Ignimbrite)								TW31 (Ignimbrite)						TW29(Ignimbrite)		
	Amphiboles					Glass			Amphiboles						Glass		
SiO_2	50.98	50.39	50.56	51.21	50.78	71.12	66.20	68.66	51.54	51.09	51.10	50.93	50.60	51.01	73.68	72.76	72.05
TiO_2	2.26	2.29	2.18	2.18	2.23	0.55	0.48	0.52	2.11	2.15	2.18	2.38	2.17	2.19	0.34	0.33	0.27
Al_2O_3	1.85	1.29	1.23	1.43	1.45	9.23	8.80	9.02	1.17	1.17	1.15	1.22	1.28	1.19	9.67	9.75	9.98
FeO	17.01	21.24	21.23	19.71	19.80	6.66	5.60	6.13	21.73	21.33	21.78	21.65	20.86	21.46	4.83	4.70	5.01
MnO	1.01	1.49	1.40	1.20	1.27	0.31	0.31	0.31	1.40	1.39	1.35	1.39	1.37	1.38	0.20	0.21	0.25
MgO	11.83	8.69	9.19	10.74	10.11	0.24	0.21	0.22	9.17	9.01	9.17	9.00	9.28	9.12	0.04	0.03	0.00
CaO	6.03	4.94	4.92	5.32	5.30	0.22	0.13	0.18	4.66	4.73	4.91	4.66	4.88	4.77	0.21	0.20	0.23
Na_2O	5.02	5.50	5.37	5.02	5.23	3.85	5.39	4.62	5.71	5.67	5.45	5.66	5.61	5.59	3.95	3.72	3.79
K_2O	0.79	0.93	0.82	0.86	0.85	4.50	4.34	4.42	0.87	0.97	0.94	0.94	0.90	0.92	4.06	4.04	3.98
NiO	0.032	0.005	0.000	0.074	0.028	0.000	0.014	0.007	0.037	0.000	0.000	0.000	0.079	0.019	0.076	0.028	0.066
Wt%(F)	0.023	0.022	0.024	0.016	0.021	0.006	0.017	0.012	0.026	0.026	0.016	0.022	0.018	0.019	0.018	0.011	0.008
Wt%(S)	0.017	0.007	0.011	0.000	0.009	0.000	0.079	0.040	0.000	0.011	0.000	0.024	0.002	0.009	0.002	0.025	0.029
Wt%(Cl)	0.046	0.002	0.000	0.010	0.015	0.150	0.282	0.216	0.012	0.000	0.002	0.000	0.002	0.005	0.159	0.155	0.142

Table 3.2: Microprobe analyses on amphibole and volcanic glass of rhyolitic ignimbrites

Rock type	**Rift floor Ignimbrites**			
Label	**TW29**	**TW30**		**TW31**
Phases	**Glass**	**Glass**	**Amphibole**	**Amphibole**
No of analysis points	**4**	**2**	**5**	**6**
SiO2	72.63	68.66	50.78	51.01
TiO2	0.31	0.52	2.23	2.19
Al2O3	9.84	9.02	1.45	1.19
FeO	4.82	6.13	19.80	21.46
MnO	0.19	0.31	1.28	1.39
MgO	0.02	0.23	10.11	9.12
CaO	0.22	0.18	5.30	4.77
Na2O	4.10	4.62	5.23	5.6
K2O	4.03	4.42	0.85	0.92
NiO	0.055	0.007	0.03	0.019
Average Wt% (F)	**0.011**	**0.012**	**0.021**	**0.019**
average PPM (F)	**110**	**120**	**210**	**190**
Maximum PPM (F)	**180**	**170**	**240**	**260**
Average Wt%(S)	0.024	0.040	0.009	0.009
Average Wt%(Cl)	0.143	0.216	0.015	0.005

Table 3.3: Summerized (average and maximum) concentrations from microprobe analyses on amphibole and volcanic glass of rhyolitic ignimbrites

4. Hydrogeochemistry of MER waters

4.1. Introduction

The geochemistry of natural waters involves the study of the composition and sources of chemical elements as well as the understanding of processes that control the composition of geochemical anomalies in waters. This chapter provides a brief discussion on the lithologic and hydrochemical controls on the chemical composition of waters. Considering that in the study area people principally relies on groundwater wells and springs for portable water resources, the investigation mainly focuses on toxic elements (such as F^-) which is negatively affecting the health of millions of the local populations.

4.2. Water sampling and analytical techniques

Water samples were collected during dry seasons in January 2006 and 2007 from 53 sites including 12 hot springs, 2 cold springs, 23 groundwater wells, 8 rivers, and 6 lakes in the Ziway-Shala basin of the MER valley, for the analysis of major ions (Na^+, K^+, Ca^{2+}, Mg^{2+}, F^-, Cl^-, NO_3^-, SO_4^{2-} and HCO_3^-) and trace elements (Li, Be, B, Al, V, Cr, Mn, Fe, Co, Ni, Cu, Zn, Ga, As, Rb, Sr, Mo, Ag, Cd, Sb, Te, Ba, Hg, Tl, Pb, Bi, U). Samples were stored in 100 ml polyethylene bottles after filtering through 0.45 μm membrane filters. For trace element analysis, samples were filtered and acidified with ultra-pure concentrated nitric acid. pH, electrical conductivity, and temperature were measured in situ.
Analyses were carried out at the Department of Earth Sciences of the University of Ferrara using AA spectrometry for cations (Na^+, K^+, Ca^{2+}, Mg^{2+}), ion chromatography and spectral photometry for anions (F^-, Cl^-, NO_3^-, SO_4^{2-}). Titration techniques were used to analyze total alkalinity (CO_3^{2-} + HCO_3^-). Analytical precision and accuracy are estimated as better than 5% (10% at sub-ppm levels) for both anions and cations on the basis of repeated analysis of samples and standards. The reproducibility of the data has been also cross-checked in the external laboratories of the Technical-Industrial Institute (ITI) of Ferrara.

Inductively Coupled Plasma Mass Spectrometry (ICP-MS) analyses were done using Thermo Electron series X Spectrometer. Quantitative determinations were performed by external calibration with multi-

element standards in aqueous matrices using Rh, In and Re as internal standard to correct instrumental drifts. Precision based on replicate analyses are estimated on average better than 4 % for As, B, Cr, V, Co, Fe, Zn, Cu, Ga, Pb, Ni, Cd, Mo, Sb, Al, Ba and about 15 % for the rest (Li, Be, Mn, Rb, Sr, Te, Hg, Bi and U). Accuracy, based on analysis's results of certified reference material (CRM) is on average better than 12% for all elements.

4.3. Geochemical composition of the MER waters.

4.3.1. Major ion compositions

The major ions geochemical analyses of the different MER water types are reported in **Table 4.1**, show extremely variable composition, ranging from low TDS (and e.g. low F^-) in rivers to very high TDS (and e.g. high F^-) in the rift groundwater wells, hot springs and lakes (see sampling points on **Figure 4.1**).

ID	TYPE	X	Y	T(^oC)	EC	pH	TDS	Na^+	K^+	Mg^{2+}	Ca^{2+}	F^-	Cl^-	HCO_3^-	SO_4^{2-}	NO_3^-
1	RI	38.651	7.726	22.2	500	8.4	425	64	15	9.4	25.9	2.2	15	287	7	3.8
2	RI	38.822	8.153	23.3	530	8.7	583	56	12	20.9	42	1.5	16	409	25	2.0
3	RI	39.003	8.046	21.5	180	7.8	174	15	5	5.2	16.8	1.6	4	125	1	2.6
4	RI	39.054	7.801	18.7	90	8.3	98	5	2	2.7	18.5	0.2	1	67	0.8	2.0
5	RI	38.892	7.521	10.6	60	7.9	73	5	3	1.4	10.7	0.1	2	49	1.5	6.2
6	RI	38.863	7.465	11.5	40	7.8	53	3	2	1.2	8.4	0.1	1	37	0.2	1.8
7	RI	38.743	7.487	16.9	150	7.9	118	13	5	2.3	17.9	0.5	3	73	2.3	11.9
8	RI	38.657	7.262	14.0	150	7.9	156	16	7	2.2	40.7	0.3	7	79	4.1	10.2
9	HS	38.628	7.489	48.5	2750	8.9	1600	593	18	bdl	0.9	19.6	279	988	3.3	bdl
10	HS	38.634	7.477	93.4	14440	8.2	7919	2288	25	bdl	0.3	97	1462	3434	612	43.3
11	HS	38.634	7.477	57.3	10570	7.8	7501	2416	26	bdl	1.4	64	1324	3642	28	bdl
12	HS	38.634	7.477	91.4	13190	8.0	6589	2109	1	bdl	1.9	55	1148	3251	22	bdl
13	HS	38.637	7.477	52.6	1780	8.2	1141	346	26	bdl	3.2	8.4	196	561	bdl	bdl
14	HS	38.423	7.402	59.3	4630	7.3	3600	969	66	8	8.8	17.5	321	2141	68.8	bdl
15	HS	38.436	7.422	51.8	4870	8.2	3896	1122	64	0.6	1.7	17.6	356	2267	66	bdl
16	HS	38.811	7.664	38.8	630	7.3	499	105	11	5.5	22	1.9	27	293	32.6	0.3
17	HS	38.773	7.712	62.0	3900	7.0	2766	802	60	0.7	13.9	23.4	435	1407	23	bdl
18	HS	38.773	7.690	96.0	4530	8.4	1830	170	39	bdl	0.9	23.5	429	915	253	34.4
19	HS	38.628	7.447	45.0	4665	9.1	3679	945	47	0.2	0.9	45.9	488	2098	54	bdl
20	HS	38.853	7.934	78.0	2040	6.8	1728	398	29	3.3	11	13	128	1110	35	bdl
21	GWL	38.798	7.793	82.0	2160	7.4	1297	306	110	bdl	0.5	13.6	162	653	52.9	bdl
22	GWL	38.796	7.788	85.6	4600	8.2	3051	771	152	bdl	0.8	40	207	1842	37.7	bdl
23	LW	38.684	7.538	24.2	1730	9.0	1377	387	21	0.5	9.7	12.5	131	769	46.5	4.7

24	LW	38.448	7.127	22.1	800	8.8	715	161	27	6	13.5	7.4	24	476	0.6	1
25	LW	38.424	7.403	24.6	>20000	10.1	64267	17725	1109	bdl	bdl	233	6330	38583	288	bdl
26	LW	38.435	7.423	25.8	>20000	9.6	11563	3426	125	0.6	4.5	90	1326	6497	95	bdl
27	LW	38.595	7.671	27.6	>20000	9.7	52725	15212	619	bdl	0.2	384	5361	30596	553	bdl
28	LW	38.736	7.919	25.2	420	8.6	379	61	11	7.6	27.3	1.5	10	253	6.6	2.4
29	WL	38.689	7.875	24.6	840	8.1	876	180	67	5.7	7.8	4.2	9	598	4	0.4
30	WL	38.724	7.841	26.0	1160	8.3	1164	241	33	4.9	4.4	2.8	16	857	5	1.6
31	WL	38.800	7.542	24.5	210	8.3	188	31	5	0.8	7.3	1.2	1	140	1	0.2
32	WL	38.772	7.520	21.5	340	7.6	323	18	6	7.7	45.7	0.4	2	244	bdl	0.5
33	WL	38.699	7.926	28.2	1020	8.3	1013	232	18	3.1	6.7	2.1	12	738	2	1.3
34	WL	38.834	8.159	24.4	640	7.7	623	90	11	11.5	33.4	3.6	20	448	6	4.3
35	WL	38.812	8.145	25.1	2750	7.8	2227	565	25	6.7	20.8	20	176	958	456	104
36	WL	38.999	8.053	25.3	300	7.8	267	50	5	2.7	10.2	1.8	2	195	bdl	1
37	WL	38.709	7.976	28.3	3360	8.2	3564	858	31	4.2	3.7	13.6	106	2547	7	bdl
38	WL	38.680	7.991	27.3	2180	8.8	1884	467	17	bdl	1.6	21.4	167	1025	186	29.5
39	WL	38.934	8.145	25.6	470	7.6	367	81	8	2.4	22.5	2.4	4	183	63.5	6.4
40	WL	38.966	8.120	24.6	350	7.5	871	61	9	2.3	27.7	3.1	145	226	397.7	15
41	WL	39.015	8.038	22.6	200	7.6	204	30	14	1.9	13.5	0.8	1	140	2	1.6
42	WL	38.749	7.482	22.5	220	8.3	211	33	2	1.1	24.7	1.5	1	146	0.8	0.4
43	WL	38.706	7.331	24.0	220	7.3	266	30	4	2.6	25	2	1	201	0.5	0.7
44	WL	38.395	7.152	23.2	1320	8.1	1252	307	12	5.6	17	13.1	17	872	7.8	bdl
45	WL	38.854	7.841	30.6	520	7.6	501	86	10	10.4	34	4.1	11	342	4	0.2
46	WL	38.838	7.821	32.3	2260	7.6	1952	480	28	30.5	30.7	7.1	266	1077	33.5	2.7
47	WL	38.637	7.833	36.0	2390	8.1	1949	557	26	0.1	29	14.3	153	1092	107	bdl
48	WL	38.648	7.720	23.6	460	7.1	420	69	12	4.6	41	1.7	11	271	8.7	bdl
49	WL	38.822	8.159	25.2	490	7.8	489	55	2	11.2	68	0.9	4	342	5.8	0.1
50	WL	38.742	8.066	23.7	1770	8.7	1735	443	21	1.9	7.2	10	19	1229	3.7	bdl
51	WL	38.532	7.006	36.4	730	7.9	668	140	15	3.2	18.9	3.1	7	475	6.4	bdl
52	CS	38.743	7.487	22.5	180	6.6	137	17	5	2.1	22.7	0.7	5	79	4.8	24
53	CS	38.869	7.891	27.6	280	7.8	258	40	6	4.2	22	1.3	2	180	2.2	bdl

Table 4.1: Major ion hydrochemical compositions (in mg/L) of MER waters from rivers, hot springs, geothermal wells, groundwater wells, cold springs, and lakes in the Ziway-Shala basin. WL=Groundwater wells, HS=Hot springs, CS=Cold springs, GWL=Geothermal wells, LW= Lakes (ID: 23=Langano, 24=Awasa, 25=Chitu, 26=Shala, 27=Abijata, 28=Ziway), RI= Rivers (ID: 1=Bulbula, 2=Meki, 3=Ketar); bdl = below detection limit; X and Y are geographic coordinates expressed in degree decimal.

The average TDS values in the groundwater wells and hot springs (39-96 ^{o}C) are 1050 and 3610 mg/L respectively. TDS is even more variable in lake waters, with values which vary from the fresh water Ziway lake (379 mg/L), brackish water Langano lake (1377 mg/L) to the saline Shala, Abijata and Chitu lakes (11563, 52725 and 64267 mg/l respectively). pH ranges between neutral to alkaline (6.8-9.1) in

groundwater wells, thermal springs and rivers whereas the lakes have pH range of 8.6-10, with the highest value recorded in the alkaline lake Chitu.

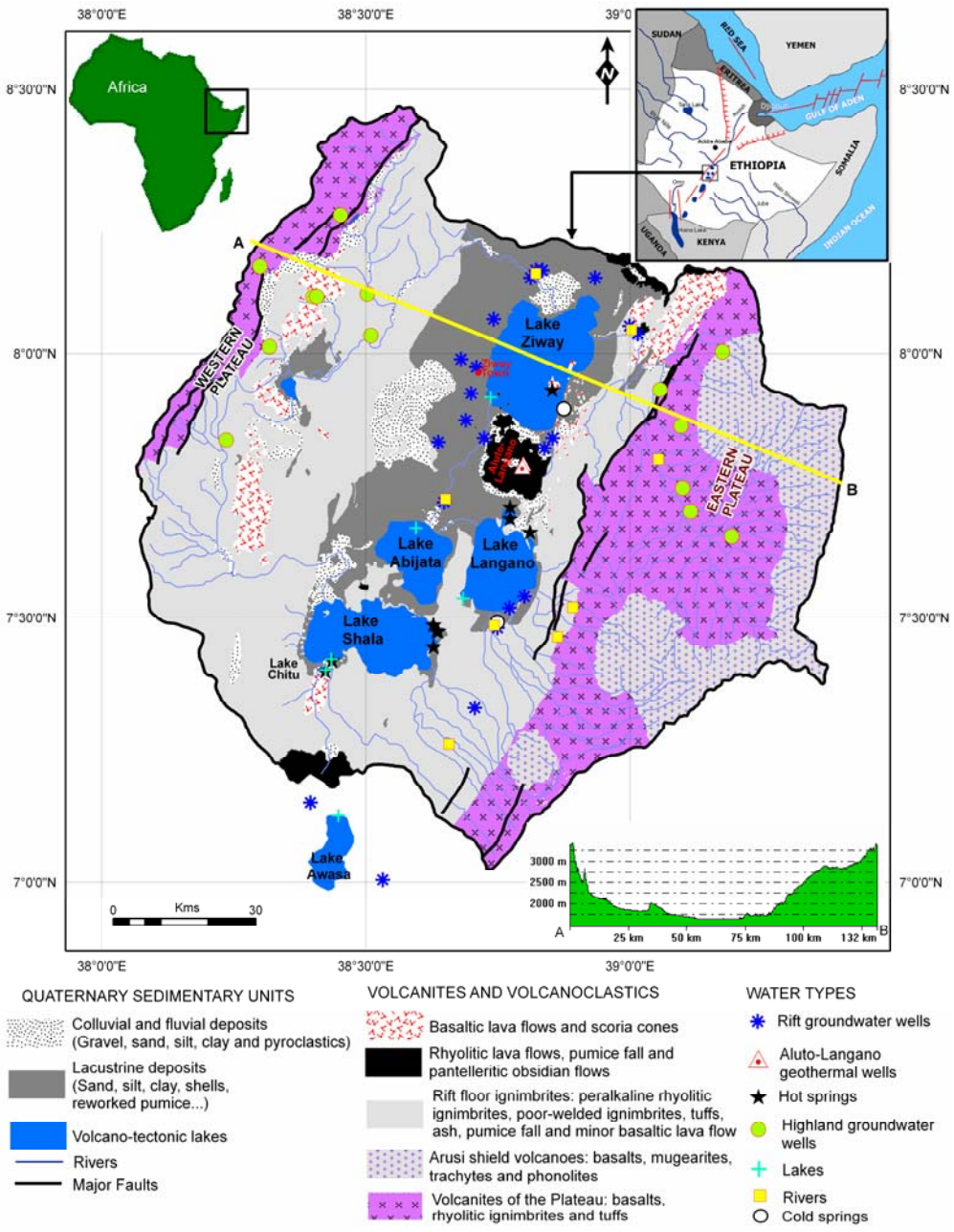

Figure 4.1: Simplified geologic map of the study area (Ziway-Shala lakes basin) modified from (Dainelli et al., 2001) reporting the localities of water sampling.

Comparing the relative concentration of major ions in the waters from the central MER valley, Na^+ is always higher than K^+, since Na is more abundant than K in the host rocks, and K-minerals in primary volcanic parageneses are more resistant to weathering than Na-minerals (i.e. plagioclase is more alterable than K-feldspar); moreover K^+ is easily stabilized in neo-formation minerals (clay minerals). Mg^{2+} is lower in concentration than Ca^{2+}, probably due to the low abundance of Mg^{2+}in the outcropping rocks. Depletion of Ca^{2+} and Mg^{2+} and enrichment in Na^+ and K^+ is observed along the groundwater flow paths, moving from the highlands to the rift axial zone. The high concentration of bicarbonate is not related to calcite dissolution (carbonates are not present in the studied area) and therefore it is induced by magmatic outgassing (CO_2 can upraise along the many faults still active in the rift). CO_2 also increases the water aggressivity, i.e. its capability to trigger water/rock interaction processes thus explaining a close geochemical link between HCO_3^- and other parameters such as Na^+, Cl^-, and F^-. A few groundwater samples were identified with high concentration of NO_3^- and SO_4^{2-} reaching up to 104 mg/L and 456 mg/L respectively, which is most probably caused by anthropogenic pollutions (agricultural and human activities).

Different hydrochemical facies were identified on the basis of the (Langelier and Ludwig, 1942) diagram reported in **Figure 4.2**. In this diagram the different water types, i.e. groundwater wells (in the rift and highlands), geothermal wells, hot springs, rivers and lakes are represented by distinct symbols. Groundwater from the highlands (Ayenew, 2005) typically show a $Ca^{2+}(Mg^{2+})$- HCO_3^- hydrochemical facies similar to that of rivers and cold springs where the sum of Ca^{2+} and Mg^{2+} exceeds Na^+ and K^+. On the contrary hot springs and most groundwater in the rift display a Na^+- HCO_3^- fingerprint, with Na^+ and HCO_3^- proportions constituting more than 80 % of all the ionic species in the solution.

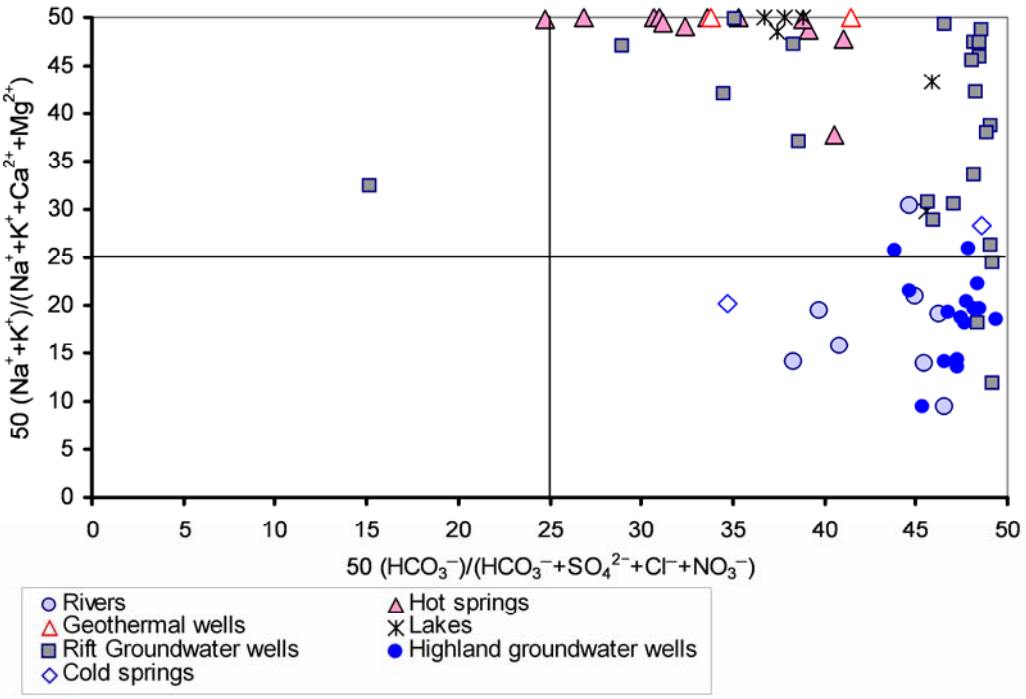

Figure 4.2: Langelier and Ludwig, 1942 diagram showing compositions of different water types of the central MER in Ziway-Shala basin.

Therefore, it can be concluded that there is a general compositional change from a Ca^{2+}-Mg^{2+}/HCO_3^- to a Na^+-HCO_3^- hydrochemical facies along the groundwater flow path from the highlands to the rift floor. This result is consistent with other hydrochemical studies of the area (Darling et al., 1996; Chernet et al., 2001; Ayenew, 2005). Fluoride concentration increases during this evolution displaying low values in Ca^{2+}-Mg^{2+}/HCO_3^- waters from the highlands and higher values in the Na^+-HCO_3^-waters from the rift. The average concentration of fluoride is 0.8 mg/L in rivers, 32 mg/L in thermal springs, 27 mg/L in deep (>2 kms) geothermal wells, 6 mg/L in groundwater wells, and 121 mg/L in lakes. 38% of rivers, 87 % of the groundwater wells and 100 % of lakes, thermal and geothermal waters have fluoride value beyond the safe drinking water limit (WHO, 2006).

4.4. Source of fluoride

4.4.1. Chemical and mineralogical composition of rocks

In chapter 3, the chemical and mineralogical composition rocks were briefly described and the result indicated that the prevalent volcanic rocks are rhyolites (i.e. felsic magmas) and that the fluvio-volcano lacustrine sediments represent the weathered (re-deposited) products of the above mentioned volcanic rocks. The microprope result also showed that most of the fluorine budget is concentrated in the glassy matrix. This glassy matrix is reactive and easily affected by weathering processes that induce the neo-formation of clay minerals that can potentially trap fluorine (as F^- can replace OH^- in phyllosilicates).
This implies that the weathering products of these volcanic rocks, i.e. the clay-rich fluvio-volcano lacustrine sediments, are enriched in $F^-$with respect to the original mother rocks.

A plausible hypothesis is that during explosive volcanic eruption, volcanic gases such as H_2O, CO_2, SO_2, HCl, H_2S and HF may have been trapped within the tephra (Giggenback, 1996). The adsorption process is effective on smaller particles having large surface area (Oskarsson, 1980) such as ash particles (<2 mm). Since fluorine is highly soluble in water, it can be subsequently transferred in the water system if the volcanic deposits are leached by water (Gregory, 1996) during water-rock interactions. In this hypothesis, the anomalous F^- concentration recorded in thermal water may not reflect a direct magmatic contribution (presence of juvenile F^--rich fluids), but it probably simply means that hot water is more aggressive and capable to leach the aquifer matrix.
To verify the mentioned process we performed laboratory leaching-tests on representative lithotypes outcropping in the rift valley. The powdered samples were mixed with distilled water having a pH of about 5.5, at a ratio of 1:5 (10 g/50 ml; room temperature), and shaken for 12 months at a frequency of 100 rev/min. The experiment was carried out in closed system, i.e. utilizing closed plastic bottles which did not allow interaction with atmospheric gases (such as CO_2).
The concentration of F^- in the real natural water can be higher than those recorded in the experimental leachates, as the resulting F^- concentration in experimental leachates is expected to increase with the increase of time. Higher temperature and introduction of CO_2 have to be considered as additional factors favouring high fluoride in the natural waters of the rift. These tests, that simulate the water-

rock/sediment interaction processes, highlight the potential contribution (i.e. the leachability) of each investigated lithotype to the release of fluorine in the water system.

The result highlights a clear relationship between high pH and high fluoride concentration. In particular, relevant increases in pH and F^- (up to 7.6 mg/l) have been recorded in the leaching tests of the fluvio-volcano lacustrine sediments. Therefore, these data confirm that the fluvio-volcano lacustrine sediments are the main reservoir of fluorine in the area and that they can release it into the water system. The water-sediment interaction is also reflected in higher TDS and EC (**Table 4.2**). Accordingly, high fluoride concentration is found in leachates characterized by high pH, Na^+ and HCO_3^- (**Figure. 4.3** a, b, c, d). The rock/sediment leachates are generally characterized by a Na^+/HCO_3^- hydrochemical facies with high pH values (near neutral to alkaline) similar to natural waters of the study area (**Figure 4.4**).

The major ions chemical composition of the silicic volcanic rock and sediment leachtes is displayed on **Table 4.2.**

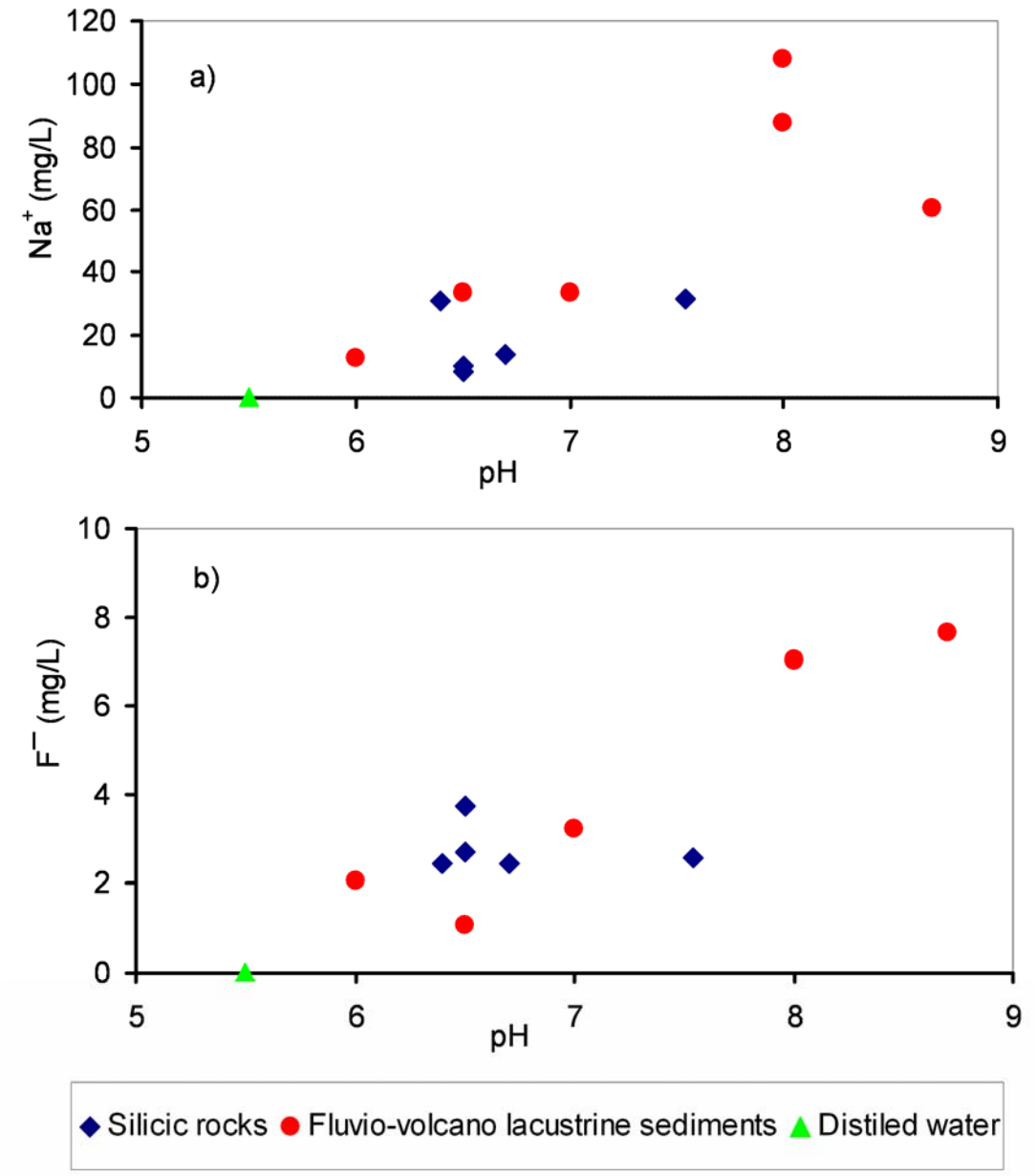
a)
Na^+ (mg/L)
120
100
80
60
40
20
0
5
6
7
8
9
pH
b)
F^- (mg/L)
10
8
6
4
2
0
5
6
7
8
9
pH
Silicic rocks
Fluvio-volcano lacustrine sediments
Distiled water

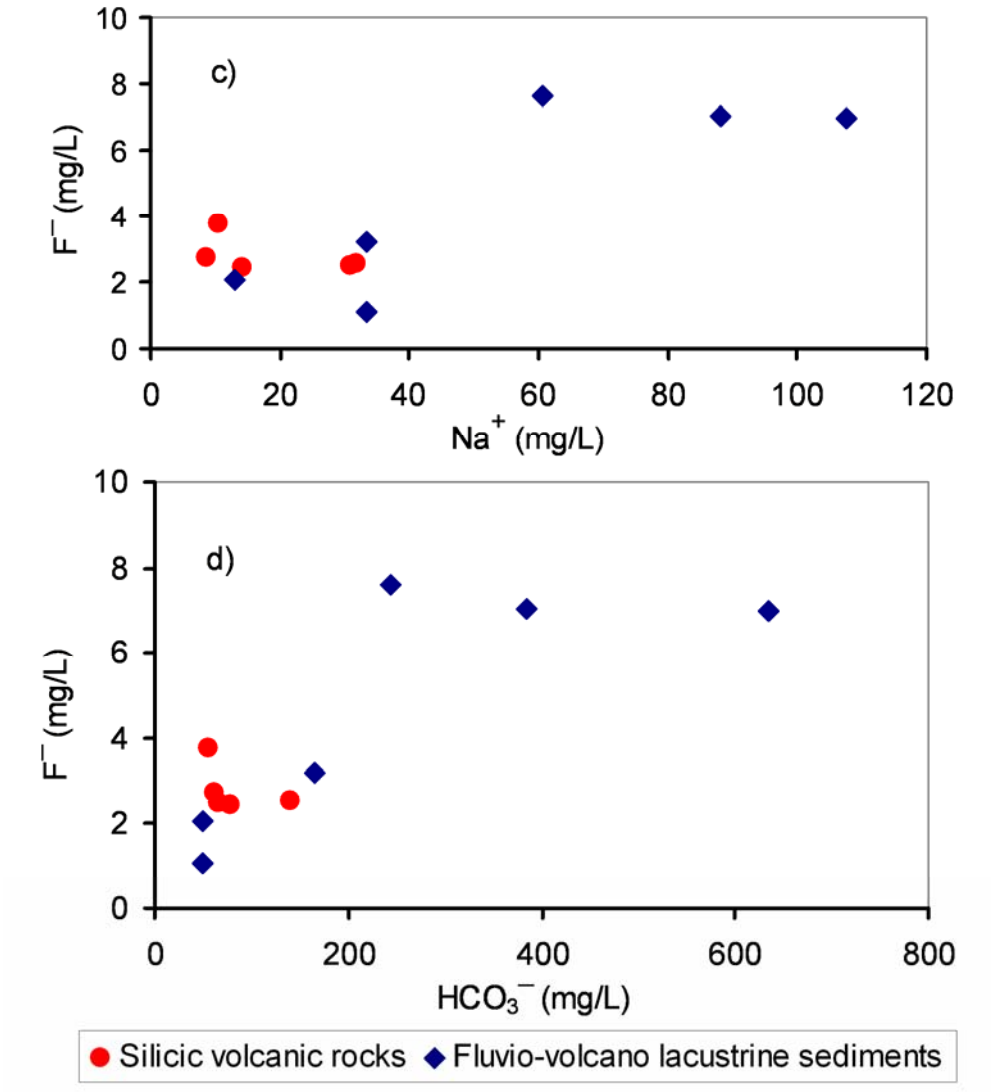

Figure 4.3: Leaching test results: a) Na^+ versus pH; b) F^- versus pH c) F^- versus Na^+ d) F^- versus HCO_3^-.

	Rhyolites					Fluvio-volcano lacustrine sediments					
In mg/L	TW9	TW11	TW29	TW30	TW31	TW14	TW15	TW22	TW34	TW39	TW43
Na^+	31.9	31.0	10.6	8.75	14.2	33.4	108	88.0	33.5	12.9	60.5
K^+	1.90	17.34	10.44	4.71	4.40	4.22	34.00	25.53	7.24	4.24	9.08
Ca^{2+}	13.3	118	9.27	6.42	8.77	20.2	9.47	18.0	18.6	5.48	15.6
Mg^{2+}	1.20	3.76	0.28	0.26	0.21	1.20	2.02	2.43	3.53	0.14	0.66
F^-	2.55	2.47	3.74	2.72	2.44	3.20	6.98	7.03	1.06	2.08	7.63
Cl^-	1.45	69.15	1.72	2.09	1.50	2.28	14.4	13.3	28.9	6.69	1.81
HCO_3^-	140	67.0	55.0	61.0	79.3	165	634	384	49.0	49.0	244
NO_3^-	bdl	212.5	5.49	0.15	0.53	8.33	44.7	6.49	64.3	16.7	bdl
SO_4^{2-}	0.98	16.9	5.60	2.51	1.23	5.19	21.5	16.2	16.2	2.94	1.45
TDS	53	472	48	28	33	78	244	177	174	51	97
EC	230	770	140	120	120	290	1140	840	360	130	380
pH	7.5	6.4	6.5	6.5	6.7	7	8	8	6.5	6	8.7

Table 4.2: Major ion chemical compositions of the leachates with TDS, EC and pH values.

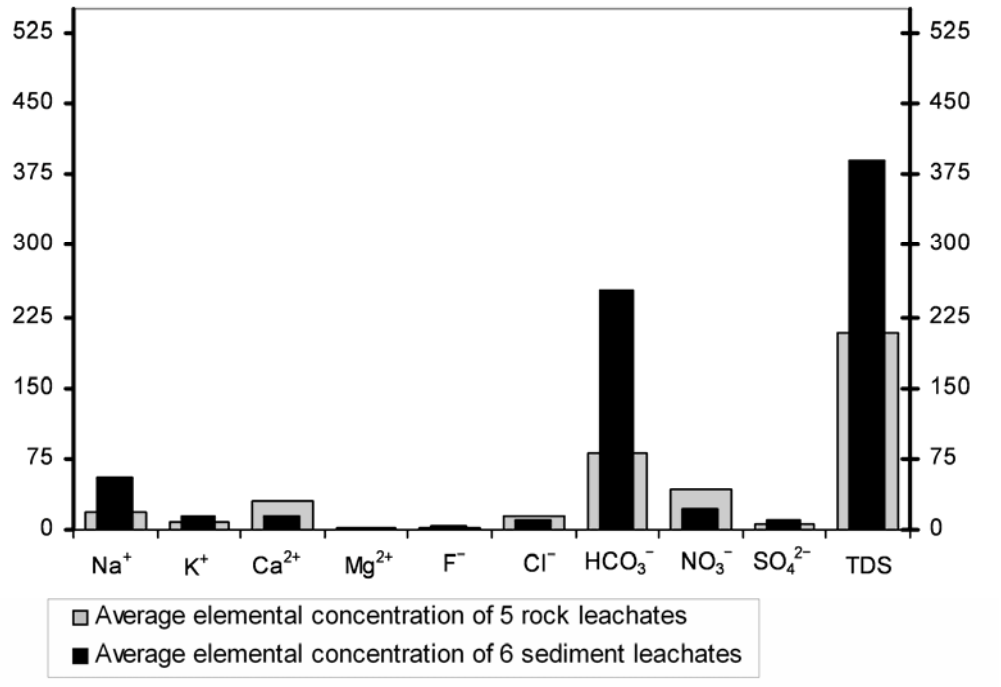

Figure 4.4: Average elemental concentrations of the leachates: Sediment leachates are more enriched by Na^+ and HCO_3^- than the rock leachates (Values are expressed in mg/L).

Similar trends of high F^- is associated with high pH, Na^+, and HCO_3^- values, whereas F^- is inversely related to Ca^{2+} and Mg^{2+} in the groundwater wells, hot springs and geothermal wells of the Main Ethiopian Rift (**Figure 4.5**).

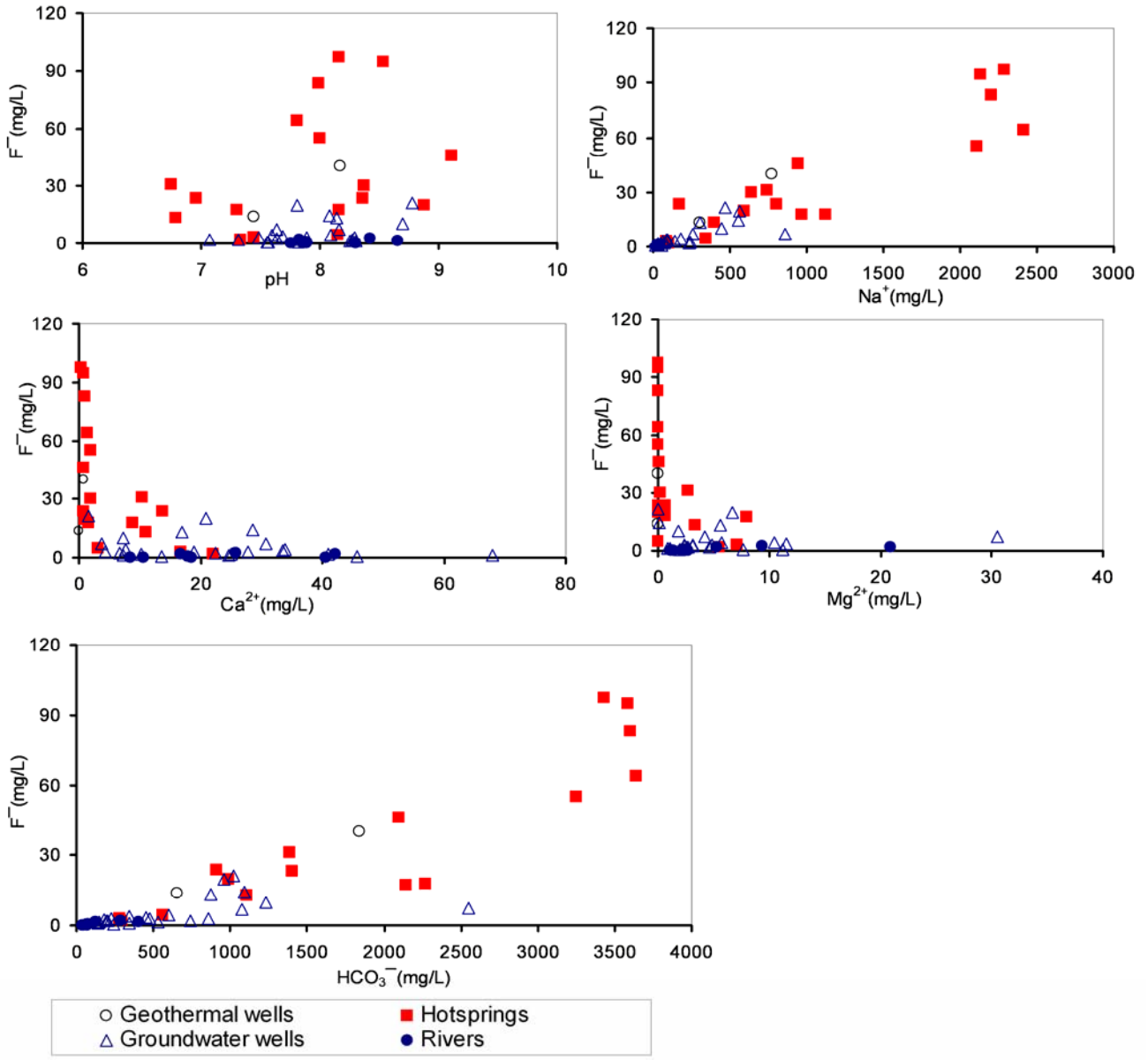

Figure 4.5: Relationship between pH, F^-, Na^+, HCO_3^-, Ca^{2+} and Mg^{2+} in waters of the central MER in Ziway-Shala basin.

The variation of pH (the original distilled water had pH 5.5) towards alkaline values observed in the experiments, shows that the system consumes H^+ (probably during hydrolysis reactions), and that the resulting alkaline conditions favours the substitution of OH^- with exchangeable F^- in fluoride-rich minerals (Guo et al., 2007).

The chemistry of the lake water appears even more complicated due to evaporation processes, which ultimately lead to very extreme compositions such as those of Lake Abijata. In this framework, further input of fluorine can be attributed to peculiar minerals included in the relative sediments, such as trona ($Na_2CO_3{-}NaHCO_3{-}2H_2O$) which usually contains trace amounts of fluoride.

4.5. Fluoride enrichment mechanism

4.5.1. Base-exchange softening

Base-exchange softening is an adsorption phenomenon. A substrate that possesses negative charges on its surface will have cations adsorbed. Different cations have different affinities for adsorption (Ca^{2+} more than Na^+). Higher affinity ions will replace lower affinity ions; the concentration of the high affinity ion decreases and the low affinity ion increases. Because of this, Ca^{2+} can be removed from solution and the dissolution calcium-containing minerals (such as CaF_2) will increase. Moreover, pH increases, and hydroxyl ions can replace fluoride. In both cases, fluoride concentration increases in solution.

Fluorine occurrence is associated with the presence of silicic rocks and their weathering products. The fluoride activity in the solution is controlled by the solubility product, $K_{fluorite}$: (Edmunds and Smedley, 2005) as expressed below:

$CaF_2 = Ca^{2+} + 2F^-$

$K_{fluorite}$: $(Ca^{2+})\,(F^-)^2 = 10^{-10.57}$ at 25ºC

This suggests that the fluoride concentration in natural waters is inversely related to Ca^{2+}. This permits free mobility of the fluoride ion into the solution at lower Ca^{2+} content. Such conditions are sometimes recorded in aquifers constituted by volcanic rocks (Kilham and Hecky, 1973; Ashley and Burley, 1994).

This effect (Ca^{2+} deficiency) is magnified in the rift (MER) where cation exchange took place within the sediments (fluvio-lacustrine, volcano-lacustrine) causing the removal of ions from the solution (mainly Ca^{2+}) by replacement with Na^{+} ions from the clay exchange sites. Such hydrogeochemical processes are responsible for the evolution of Ca^{2+}-Mg^{2+}/HCO_3^- to Na^{+}/HCO_3^- types of groundwater and thermal water.

During this study the software package (PHREEQC-2) (Parkhurst and Appelo, 1999) was used to calculate the saturation indices of the major mineral phases. Generally, the saturation indices are used to express the water tendency towards precipitation or dissolution. The degree of water saturation with respect to a mineral is given by:

$$\mathbf{SI = \log (K_{IAP} / K_{sp})}$$

Where: K_{IAP} is the ionic activity product,
K_{sp} is the solubility product, and
SI is the saturation index of the concerned mineral.

When SI is equal to zero then the water is at equilibrium with the mineral phase, whereas SI values less than zero (negative values) indicate under-saturation and that the mineral phase tends to dissolve, while SI values over zero (positive values) indicate super-saturation and that the mineral phases tends to precipitate.

Saturation indices (SI) of fluorite (CaF_2) and calcite ($CaCO_3$) were calculated to constrain the observed chemical evolution (Appelo and Postma, 2005). Calculations were carried out using the standard PHREEQC, WATEQ4F database (Ball and Nordstrom, 1991), and a database derived from MINTEQA2 (Allison et al., 1990). The saturation indices of fluorite obtained with the different databases show only 5−8% of variations, and the result showed that: river samples and groundwater samples from highlands have the more negative SI (average values of -2.06 and -1.92 respectively); geothermal wells have an average value of -1.12, and hot springs have an average value of -0.48; groundwater from rift floor have an average value of -0.69; lakes have an average value of -0.42. Therefore, although a slight increase of fluorite SI can be observed along the flow path, fluorite precipitation is unlikely. The Calcite SI of all groups oscillates around zero, suggesting conditions close to equilibrium for this mineral phase and

calcite precipitation is unlikely, and can not be considered the major cause of calcium depletion. This means that the observed hydrochemical evolution of groundwater from the highlands to the rift cannot be related to significant calcite precipitation. This in turn implies that cation exchange is the most probable process which leads to increase of F^- concentration in the local groundwater. The saturation indices of various water types are showed on (**Figure 4.6 and Appendix 4.1 and 4.2**).

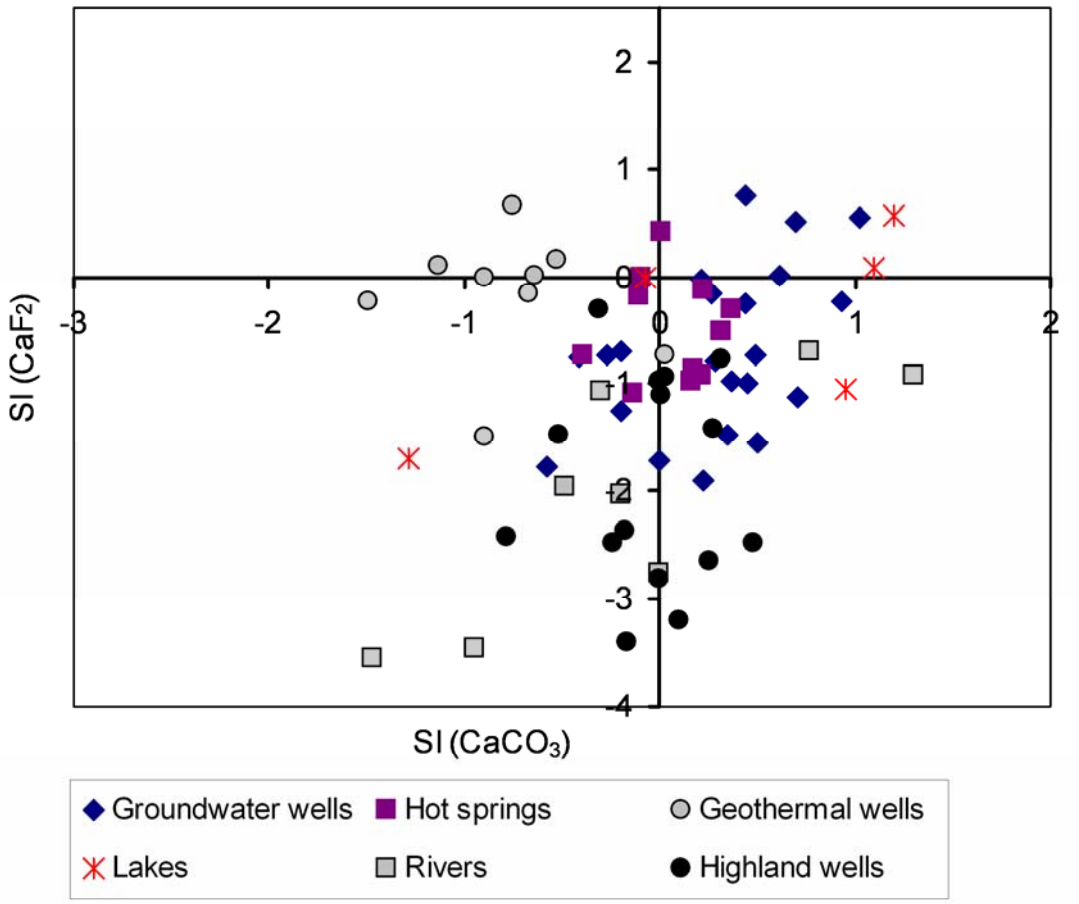

Figure 4.6: Fluorite and calcite Saturation indices of various water types of the central MER in Ziway-Shala basin.

Fluoride ion is a strong ligand; it could form a number of complexes with cations such as Al, Mg, Fe, (Nodstrome and Jenne, 1977). However, the higher pH of the rift waters does not allow the formation of these complexes and the fluoride persists freely in solution.

An investigation of the Na^+/HCO_3^- ratio (expressed in mmoles/L) was carried out in order to support the existence of Base Exchange softening processes.

Weathering of primary feldspar-rich volcanic parageneses in clay-rich saprolites can be idealized by the subsequent reaction (Deer et al. 1992):

$$NaAlSi_3O_8\ (s) + H_2CO_3 + 4.5H_2O \rightarrow Na^+ + HCO_3^- + 2H_4SiO_4 + 0.5Al_2Si_2O_5(OH)_4\ (s)$$

The stoichiometry suggests a Na^+/ HCO_3^- ratio close to 1 in the interacting water.

Therefore, Na^+/ HCO_3^- ratio higher than one, indicates that the incongruent dissolution of feldspars (important constituent minerals of volcanic rocks) by interaction with carbonic acid is not the only controlling hydrogeochemical process.

It is interesting to note that F^- rich waters are those affected by base exchange and thus typically characterized by a high Na^+/ HCO_3^- ratio exceeding unity (**Figure 4.7 and Appendix 4.3**). This water groups are also characterized with TDS values above ~1000mg/L.

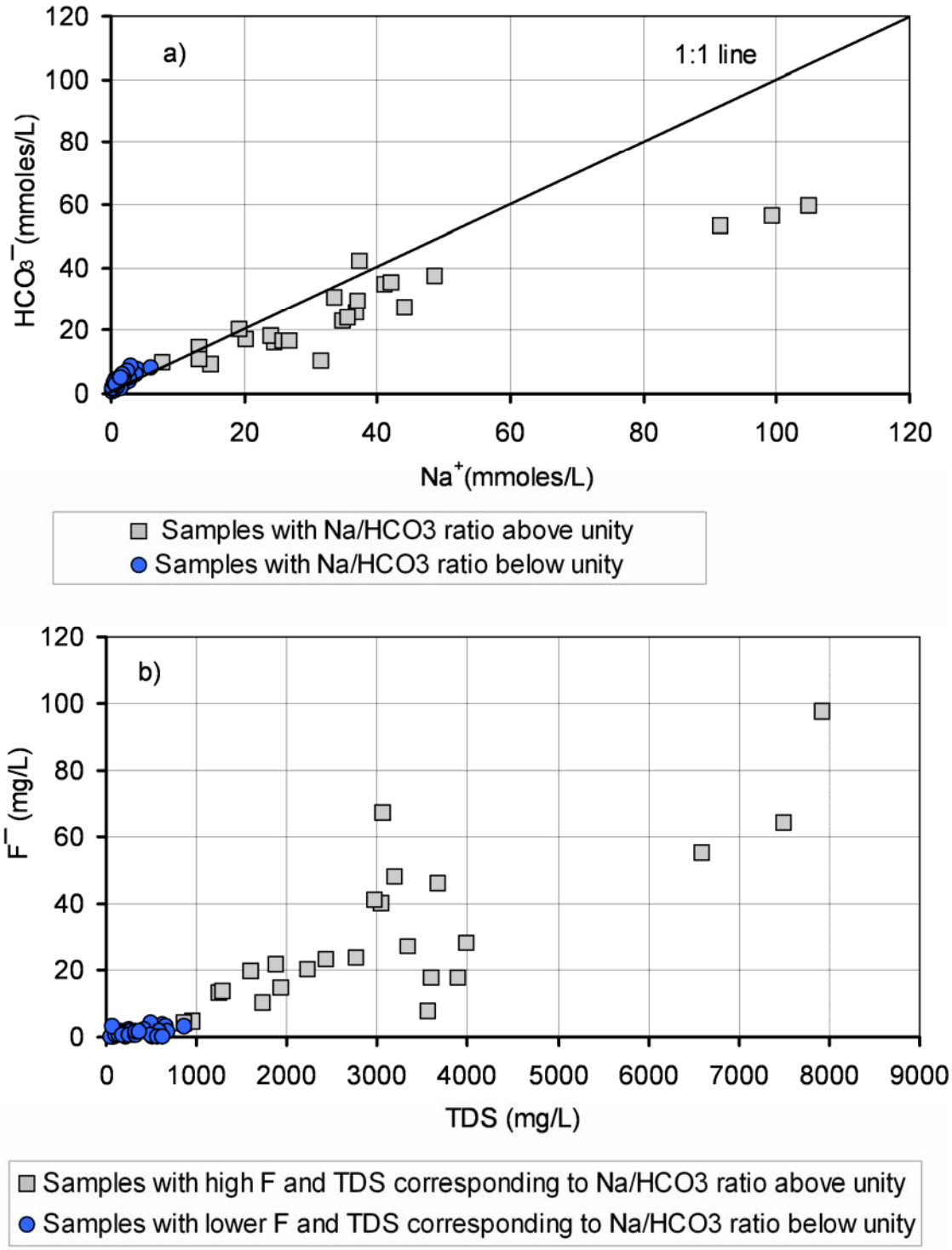

Figure 4.7: a) HCO_3^- versus Na^+ and, b) F^- versus TDS in waters of the Ziway-Shala basin. Note the different behaviour of samples characterized by Na^+/ HCO_3^- ratio above and below unity

It is plausible to assume that ion exchange (base exchange softening) hydrogeochemical processes are the main controlling mechanisms for the elevated content of fluoride in the rift waters; this mainly takes place where water is hosted in the fluvio/volcano lacustrine sediments. The higher Ca and Mg content of the original low TDS groundwater is affected by a base exchange softening reaction:

Na^{+}-clay + (Ca^{2+} +Mg^{2+}) groundwater = (Ca^{2+} +Mg^{2+}) clay + (Na^{+}) groundwater

This reaction would decrease the concentrations of Ca^{2+} and Mg and increase the concentration of Na in groundwater (Hidalgo and Cruz-Sanjulian, 2001). This is supported by the enrichment of fluoride in waters characterized by high Na^{+} and low Ca^{2+} (Mg^{2+}) concentrations, with the parallel increase of pH (the competition of OH^{-} ions at high pH permits the release of F^{-} from the clay-minerals sites).
This hypothesis is supported by the spatial distribution of the different water types, with the occurrence of the Ca^{2+} (Mg^{2+})- HCO_3^{-} hydrochemical facies in the highlands (and the escarpment) and the presence of Na^{+}/ HCO_3^{-} water signature in the rift, where ion exchange with sediments occurs.

5. Geochemistry of elements in natural waters and experimental leachates

5.1. Trace (and Major) elements composition in natural waters.

Water quality evaluation of the various water types were done based on comparison with the currently existing drinking water guidelines. The main parameters of concern were the major and trace elements. In order to sort out potentially hazardous geochemical anomalies, the measured concentrations of major ions (Na^+, K^+, Ca^{2+}, Mg^{2+}, F^-, Cl^-, NO_3^-, SO_4^{2-} and HCO_3^-; **Table 4.1** in chapter 4) and trace elements (As, Mo, Sb, U, Li, Al, V, Cr, Mn, Fe, Co, Cu, Zn, Ga, Rb, Sr, Mo, Sn, Be, Bi, Te, Ba, Hg, Tl, Ag, Cd, Pb, Ni, Cd; **Table 5.1**) in MER natural waters were compared with existing drinking water standards recommended by the authorities (WHO 2006; EU directives, 1998 and USEPA, 2003).

ID	Type	As	V	B	Al	Fe	Mn	Cr	U	Li	Mo	Rb	Sr	Ba	DF
LOD		0.1	0.05	0.5	0.1	0.15	0.05	0.03	0.01	0.01	0.07	0.02	0.02	0.15	
1	RI	3.39	10.1	114	nm	135	2.00	17.4	1.30	2.73	5.27	9.82	185	6.55	10
2	RI	3.36	13.3	11.1	nm	67.0	7.10	1.91	5.40	5.08	8.86	8.53	210	34.8	10
3	RI	bdl	3.31	Bdl	nm	276	146	4.57	0.50	3.73	1.30	5.90	86.2	10.3	10
4	RI	bdl	1.71	5.62	322	308	16.7	1.18	bdl	bdl	0.40	1.21	56.2	10.5	5
5	RI	bdl	0.63	1.04	307	416	9.40	1.18	bdl	0.14	0.35	3.33	37.3	10.1	5
6	RI	bdl	0.29	Bdl	90.0	353	6.70	1.13	bdl	bdl	bdl	2.12	33.1	7.59	5
7	RI	bdl	1.32	2.50	472	398	10.9	1.71	0.10	2.02	0.46	5.03	53.5	6.69	5
8	RI	bdl	0.59	3.86	96.0	76.0	bdl	2.10	0.10	1.78	0.63	7.24	62.7	10.9	5
9	HS	5.63	2.94	906	48.0	137	bdl	22.6	bdl	20.2	87.6	7.62	25.8	bdl	50
10	HS	13.6	14.9	4635	114	356	bdl	51.7	bdl	388	96.4	107	179	18.0	100
11	HS	14.8	16.3	4975	131	320	bdl	47.7	bdl	416	103	115	201	bdl	100
12	HS	12.8	13.8	4356	182	463	6.10	57.3	bdl	365	95.1	101	254	27.8	100
13	HS	5.00	2.50	612	23.0	110	bdl	20.2	bdl	73.0	52.5	14.4	44.2	bdl	50
14	HS	16.3	2.96	762	38.0	186	26.3	24.8	0.90	6.42	314	58.2	124	9.9	50
15	HS	7.96	4.46	930	16.0	114	bdl	25.4	bdl	bdl	304	37.7	54.9	bdl	50
16	HS	2.34	8.38	200	249	180	0.50	3.49	0.60	23.9	16.9	20.6	72.2	6.14	10
17	HS	72.1	2.57	2099	192	376	128	20.3	bdl	427	58.8	53.0	66.3	14.5	50
18	HS	156	4.80	3084	1382	688	207	21.4	bdl	84.1	2.44	264	23.8	4.90	20
19	HS	109	15.9	3391	1157	415	34.0	22.1	bdl	716	12.4	382	32.4	bdl	50
20	HS	52.8	34.8	4250	nm	373	16.0	91.6	bdl	567	70.4	203	445	212	10
21	GWL	195	4.05	2888	nm	506	9.10	Bdl	2.90	91.4	128	68.1	92.5	bdl	50
22	GWL	278	0.89	1253	nm	188	106	3.90	0.50	451	3.50	146	267	195	50
23	LW	7.85	8.10	560	72.0	159	bdl	10.8	1.70	3.53	32.0	5.60	35.7	7.50	20
24	LW	1.35	0.95	107	72.0	34.0	bdl	5.70	0.20	81.1	6.98	30.1	79.3	15.7	10
25	LW	405	89.1	14770	42.0	503	bdl	202	73.5	bdl	6927	974	156	22.1	100
26	LW	23.2	15.8	3861	16.0	332	bdl	67.9	9.20	14.0	425	53.7	57.2	11.3	100
27	LW	21.4	20.6	513	1364	1752	2939	45.4	6.50	72.9	65.0	62.6	1402	162	100
28	LW	0.91	4.61	45.4	184	117	bdl	4.38	0.80	0.22	2.84	3.40	123	21.6	10
29	WL	30.1	87.1	302	nm	240	2.60	bdl	5.70	26.4	5.76	13.4	115	bdl	10

30	WL	8.96	147	286	nm	483	4.40	13.9	2.50	15.47	6.94	10.0	67.4	bdl	10
31	WL	1.29	7.39	14.4	nm	2.00	0.80	bdl	0.20	17.2	3.31	8.76	25.7	bdl	10
32	WL	1.96	0.71	20.4	nm	bdl	210	bdl	0.40	8.49	2.00	2.77	219	51.4	10
33	WL	50.9	36.1	332	nm	bdl	2.50	bdl	6.40	41.8	11.1	16.9	121	bdl	10
34	WL	6.23	3.51	23.3	nm	9.00	5.20	bdl	12.5	58.7	2.76	17.3	273	bdl	10
35	WL	61.4	148	423	nm	bdl	bdl	bdl	49.9	49.1	61.6	26.9	149	4.72	20
36	WL	1.27	1.34	Bdl	nm	219	268	3.71	bdl	13.4	3.85	7.21	53.6	6.13	10
37	WL	157	40.7	5408	nm	104	3.30	104	43.9	0.56	446	73.8	33.2	51.4	20
38	WL	81.0	91.1	20.9	nm	12.0	2.10	4.26	41.7	67.0	96.2	7.95	37.8	bdl	10
39	WL	bdl	2.64	10.6	77.0	72.0	5.60	3.04	0.40	20.0	6.72	11.3	49.3	1.91	10
40	WL	1.00	3.12	9.44	89.0	105	2.30	3.24	0.90	21.5	3.49	8.02	14.4	5.50	10
41	WL	1.24	3.62	6.05	19.0	17.0	25.6	1.36	0.40	9.06	1.80	9.28	4.63	bdl	5
42	WL	1.23	1.07	7.12	6.00	13.0	0.25	1.56	0.20	13.4	2.55	0.84	45.8	1.91	5
43	WL	1.00	8.78	5.00	76.0	76.0	0.50	3.89	0.20	5.94	2.43	2.00	37.6	3.97	10
44	WL	bdl	Bdl	29.4	5.00	30.0	26.0	2.06	0.70	27.5	1.97	2.24	20.0	bdl	20
45	WL	1.77	1.22	55.2	186	99.0	162	3.94	bdl	16.4	12.9	5.29	82.5	13.5	10
46	WL	9.83	52.5	664	Bdl	145	51.6	20.4	8.80	55.7	51.0	11.6	122	12.7	50
47	WL	21.5	37.7	492	382	372	bdl	24.6	21.2	58.3	47.1	4.80	57.3	bdl	50
48	WL	23.8	5.59	1707	6.00	45.0	bdl	17.1	8.30	bdl	105	13.0	14.2	2.62	10
49	WL	bdl	1.03	26.7	127	61.0	1.40	6.24	0.90	14.9	1.01	1.23	188	3.01	10
50	WL	26.3	38.5	359	273	232	8.70	9.89	11.2	32.4	5.53	8.69	101	9.85	20
51	WL	2.48	2.00	57.9	214	115	0.50	4.35	1.50	33.6	5.10	9.91	64.2	14.1	10
52	CS	0.83	2.38	42.2	3339	2023	12.8	4.06	0.90	5.57	0.53	9.71	35.8	2.35	5
53	CS	1.18	12.4	14.3	189	93.0	bdl	4.13	0.80	6.91	4.38	5.11	63.1	2.89	10

ID	**Type**	**Be**	**Co**	**Ni**	**Zn**	**Cu**	**Ga**	**Ag**	**Cd**	**Sb**	**Te**	**Tl**	**Pb**	**Bi**	**DF**
LOD		0.04	0.2	0.1	0.25	0.1	0.02	0.03	0.04	0.02	0.06	0.01	0.01	0.03	
1	RI	bdl	0.18	0.99	bdl	bdl	0.29	bdl	bdl	0.94	bdl	0.33	bdl	bdl	10
2	RI	bdl	0.39	9.36	bdl	1.14	1.93	bdl	bdl	bdl	bdl	bdl	bdl	bdl	10
3	RI	bdl	0.26	3.39	7.87	bdl	0.52	bdl	bdl	bdl	bdl	bdl	0.44	bdl	10
4	RI	bdl	0.08	bdl	bdl	bdl	0.32	bdl	bdl	1.24	bdl	0.06	bdl	bdl	5
5	RI	bdl	bdl	bdl	bdl	bdl	0.30	bdl	bdl	1.1	bdl	bdl	bdl	bdl	5
6	RI	bdl	bdl	bdl	bdl	bdl	0.14	bdl	bdl	bdl	bdl	bdl	bdl	bdl	5
7	RI	bdl	bdl	bdl	bdl	bdl	0.26	bdl	bdl	0.78	bdl	bdl	bdl	bdl	5
8	RI	bdl	bdl	bdl	8.25	bdl	0.26	bdl	bdl	0.1	bdl	bdl	bdl	bdl	5
9	HS	bdl	bdl	bdl	bdl	bdl	bdl	bdl	bdl	bdl	bdl	bdl	bdl	bdl	50
10	HS	9.92	bdl	bdl	bdl	bdl	bdl	bdl	bdl	bdl	bdl	bdl	bdl	bdl	100
11	HS	14.7	bdl	bdl	bdl	bdl	bdl	bdl	bdl	bdl	bdl	bdl	bdl	bdl	100
12	HS	7.75	bdl	bdl	bdl	bdl	bdl	bdl	bdl	bdl	bdl	bdl	bdl	bdl	100
13	HS	bdl	bdl	bdl	bdl	bdl	bdl	bdl	bdl	bdl	bdl	bdl	bdl	bdl	50
14	HS	bdl	bdl	bdl	bdl	bdl	bdl	bdl	bdl	bdl	bdl	bdl	bdl	bdl	50
15	HS	bdl	bdl	bdl	bdl	bdl	bdl	bdl	bdl	bdl	bdl	bdl	bdl	bdl	50
16	HS	0.54	bdl	bdl	19.3	bdl	bdl	bdl	bdl	bdl	bdl	bdl	4.79	bdl	10
17	HS	2	bdl	bdl	bdl	bdl	bdl	bdl	bdl	bdl	bdl	bdl	bdl	bdl	50
18	HS	8.26	bdl	bdl	bdl	bdl	1.51	bdl	bdl	0.29	bdl	0.77	bdl	bdl	20
19	HS	9.89	bdl	bdl	bdl	bdl	3.58	bdl	bdl	6.31	bdl	bdl	bdl	bdl	50
20	HS	2.38	1.33	3.77	49.4	10.1	6.28	0.35	5	22.6	3.43	3.46	35	bdl	10

21	GWL	bdl	bdl	0.97	54.1	5.87	bdl	bdl	bdl	1.35	bdl	bdl	71.7	0.54	50
22	GWL	bdl	0.12	3.64	6.26	bdl	11.5	bdl	bdl	5.09	bdl	bdl	0.94	bdl	50
23	LW	bdl	bdl	bdl	bdl	bdl	bdl	bdl	bdl	bdl	bdl	0.05	bdl	bdl	20
24	LW	bdl	bdl	bdl	84.1	bdl	0.22	bdl	bdl	bdl	bdl	bdl	2.12	bdl	10
25	LW	bdl	bdl	bdl	bdl	bdl	bdl	bdl	9.67	bdl	bdl	bdl	bdl	bdl	100
26	LW	bdl	bdl	bdl	bdl	bdl	bdl	bdl	bdl	bdl	bdl	bdl	bdl	bdl	100
27	LW	bdl	bdl	bdl	1901	bdl	bdl	bdl	bdl	bdl	bdl	bdl	39.4	bdl	100
28	LW	0.000	0.000	bdl	20.3	bdl	0.31	bdl	bdl	bdl	bdl	bdl	3.19	bdl	10
29	WL	bdl	0.030	bdl	160	bdl	bdl	bdl	bdl	0.33	bdl	0.2	bdl	bdl	10
30	WL	bdl	bdl	0.79	102	21.5	bdl	bdl	bdl	0.2	bdl	0.22	1.47	bdl	10
31	WL	bdl	bdl	2.32	398	bdl	bdl	bdl	bdl	bdl	bdl	bdl	9.26	bdl	10
32	WL	bdl	0.194	1.69	211	bdl	2.83	bdl	bdl	bdl	bdl	bdl	bdl	bdl	10
33	WL	bdl	bdl	bdl	10.8	bdl	bdl	bdl	bdl	0.61	bdl	bdl	bdl	bdl	10
34	WL	bdl	bdl	0.73	63.6	3.20	bdl	bdl	bdl	bdl	bdl	bdl	bdl	bdl	10
35	WL	bdl	bdl	bdl	20.9	5.79	bdl	bdl	bdl	bdl	bdl	bdl	bdl	bdl	20
36	WL	bdl	0.350	3.7	832	3.89	0.2	bdl	bdl	bdl	bdl	0.03	17.7	bdl	10
37	WL	bdl	bdl	bdl	5.14	bdl	2.3	bdl	0.79	bdl	1.89	bdl	10.2	bdl	20
38	WL	bdl	bdl	bdl	8.8	bdl	bdl	bdl	bdl	0.62	bdl	bdl	0.84	bdl	10
39	WL	bdl	bdl	bdl	16.1	bdl	bdl	bdl	bdl	bdl	bdl	bdl	0.31	bdl	10
40	WL	bdl	bdl	bdl	230	bdl	bdl	bdl	bdl	bdl	bdl	bdl	3.06	bdl	10
41	WL	bdl	bdl	bdl	870	bdl	bdl	bdl	bdl	bdl	bdl	bdl	0.98	bdl	5
42	WL	bdl	bdl	bdl	104	bdl	bdl	bdl	bdl	bdl	bdl	bdl	bdl	bdl	5
43	WL	bdl	bdl	bdl	12.5	bdl	bdl	bdl	bdl	bdl	bdl	bdl	2.80	bdl	10
44	WL	0.036	bdl	bdl	bdl	bdl	bdl	bdl	bdl	bdl	bdl	bdl	bdl	bdl	20
45	WL	bdl	bdl	bdl	91.6	1.49	0.09	bdl	bdl	bdl	bdl	bdl	6.98	bdl	10
46	WL	bdl	bdl	bdl	bdl	bdl	bdl	bdl	bdl	bdl	bdl	bdl	bdl	bdl	50
47	WL	bdl	bdl	bdl	bdl	bdl	bdl	bdl	bdl	bdl	bdl	bdl	bdl	bdl	50
48	WL	bdl	bdl	bdl	bdl	bdl	bdl	bdl	bdl	bdl	bdl	bdl	bdl	bdl	10
49	WL	bdl	bdl	bdl	78.8	bdl	bdl	bdl	bdl	bdl	bdl	bdl	1.93	bdl	10
50	WL	bdl	bdl	bdl	77.5	bdl	bdl	bdl	bdl	bdl	bdl	bdl	5.89	bdl	20
51	WL	bdl	bdl	bdl	37	bdl	0.07	bdl	bdl	bdl	bdl	bdl	3.01	bdl	10
52	CS	0.878	0.074	1.17	1.76	bdl	1.08	0.11	bdl	1.43	bdl	0.10	0.22	bdl	5
53	CS	0.013	0.000	bdl	38.4	bdl	bdl	bdl	bdl	bdl	bdl	bdl	6.17	bdl	10

Table 5.1: Trace elements hydrochemical composition (in µg/L) of MER waters from rivers, hot springs, geothermal wells, groundwater wells, cold springs, and lakes in Ziway-Shala basin. WL= Groundwater wells, HS=Hot springs, CS=Cold springs GWL= Geothermal wells, LW= Lakes, RI= Rivers, nm= not measured, LOD= Limit of Detection in diluited samples, DF= Dilution Factor applied in each samples, bdl = below detection limit. The geographic coordinate from major elements (Table 4.1) is applicable for the trace elements as well.

This comparison between the international quality standards, and the major ions and trace elements of different MER water groups (groundwater wells, geothermal wells, hot springs, lakes, and rivers) show that major ions (F^-, Na^+, Cl^-, SO_4^{2-} and NO_3^-) and trace elements such as As, B, Mo, U, Fe, Al, Cr and

Mn often exceed the tolerance limit of drinking water fixed by the authorities (**Table 5.2**). Other trace elements such as Co, Bi, Tl, Te, Ag, Cd, Ni, Cu, Ga, Sb, Be, Zn and Pb were undetected or measured in extremely low concentrations and are not expected to cause harm to the local people.

Drinking water quality standards, in ppm	**F**	**As**	**Fe**	**Al**	**B**	**Mo**	**Cr**	**Mn**	**U**	**Na^+**	**Cl^-**	**SO_4^{2-}**	**NO_3^-**
WHO guidelines, 2006	**1.5**	**0.01**	NG	**0.2**	**0.5**	**0.07**	**0.05**	0.4	**0.015**	NG	NM	NG	50
EU directives, 1998	**1.5**	**0.01**	**0.2**	**0.2**	1	NM	**0.05**	**0.05**	NM	**200**	**250**	**250**	50
USEPA, 2003	4	**0.01**	0.3	0.05-0.2	NM	NM	0.10	**0.05**	NM	**200**	**250**	**250**	**10**
% exceeding the minimum standard within each water groups													
Out of 23 **WL**	87	35	38	27	13	13	0	9	17	39	4	9	13
Out of 14 **HS** (plus 2 **GWL**)	100	70	57	27	93	50	21	14	0	86	75	17	17
Out of 6 **LW**	100	17	50	20	67	33	33	17	17	67	50	33	0
Out of 8 **RI**	38	0	63	60	0	0	0	13	0	0	0	0	25

Table 5.2: International water quality standards of drinking water, and percentage of MER water samples exceeding the minimum threshold defined by the authorities. Note: WL= Groundwater wells, HS=Thermal springs, GWL= Geothermal wells, LW= Lakes, RI= Rivers NG (no guidelines), NM (not mentioned), Bold font: (the minimum standard considered).

As showed in **Table 5.2**, the fluoride anomaly consists of high level in all water groups including even 38% of the rivers, and is often coupled with an arsenic anomaly.

Al, Mn, Fe, Cl^- and SO_4^{2-}, although not considered as poisoning components, may cause water to become undrinkable due to odour, metallic taste and dark colour, and are regulated by secondary (non-enforceable) guidelines (USEPA, 2003). In this light, MER Rivers often contain high level of Fe, Al, F and Mn that do not meet these drinking water quality standards. High level of Al in drinking waters has reported linked to Alzheimer's disease (Martyn et al., 1989). V also appears in considerable amount in the waters though their drinking water limits has not been determined in any of the authorities although it can induce genotoxicity and irritation of the respiratory tract (Costigan et al., 2001).

Therefore, these new analyses demonstrate that the problem of F^- in the MER waters is potentially coupled with high content of other toxic elements (e.g.: As, B, Mo, V, U, Al, Cr, Fe, Mn), and as far as we know the possible health impact related to the latter elements is not studied and understood yet. Concentrations are generally higher in thermal waters. Unfortunately, the limited availability of drinking water in the rift forces the people to consume any existing water resources including cooling of hot springs (local people, personal communication)

The average concentration of fluoride is 0.8mg/L in rivers, 32 mg/L in thermal springs, 27 mg/L in deep (>2 kms) geothermal wells, 6 mg/L in groundwater wells, and 121 mg/L in lakes. Some 38% of rivers, 87 % of the groundwater wells and 100 % of lakes, thermal and geothermal waters have fluoride values beyond the safe drinking water limit (WHO, 2006).

The result showed that among trace elements, arsenic represent another geochemical anomaly, as the natural Na-HCO_3 type of waters in MER often show high concentrations of this element. The average concentration of arsenic is 0.9µg/L in rivers, 39µg/L in thermal springs, 236µg/L in deep geothermal wells, 21.4µg/L in groundwater wells and 77µg/L in lakes, with maximum values of 3µg/L, 156µg/L, 278µg/L, 157µg/L and 405 µg/L respectively. It has to be noted that 35 % of the MER groundwater wells (the main source of potable water) contain more than the safe limit 10 µg/L (WHO, 2006).

In chapter 4, the F^- geochemistry is discussed in detail and F^- correlations with pH, Na^+, HCO_3^- and Ca^{2+} in all water types of MER is displayed in (chapter 4; **Figure 4.5**).

Here F^- and As relationship with some major and trace elements were investigated in the groundwater wells. F^- in MER groundwater wells positively correlated with Na^+ (R^2 =0.7), HCO_3^- (R^2=0.5), TDS (R^2=0.64) and EC (R^2=0.73) and similarly arsenic shows a positive correlation with Na^+ (R^2=0.63), HCO_3^- (R^2=0.7), TDS (R^2=0.6) and EC (R^2=0.67) (**Figure 5.1**). Arsenic also correlates with some trace elements such as Mo (R^2=0.79), V (R^2=0.68), and U (R^2=0.70), whereas no correlation with Fe and Mn (**Figure 5.2**) were observed. F^- and As distribution map is showed on **Figure 5.3 and 5.4** respectively. The lack of positive correlation between As and Fe, supports the theory that As origin is likely to be unrelated to sulphide minerals but is principally linked to volcanic glass.

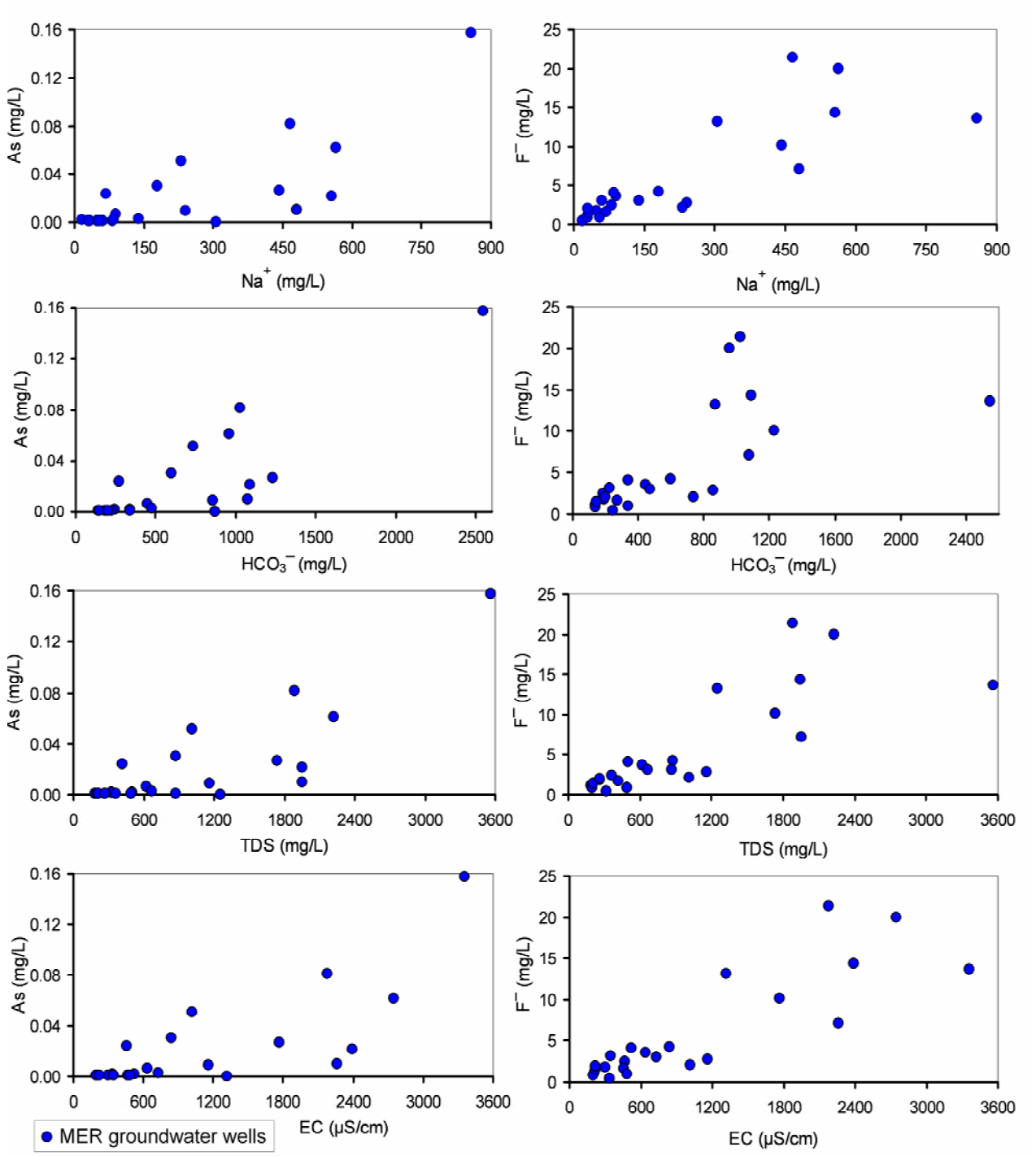

Figure 5.1: As and F^- relationships with Na^+, HCO_3^-, TDS and EC in the MER groundwater wells.

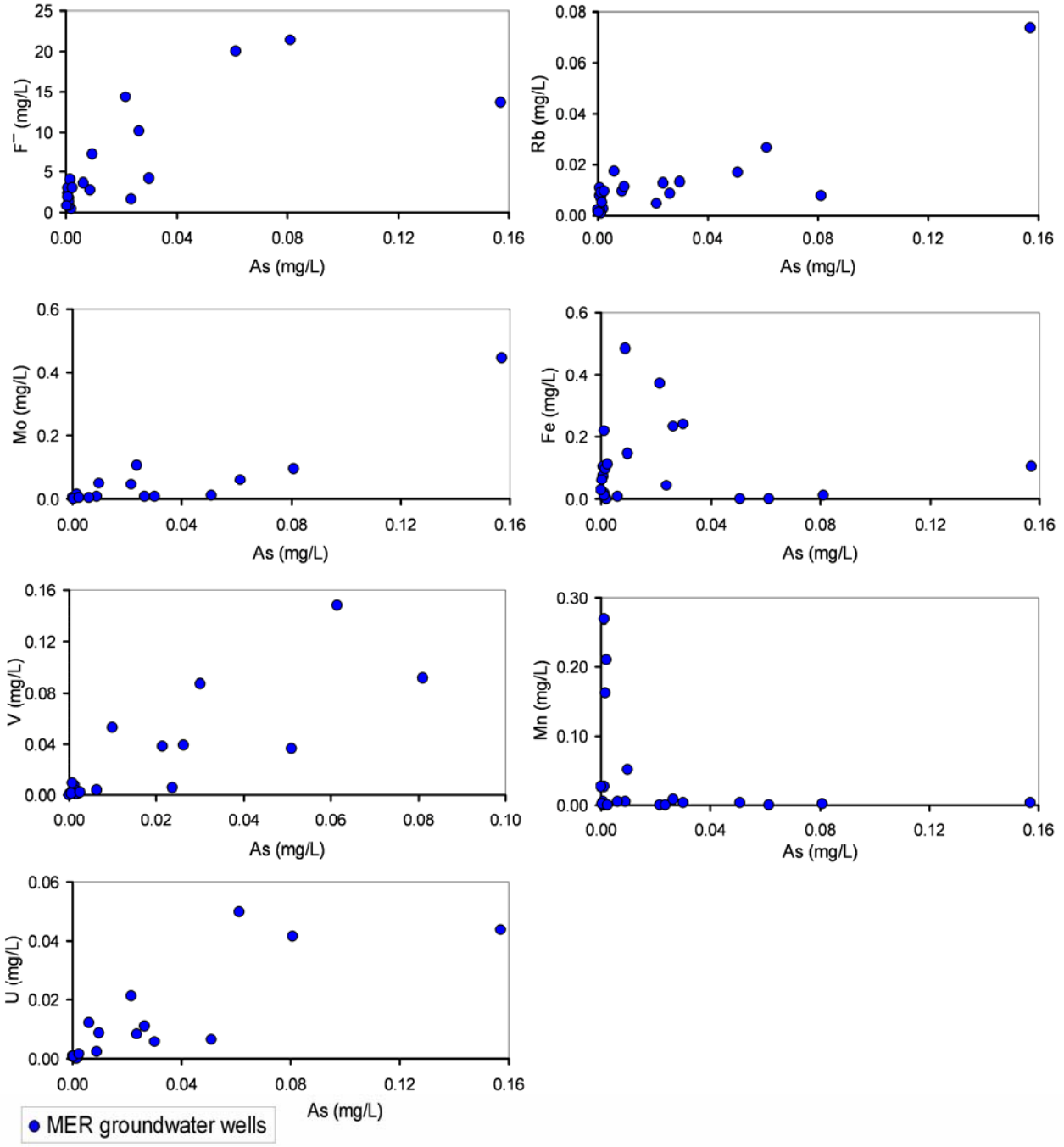

Figure 5.2: Arsenic relationships with F^-, Mo, V, U, Rb, Fe and Mn in the MER groundwater wells.

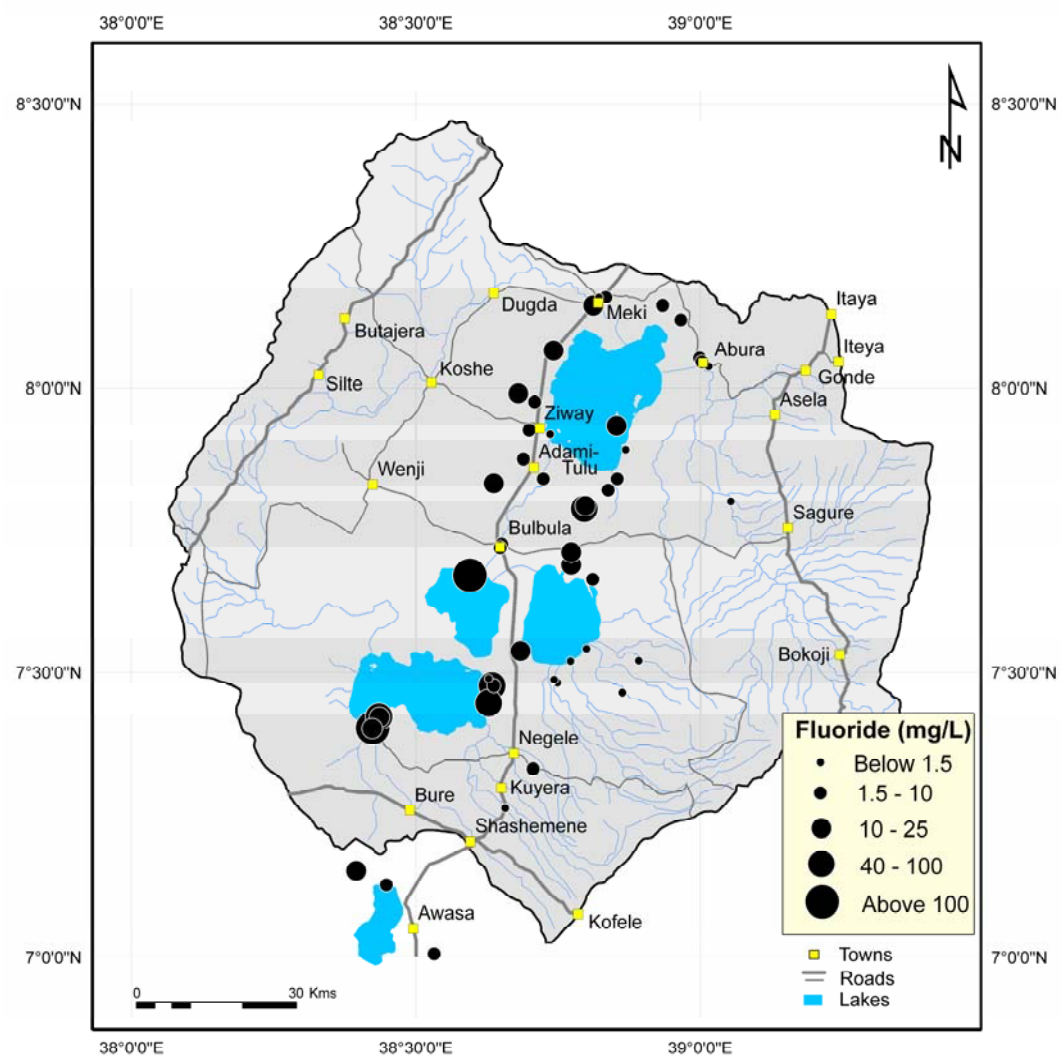

Figure 5.3: Map of F^- distribution in the MER natural waters.

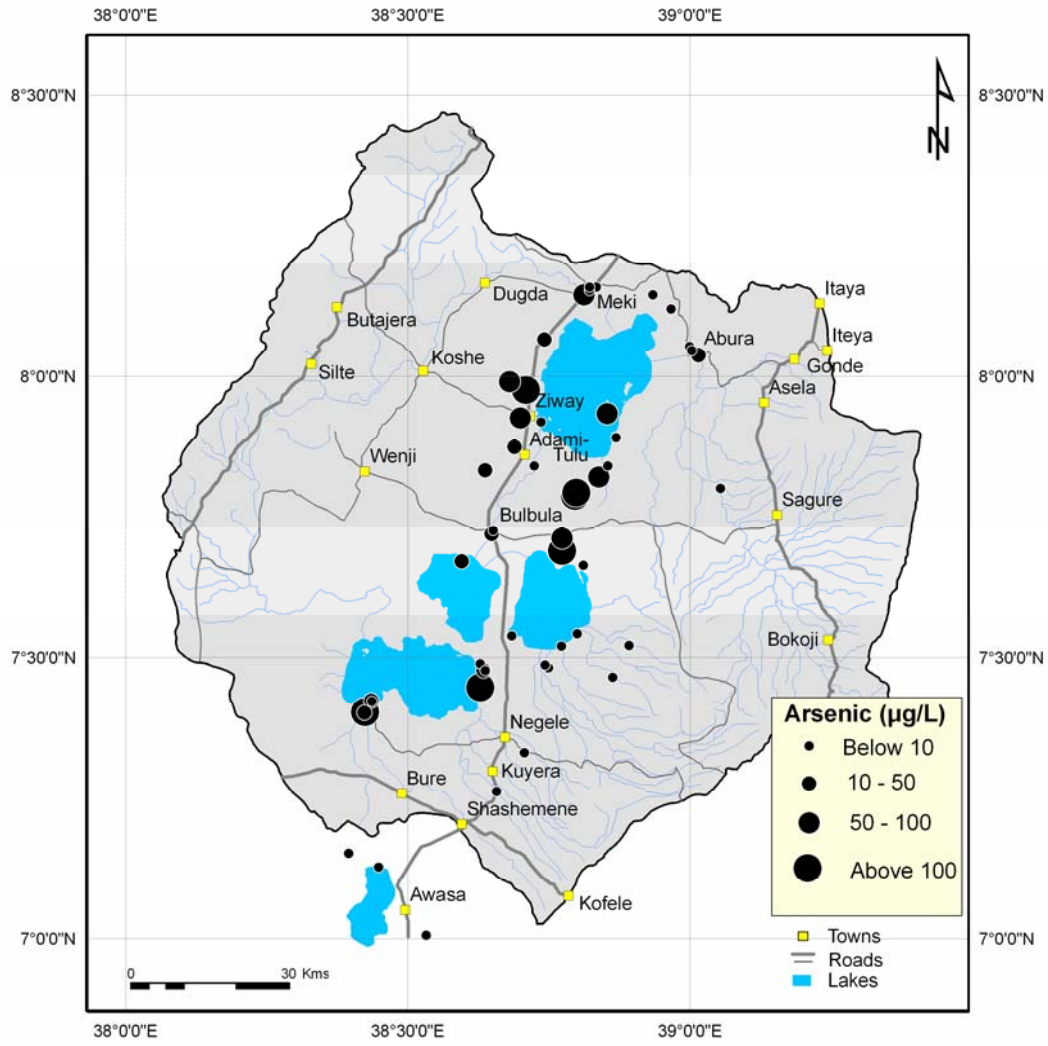

Figure 5.4: Map of As distribution in the MER natural waters.

Higher level of F^-, As, but also Li, B and Mo concentration were mainly observed in thermal springs. This doesn't necessarily imply the involvement of juvenile fluids, and is possibly related to higher reactivity of hot waters in contact with the aquifer solid matrixes.

The chemistry of the lake water appears even more complicated than the other water types due to high evaporation processes, which ultimately lead to very extreme concentrations of F^- and As on highly alkaline Lakes of Chitu, Abijata and Shala.

5.2. Trace (and major) elements composition in the experimental leachates

Laboratory leaching test experiments for major ion were discussed in chapter 4 in order to particlarly investigate the sources of the fluoride. Here the discussion will give emphasis on trace elements (e.g. As) geochemistry on the same representative lithotype leachates and the geochemistry of As is discussed with F^-.

These experiments simulate the potential extractability (leachability) of water soluble components during water-rock/sediment interaction processes. From this point of view, the approach is more appropriate than the direct bulk-analysis of rock and sediments, as the leachates composition give a more realistic idea on the chemical budget that can be extracted by the aquifer matrixes during water-rock interaction, i.e. the bioavailable fraction.

Coherently, the risk of water contamination is related to such mobile fractions rather than the total rock/sediment concentration (Adriano, 1980). Trace elements analysis result of the leachates is displayed on (**Table 5.3**).

The comparison with the tolerance limits indicated by international guidelines has been extended to the experimental leachates, showing that the concentration of elements potentially affecting human health such as F, As, Fe, Al, Mo, and U are often beyond the admissible limits (**Table 5.4 and Figure 5.5**). See also for Li, Sr and V in **Figure 5.6.** The concentration of major and trace elements in the rock and sediment leachates and the water quality guidelines are displayed on **Appendix 5.1 and 5.2**.

	Rhyolites					Fluvio-volcano lacustrine sediments					
In µg/L	**TW9**	**TW11**	**TW29**	**TW30**	**TW31**	**TW14**	**TW15**	**TW22**	**TW34**	**TW39**	**TW43**
Li	22.4	2.93	27.6	1.76	5.11	9.41	23.6	165	12.5	1.24	15.1
B	24.8	13.6	bdl	bdl	bdl	15.1	427	220	17.7	bdl	5.75
Al	68.3	bdl	192	78.1	1862	bdl	2.15	8.42	bdl	323	257
V	6.50	2.12	15.6	17.2	8.21	29.7	26.5	254	5.58	9.74	15.5
Cr	2.60	3.14	3.42	2.61	3.06	4.67	7.29	6.95	3.22	1.91	4.09
Mn	6.62	bdl	8.33	3.33	190	bdl	bdl	0.11	bdl	5.51	38.9
Fe	73.3	bdl	378	108	5223	bdl	bdl	bdl	1.98	624	1154
Co	0.59	0.57	0.20	0.39	0.15	0.35	0.45	1.52	1.53	0.07	0.17
Ni	2.64	2.28	1.68	1.57	1.96	1.72	2.49	5.57	2.61	1.31	2.37
Cu	1.58	1.56	1.51	0.29	1.12	0.83	2.10	4.79	1.52	0.45	1.49
Zn	3.37	13.6	11.9	12.9	41.1	16.9	8.77	10.5	35.5	6.78	34.8
Ga	4.08	0.01	0.31	0.11	2.65	0.05	0.05	0.02	0.10	0.37	1.14

As	2.21	1.72	2.70	0.25	4.91	11.8	17.4	220	1.23	1.96	6.62
Rb	1.66	13.8	9.55	4.12	5.64	2.58	15.3	21.8	5.03	6.83	10.2
Sr	bdl	252	4.10	4.61	5.43	62.3	107	65.5	58.4	1.92	15.3
Mo	9.61	16.3	8.59	10.4	4.44	7.86	11.3	181	6.09	5.34	2.52
Sb	0.19	0.01	0.13	bdl	0.16	0.10	0.82	5.03	4.62	0.1	0.44
Pb	0.14	0.13	0.17	0.05	3.42	0.18	0.35	0.04	bdl	0.43	0.57
U	0.95	0.24	0.05	bdl	0.36	0.75	5.04	63.6	0.05	0.17	0.83
Be	bdl	bdl	bdl	bdl	bdl	bdl	bdl	bdl	bdl	bdl	bdl
Bi	bdl	bdl	bdl	bdl	bdl	bdl	bdl	bdl	bdl	bdl	bdl
Te	bdl	0.13	bdl	bdl	0.19	bdl	bdl	bdl	bdl	bdl	0.07
Ba	bdl	97.1	bdl	bdl	bdl	bdl	bdl	bdl	bdl	bdl	bdl
Hg	bdl	bdl	bdl	bdl	bdl	bdl	bdl	bdl	bdl	bdl	bdl
Tl	0.49	0.20	bdl	bdl	bdl	0.02	0.05	bdl	bdl	bdl	bdl
Ag	bdl	bdl	bdl	bdl	0.03	bdl	bdl	bdl	bdl	bdl	bdl
Cd	bdl	0.17	0.13	0.06	3.25	0.02	bdl	bdl	0.05	0.25	0.49

Table 5.3: Concentrations of trace elements in the leachates

Elements	Drinking water quality standards (in µg/L)	Number of samples beyond standard, out of 6 sediment leachates	Number of samples beyond standard, out of 5 rock leachates
Fluorine (F)	1500	6	4
Arsenic (As)	10	3	0
Aluminium (Al)	200	2	2
Iron (Fe)	200	2	2
Uranium (U)	15	1	0
Molybdenum (Mo)	70	1	0
Manganese (Mn)	50	0	1

Table 5.4: Elements found in the leachates exceeding the concentration limit set by (WHO, 2006) applied for F^-, As, Al, U and Mo, and (EU directives, 1998) for Fe and Mn.

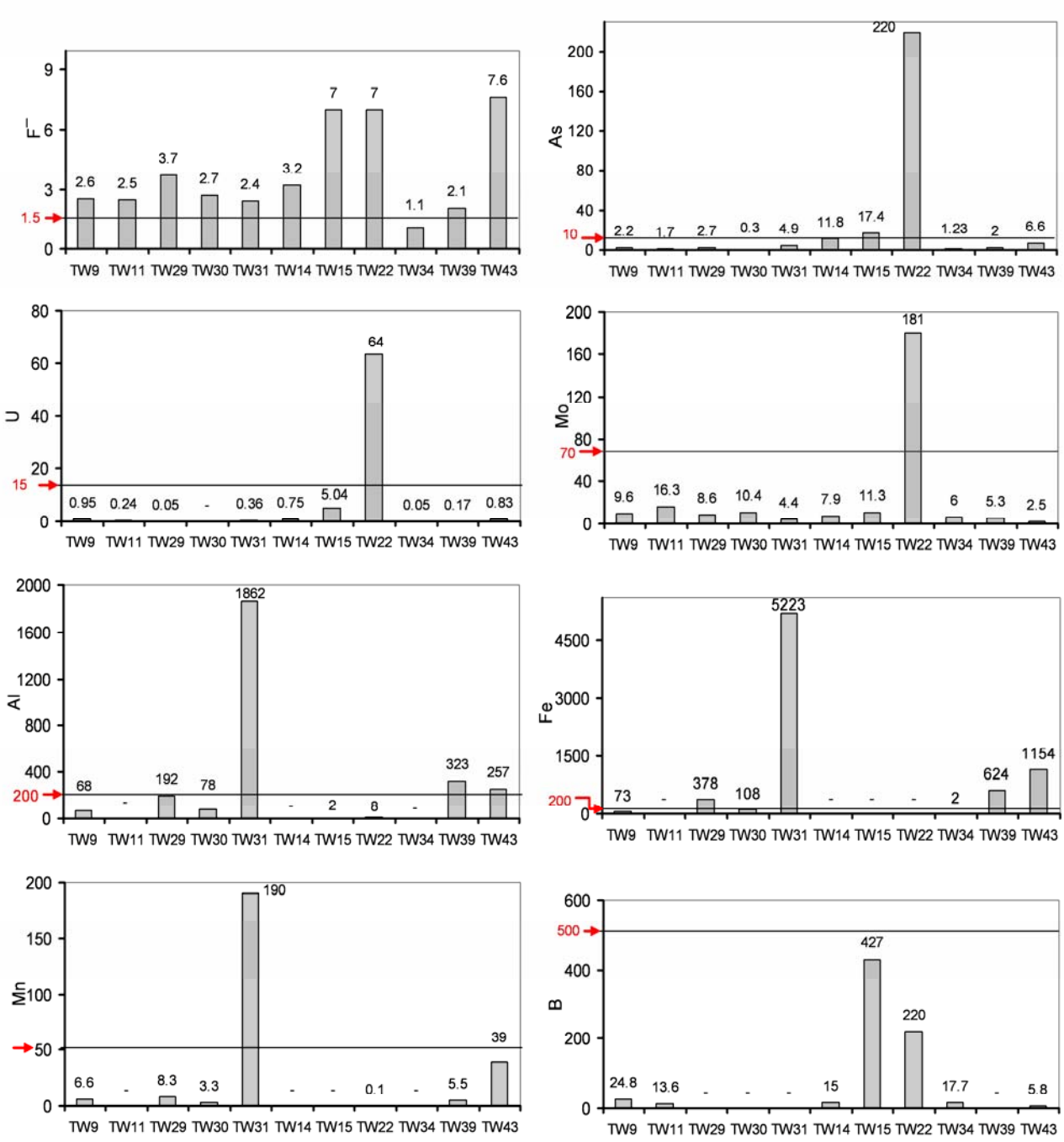

Figure 5.5: Concentrations of F^-, As, Fe, Al, Mn, Mo and U in leachates compared with WHO (EU directives, 1998 for Fe and Mn) guideline values (dotted lines). Note that all concentrations are expressed in µg/L except for F^- (in mg/L). TW9, TW11, TW29, TW30 and TW31 are rocks and TW14, TW15, TW22, TW34, TW39 and TW43 are sediments. -: below detection limit.

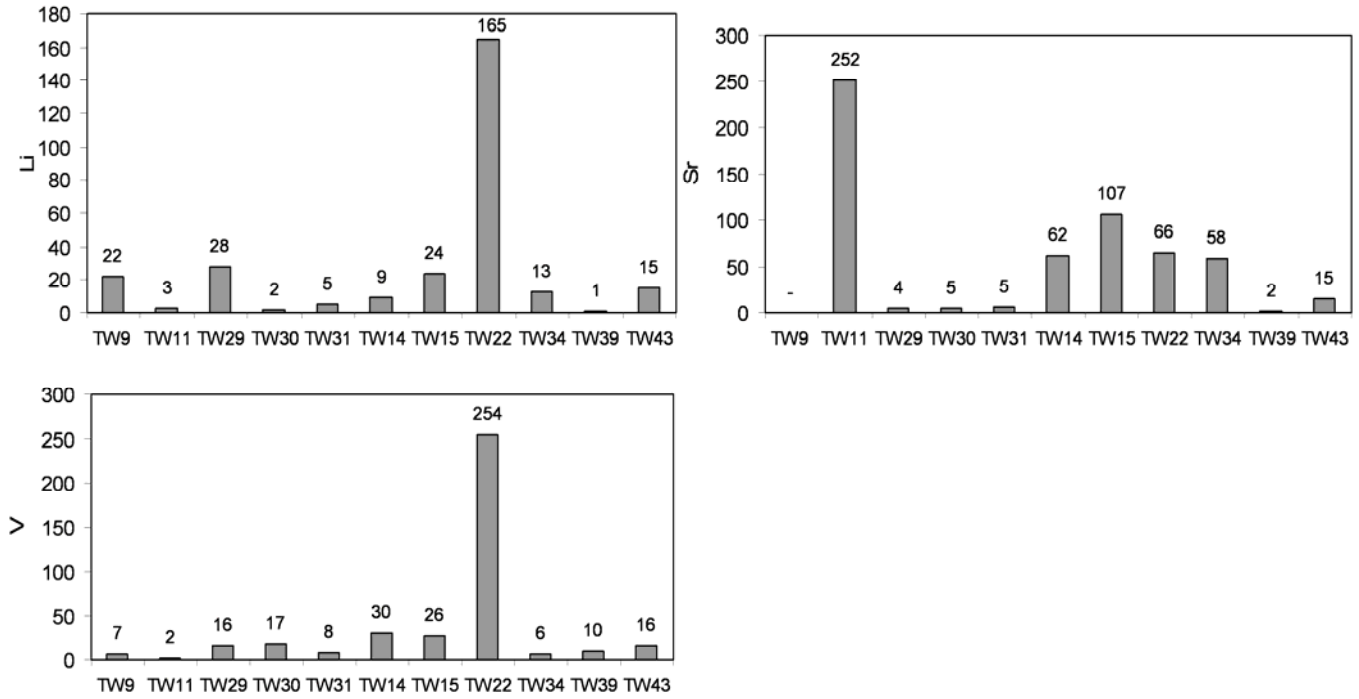

Figure 5.6: Concentrations of Li, Sr and V in leachates. Note that all concentrations are expressed in µg/L TW9, TW11, TW29, TW30 and TW31 are rocks and TW14, TW15, TW22, TW34, TW39 and TW43 are sediments.

For instance, fluoride concentrations exceeded the drinking water standard of 1.5 mg/L in 10 out of 11 leachates, arsenic concentrations exceeded the standard of 10 µg/L in 3 out of 11 leachates, iron concentrations exceeded the standard of 200 µg/L in 4 out of 11 leachates and aluminium concentrations exceeded the standard of 200 µg/L in 3 out of 11 leachates (**Table 5.4**). It is also very interesting to note that leachates from sediments display higher concentration of toxic elements with respect to those obtained from volcanic rocks. This indicates that the sediments are the major reservoir and source of toxic elements. Relatively higher level of Sr, Rb, Li and V were also measured on leachates and on some MER natural waters

The percentage proportion of trace elements extracted in all leachates (rocks and sediments) is showed on **Figure 5.7**.

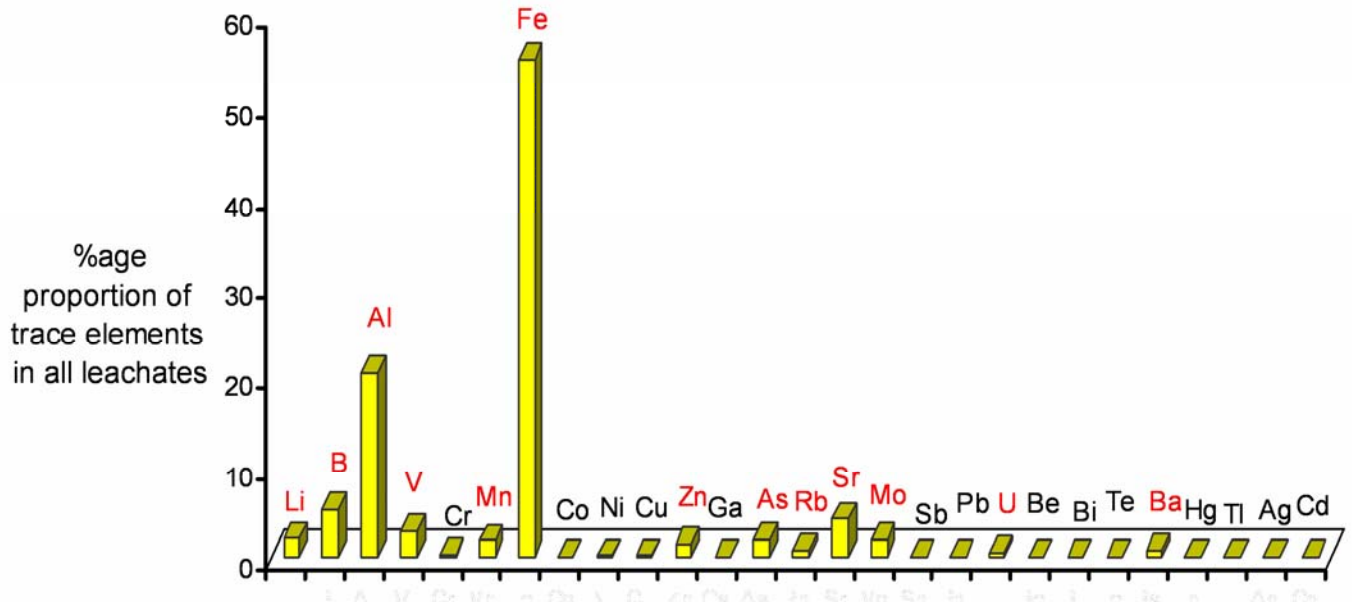

Figure 5.7: Percentage proportion of trace elements extracted in leachates (average of all the available rocks and sediments leachates).

F^- and As concentrations in natural water can be higher than those recorded in experimental leachates, as the resulting F and As concentrations in experimental leachates are expected to increase with time. Higher temperature and the introduction of CO_2 have also to be considered as additional factors favouring high fluoride and arsenic concentrations in the natural waters of the rift. These tests, that simulate water-rock/sediment interaction processes, simply highlight the potential contribution (i.e. the leachability) of each investigated lithotype to the release of fluorine and arsenic in the water system.

The results highlight a clear relationship between high pH and high arsenic and fluoride concentration. The highest As (220µg/L) and F^- (7.6 mg/L) were recorded at pH of 8 and 8.7 respectively from fluvio/volcano-lacustrine sediment leachates. The highest measured As was found associated with the sediment sample TW22, which contains high level of sulphur (145 ppm; Table 4) suggesting the local presence of most likely coprecipitated sulphides (e.g. arsenopyrite; Edenborn et al., 1986; Rittle et al., 1995 and Morse and Luther, 1999)

Therefore, these data confirm that the fluvio-volcano lacustrine sediments are the main reservoir of As and F^- in the area and that they can release it into the water system. Accordingly, high arsenic and fluoride concentration is found in leachates characterized by high pH, Na^+, and HCO_3^- (**Figure 5.8**).

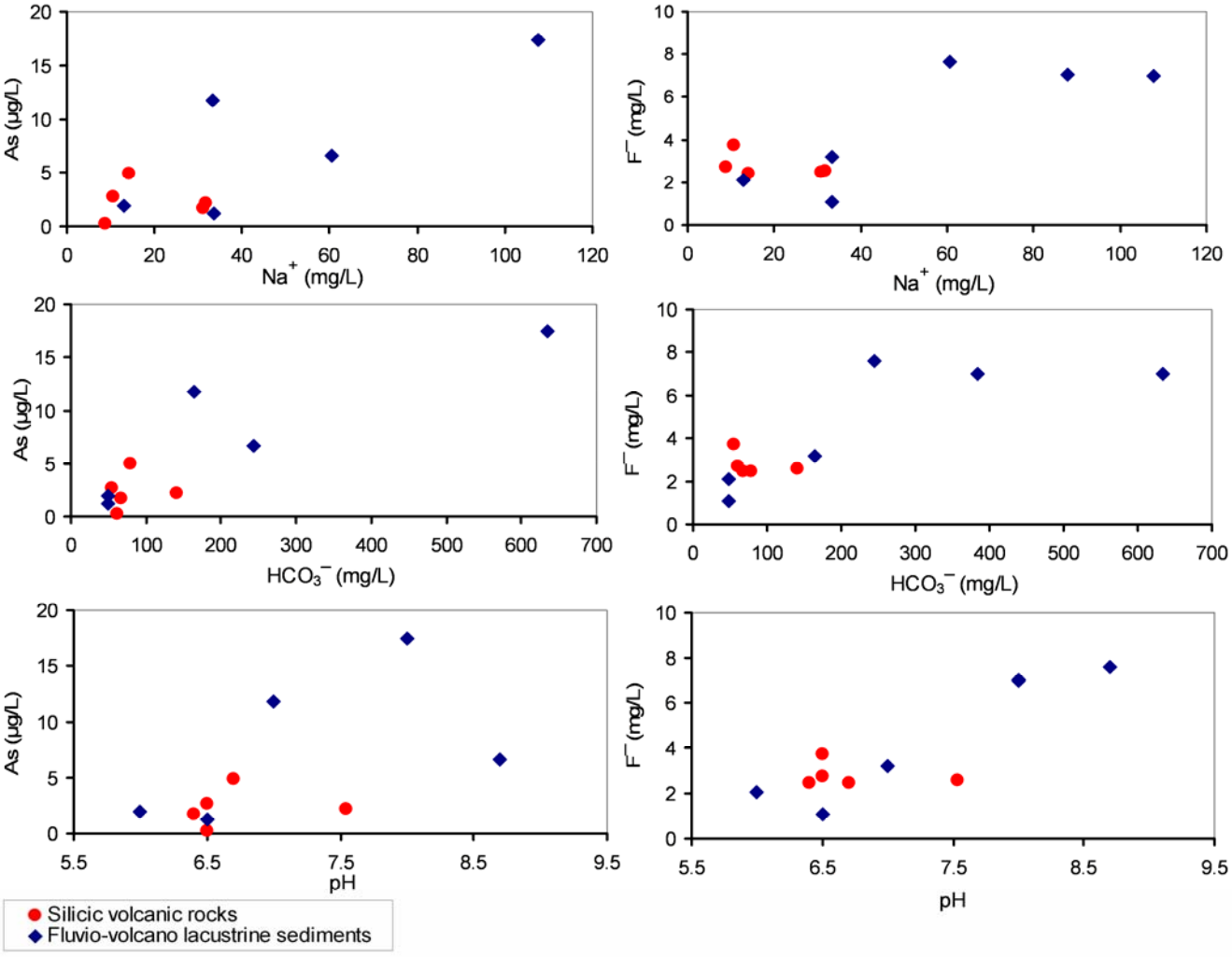

Figure 5.8: Leaching test results: Relationship between of As and F with pH, Na, and HCO_3. Note that the extreme As value (220µg/L) from the TW22 sediment leachate is excluded.

Leaching tests using a $NaHCO_3$ solution under alkaline conditions were found to be even more effective in extracting arsenic from sediments (Anawar et al., 2003; 2004; Bhattacharya, 2006). Appelo et al., 2002; Kim et al., 2000; 2003, studied the displacing (competing) effect of HCO_3^- which induces higher

mobility of As. This geochemical condition is mirrored by the positive correlation between As and HCO_3^- in the groundwater wells of the MER (**Figure 5.1**).

6. Origin and genesis of the geochemical anomalies observed in the MER waters

6.1. Origin of fluoride and arsenic

The process that accounts for the genesis of the MER felsic rocks is fractional crystallization of basalts with a minor interaction with crustal lithologies (Peccerillo et al., 2007). This magma evolution ultimately led to a progressive concentration of the incompatible elements (halogens and arsenic included) in the residual melt fractions, and thus elements such as F, Cl and As, already present in the primitive MER basalts, were subsequently enriched in the more differentiated volcanic products, i.e. the MER rhyolites.

During explosive volcanic eruptions, gases such as HCl(Cl), HF(F), and other elements showing affinity for the volatile phases (i.e. As) may probably have been released and trapped within the tephra (Taylor and Stoiber, 1973; Thomas et al., 1982; Varekamp et al., 1984; Giggenback, 1996; Allard et al., 2000; Armienti et al., 1998, 2002). This process is effective especially on the smaller particles having large surface area (Oskarsson, 1980) such as ash particles (<2 mm).

Therefore, the pristine source of fluorine and arsenic is plausibly linked to the nature of the MER magmas and their mode of emplacement.

As concerns arsenic, considering that in the MER region there are no sulphide deposits, its presence in the local water possibly implies that the described volcanic products and their re-worked products (i.e. the fluvio-volcano lacustrine sediments) can release appreciable amounts of As.

This is supported by literature studies on felsic volcanic rocks highlighting significant content of arsenic; examples are provided by pyroclastic rocks, containing over 90% of rhyolitic glass, that have As concentrations in the range 6−10 mg/kg (Nicolli et al., 1989; Castro et al., 1998; Smedley et al., 1998; 2002; Bundschuh et al., 2004).

These felsic volcanics under oxidizing and high pH conditions release high concentrations of As in water system (Nicolli et al., 2001; Smedley et al. 2002; and Claesson and Fagerberg, 2003).

It is plausibly to assume that during the weathering of these volcanic rocks arsenic is adsorbed to and/or coprecipitated with metal (Fe, Mn and Al) oxides, especially with iron oxides, and in minor amount adsorbed to clay-mineral surfaces, and/or associated with organic carbon (Welch et al., 1988; Claesson and Fagerberg, 2003). The occurrence of these weathering processes and their influence on the water composition are testified by the high SiO_2 concentration (on average more than 80 mg/L) reported by

(Gashaw, 1999) in the MER groundwaters. **Appendix 6.1** shows the composition of major ions and SiO_2 in the groundwater wells, east and northeast of Lake Ziway.

6.2 Genesis

6.2.1 Clues on the enrichment mechanism of fluoride and arsenic

The acidic volcanic material (tephra) is very reactive and volatile elements (such as fluorine and arsenic) can subsequently be transferred into the water system (Gregory, 1996) during water-rock interactions. Thus, fluorine and arsenic occurrence is plausibly associated with the presence of silicic rocks and their weathering products. Weathering of primary feldspar-bearing volcanic parageneses (important constituent minerals of volcanic rocks in MER in clay-rich saprolites is responsible for the formation of Na^+ rich clays and increasing pH of natural water. This reaction can be idealized as (Deer et al., 1992):

$$NaAlSi_3O_8\ (s) + H_2CO_3 + 4.5H_2O \rightarrow Na^+ + HCO_3^- + 2H_4SiO_4 + 0.5Al_2Si_2O_5(OH)_4\ (s)$$

Together with devitrification of volcanic glass (Di Paola, 1972; AG consult, 2006), weathering of silicic volcanic rocks is responsible for the formation of clays and metal oxides (such as Fe, Al,) that respectively trap fluorine and arsenic. Arsenic is known to be associated with volcanic glass of rhyolitic rocks (Nicolli et al., 1989; Hinkle and Polette, 1999; Bundschuh et al., 2004) and sorbed by metal oxides (Cullen et al., 1989; Nicolli et al., 1989, 2001; Smedley et al., 2002; Ladeira and Ciminelli, 2004) and in minor amounts by clays (Goldberg and Glaubig, 1988; Mohapatra et al., 2007; Smedley et al., 2002; Ladeira and Ciminelli, 2004). Sun and Doner, 1996; Waychunas et al., 1993; Foster, 2003 studied the important role of iron hydroxides (such as goethite and ferrihydrite) in aquifer sediments in controlling the mobility of arsenic.

In the MER, the volcanic glasses in rhyolites are the main sources of fluoride that is progressively enriched in the weathering products of these rocks, as progressively incorporated in clay minerals. The source and enrichment mechanism of fluoride is briefly discussed in chapter 4.

The concomitant presence of As anomalies possibly means that during weathering the As budget is directly released by the glassy rich volcanic rocks, trapped in As-bearing phases such as iron-aluminium-manganese oxides and hydro-oxides, and progressively concentrated within the fluvio-

lacustrine sediments. These phases are very sensitive to Eh-pH changes and if destabilized can release their chemical constituents within the interacting water. During water-rock interaction, the weathering of silicic materials (ash, pumice, tuff, rhyolitic ignimbrites) give rise to Na^+-HCO_3^- rich high-pH waters that favour high mobility of As. As a result As correlated with Na^+ (R^2=0.63) and HCO_3^- (R^2=0.7) in groundwater wells.

Taking into account the speciation of arsenic, hydrogeochemical modelling was performed in order to constrain its behaviour and mobility. Saturation indices with respect to arsenic adsorbing Fe, Al and Mn oxy hydroxide minerals were computed using database of WATEQ4F (Ball and Nordstrom, 1991) of the PHREEQC software. The modeling revealed supersaturation with respect to ferric oxides and hydroxides (hematite, magnetite and goethite) and aluminium hydroxide species (boehmite and gibbsite) indicating that these mineral phases are stable (do not dissolve) in water and could be assumed as potential As adsorbents (**Table 6.1**). Saturation is not reached with repect to Mn oxy-hydroxide phases. The results also showed that arsenate oxyanions, (As (v)) are predominant over arsenite (As (III)) in the water types. This probably indicates an oxidizing aquifers/environment.

Under oxidizing and high pH conditions (caused by the processes of dissolution of silicates and cation exchange) combined with Na^+-HCO_3^- hydrochemical facies can induce local destabilization of these oxide and hydroxides, with concomitant release of arsenic in the interacting water.
Further work of sequential chemical extraction would be required to quantify the metal content associated with different phases (oxides, organic matter, clays) and to clearly determine the origin of the mentioned geochemical anomalies in the MER natural waters.

Water types	Ted8 (RI)	Ted18 (HS)	Ted20 (HS)	Ted36 (HS)	TW26 (HS)	Ted43 (GWL)	Ted46 (WL)	Ted41 (WL)	Ted37 (WL)
pH	**8.3**	**7.8**	**8.2**	**7**	**9.1**	**8.2**	**8.7**	**7.1**	**8.1**
As(tot)=As(V)+As(III) in µg/L	**0.14**	**14.8**	**4.4**	**72**	**109.4**	**277**	**26.3**	**23.8**	**21.5**
mineral phases	**SI**	**SI**	**SI**	**SI**	**SI**	**SI**	**SI**	**SI**	**SI**
Fe_2O_3	8.84	4.5	3.91	4.16	5	0.95	7.77	5.09	6.9
Fe_3O_4	19.18	16.74	15.06	17.4	15.14	13.16	17.69	15.25	18.17
FeOOH	8.38	7.48	7.05	7.45	7.36	6.46	8.03	6.69	8.02
$Fe(OH)_3$(a)	2.72	0.55	0.26	0.38	0.8	-1.22	2.19	0.85	1.75
$Fe_3(OH)_8$	3.49	-3.37	-4.56	-3.17	-3.67	-9.57	1.37	-1.06	0.37
$Fe(OH)_2$.7Cl.3	6.84	5.68	5.03	5.61	5.42	3.56	6.51	5.58	6.52
$FeAsO_4$:$2H_2O$	-10.44	-8.44	-9.87	-6.35	-9.9	-9.33	-10.45	-6.8	-7.68
$Al(OH)_3$	1.62	-0.04	-0.96	0.69	0.12	-3.23	0.86	0.76	1.03
AlOOH	2.82	1.33	0.39	2.08	1.44	-1.76	2.09	1.98	2.31
$Al(OH)_3$(a)	-1.13	-2.46	-3.42	-1.7	-2.4	-5.46	-1.84	-1.95	-1.56
MnO_2	-8	-11.61	-9.23	-6.47	-2.27	0.28	-7.1	-17.24	-12.09
$Mn(OH)_2$	-5.39	-13.69	-11.5	-7.56	-5.29	-5.94	-6.11	-13.04	-11.81
MnOOH	-3.23	-12.03	-9.44	-6.7	-2.33	-3.91	-3.55	-12.08	-9.85
Calcite	-0.08	-0.1	0.19	0.05	0.32	0.03	0.88	-0.32	1.04
Fluorite	-2.75	0.02	-0.9	0.42	-0.48	-0.74	-0.22	-0.72	0.56

Table 6.1: PHREEQC calculations of saturation indices for selected mineral phases and selected water samples. WL= Groundwater wells, HS=Hot springs, CS=Cold springs, GWL= Geothermal wells, LW= Lakes, RI= Rivers and (a): amorphous phase, SI=saturation index.

7. Column experiment on volcanic ash

7.1. Introduction

Most of the rift floor is covered by silicic pyroclastic materials mainly consisting of rhyolitic ignimbrites, interlayered with basalts and tuffs, associated with layered and unwelded pumices. Ashes are frequently found inter-bedded with ignimbrites and pumice layers. This pyroclastic material (tephra) is the result of explosive volcanic eruptions. These volcanic products are the natural persistent source of toxic elements in the rift environment. During eruptive volcanism, fluorine forming gases can adsorb on to the tephra. Linked to these volcanic products, the natural waters of the Ethiopian Rift are characterized by anomalous concentration of fluoride.

In order to further understand the geochemical processes controlling the elevated fluoride concentration, leaching experiments were performed on columns filled by a pyroclastic ash. These experiments aim to simulate the elemental extractability of water soluble ions with particular emphasis on the leaching (dissolution/desorption) behaviour of fluoride during the water-ash interaction. The comparison between the amounts of fluoride leached from different grain size fractions of the same sample also provides further fundamental information in the understanding of sources and geochemical behaviour of fluoride in the waters of the MER. To characterize the flow and transport properties at the field or at the laboratory scale, tracer tests are employed (Ptak et al., 2004) and flow interruption techniques are employed to access physical non-equilibrium behaviour (Brusseau et al., 1989, 1997). Moreover, the numerical transport modelling of the above mentioned tracer tests can help to discern dilution and dispersion processes from reactions between the water and the solid phase (Appelo et al., 1990). Thus, both tracer tests with flow interruption and modelling were used to obtain information on the mobility of selected reactive and non reactive species.

7.2. Sampling and analytical techniques

The sampling location of the pyroclastic fall deposit (TW39) consisting of vitric ash (consisting pumice fragments) are indicated on **Figure 7.1.**

The sample was sieved to obtain different grain size fractions, i.e. <63µm (fine grain ash), 63µm-2mm (coarse grain ash). These different grain fractions (raw, coarse and fine) were later used in the column experiments simulating the water-rock interaction.

After a preliminary drying of the sample at 110 ^{o}C for 12 hours, the bulk rock chemical composition was characterized by X-ray fluorescence spectrometry (XRF) analysis on pressed powder pellets using wavelength-dispersive automated ARL Advant'X spectrometer with accuracy and precision (based on the analysis of certified international standards) better than 3% for Si, Ti, Fe, Ca, K, and 7% for Mg, Al, Mn, Na.

The mineralogical characterization was performed by X-ray diffraction (XRD) investigation and by in situ analyses of single grains obtained with a Zeiss EVO 50 SEM in conjunction with an Oxford Instruments INCA microanalysis suite.

Online parameters on the leaching solutions were determined with the multi-parameter instrument HANNA Multi 340i which includes: a HIcell-31 pH combined electrode with a built-in temperature sensor for pH measurement and a HIcell-21 electrode conductivity cell for EC measurements. Leaching solutions were filtered through a 0.22 µm Dionex vials caps. The major cations, anions (Na^{+}, K^{+}, Ca^{2+}, Mg^{2+}, F^{-}, Cl^{-}, NO_3^{-}, SO_4^{2-}) and oxianions (acetate and formate) were determined by an isocratic dual pump ion chromatography ICS-1000 Dionex, equipped with AS9-HC 4 x 250 mm high capacity column and ASRS-ULTRA 4mm self-suppressor for anions and CS12A 4 x 250 mm high capacity column and CSRS-ULTRA 4mm self-suppressor for anions. An AS-40 Dionex auto-sampler was employed to run analysis, Quality Control (QC) samples were run every 10 samples. The standard deviation for all QC samples run was better than 4% whereas the accuracy is reported as the average of the relative differences between the measured and known standards and it was 5% for cations and anions. Charge balance errors in all analyses were less than 5% and predominantly less than 3%. The detection limit was 2 µg/l for F^{-} and lower than 50 µg/l for all the analyzed anions and cations.

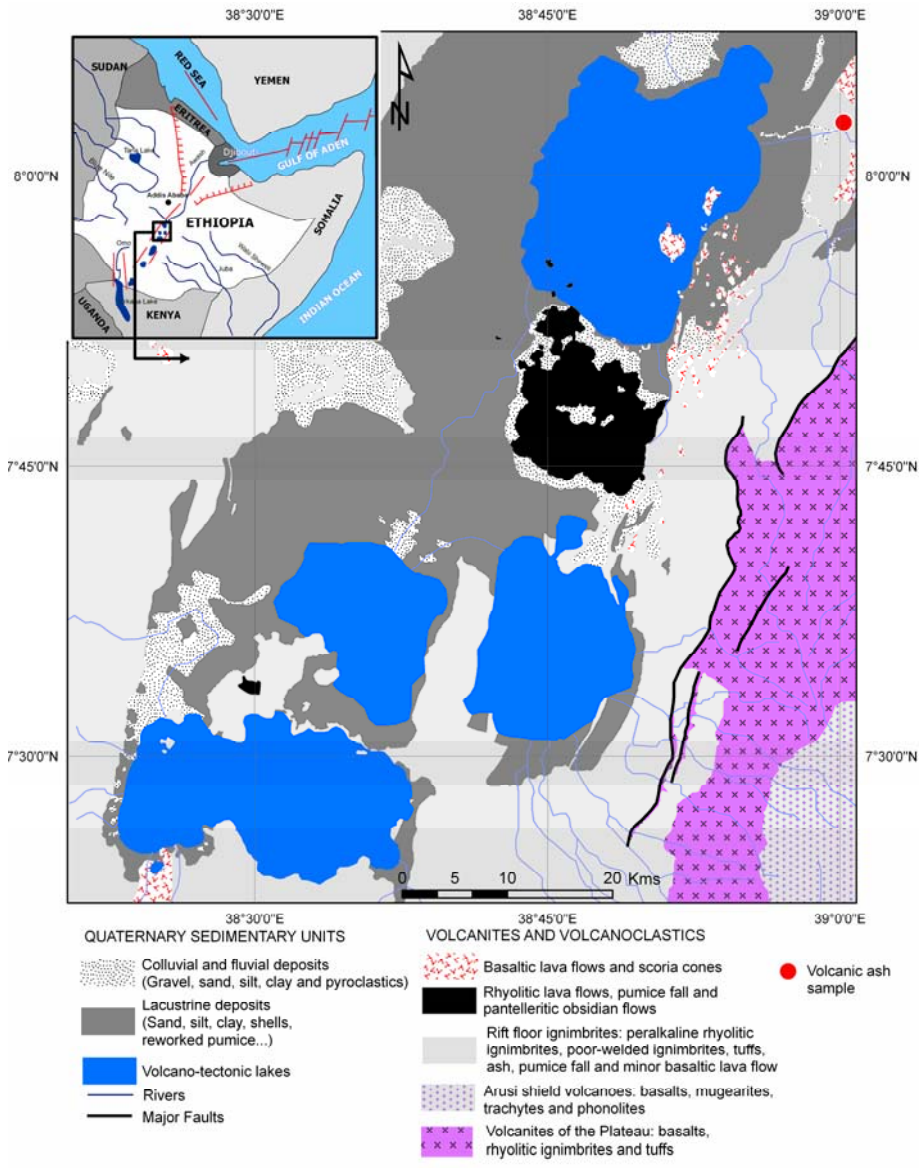

Figure 7.1: Simplified geologic map of the study area modified from (Dainelli et al., 2001) with volcanic ash sampling location.

7.3. Column transport experiments

Column experiments were conducted using polyethylene (PE) columns with internal diameter of 1.35 cm and a length of 20 cm, equipped with PE pre and post-chambers consisting of uniformly packed quartz gravel and a 50 µm NITEX mesh in contact with sediments.

Packing of air-dried sediment took place in 15−20 increments and each increment was lightly packed before the next one was placed on top.

During the experiments involving the raw ash (unsieved sample) and the coarse ash (grain size 63µm-2mm) columns were filled entirely with natural ash, while during the experiment involving the fine ash (<63µm) the column was filled with a 1:3 mixture of natural fine ash particles and inert quartz sand with well sorted grain size 0.1±0.05 mm (Merck, Germany). The latter column was filled in this way to avoid clogging of column filters and excessive entry pressure in the column due to low permeability of fine fraction. Elution experiments consisted in slowly saturating every column with synthetic rain water (pH=5.5), $CaCl_2$ 0.005 M in double deionised water (Carlo Erba, Italy), and equilibrating the ash and the pore water for approximately 1 hour. After the equilibration period, a peristaltic pump with a constant flow rate of 100 ml/h was employed to pump the synthetic rain water in each column. An effluent tube was fixed to a fraction collector (RediFrac Pharmacia LKB Biotechnology) to collect continuous effluent fractions of 2 mL. These fractions were then divided in two 1 mL aliquots for the analysis of cations and anions. After approximately 100 pore volumes, the pump was stopped and turned on again after 1 day to evaluate the amount of cation and anions leached after flow interruption. To get the standard deviation of initial concentrations, 3 small replicates were carried out using 10 mL syringes filled with 5 cm^3 of raw, coarse and fine ash and 5 mL of synthetic rain water; after 30 minutes the first mL out flowing from the syringe was sampled and analyzed. The schematic diagram of the column experiment is shown in **Figure 7.2**.

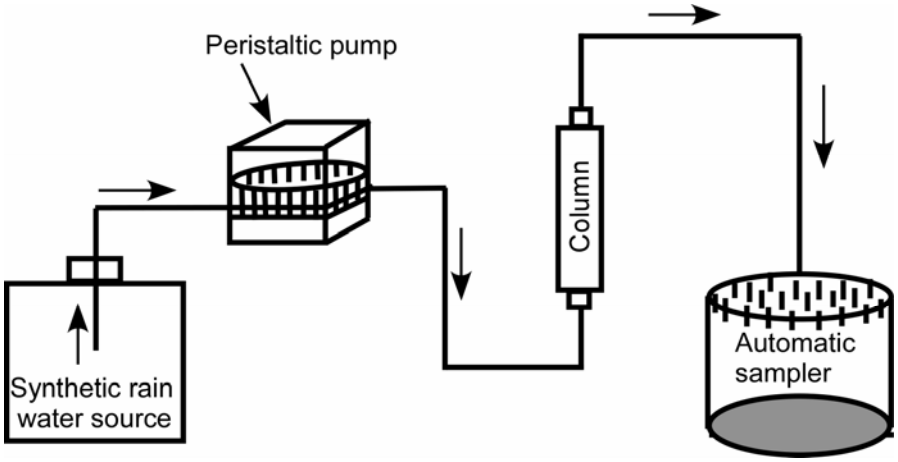

Figure 7.2: Schematic diagram of the column experimental set-up

Extra column volume was taken into account when the experimental elution curves were constructed by correcting the arrival volumes of the effluents. Tracer tests were performed on every column after elution experiments. A solution of 1 g/L of KCl dissolved in synthetic rain water was injected for 0.8 minutes into the column and immediately afterward the synthetic rain water reservoir was turned on. A small flow through cell was used to monitor KCl concentration via electrical conductivity (EC) at the column outflow and KCl concentration (mg/L) of the effluent was obtained from the measurement of EC for a series of known concentrations of KCl solutions. An additional tracer test with flow interruption was performed on every column to examine the effect of diffusive mass transfer on solute transport (Brusseau et al., 1989, 1997).

7.3. Moment analysis and numerical modelling

The breakthrough curves of saline tracer KCl were analysed with the method of moments (Eriksson et al. 1997). The zeroth normalized moment, μ_0, quantifies the fraction of tracer mass recovered in the effluent. The normalized first moment μ_1, which is the mean arrival time, gives the linear retardation factor R; the normalized central second μ_2 and third moments μ_3, measure the spreading around the centre of mass and the degree of asymmetry or skewness (S) of the breakthrough curve, with S given by the ratio $\mu_3/(\mu_2)^{1.5}$ (Vincent et al. 2007).

The finite difference USGS numerical code MODFLOW-2000 (Harbaugh et al., 2000) was employed, to simulate saturated groundwater flow within the column experiments. The flow model domain consisted of a single column and a single row with extent of 12 mm × 12 mm and of 50 layers 4 mm thick for a total column length of 200 mm. Flow boundary conditions consisted in an injection well placed in the first cell with a constant flow rate of 100 ml/hour and a constant head in the last cell, to maintain a constant flux within the column. The solute transport model MT3DMS (Zheng and Wang, 1999) was employed in order to simulate tracer test breakthrough curves and elution of conservative species. The classical formulation of the advection dispersion equation (ADE) was solved by the TVD (third-order total-variation-diminishing method) scheme, which is mass conservative. The TVD scheme solves the advection component independently from the other terms in the transport equation. The only adjustable parameter in the TVD scheme is the Courant number which represents the number of cells a particle will be allowed to move through in any direction, in one transport step, this was set equal to 0.1 to ensure stability during the calculation process (Zheng and Bennet 2005)

The injection of the tracer was simulated with a constant concentration boundary applied to the first cell for 0.8 minutes with KCl concentration of 1000 mg/L. To simulate the elution of conservative species, a flow and transport model was implemented with the same boundary conditions and parameters of the one calibrated for tracer test. The only changes were the removal of the constant concentration boundary and the imposed initial concentration of F^-, set as the initial concentration observed in the first sample collected from the effluent of each column. The comparison of the calculated conservative F^- elution curve and the observed one from different particle fractions, allowed the distinction between the readily water soluble F^- and the sorbed F^- which was slowly released from the porous matrix (Appelo et al. 1990).

7.4. Geochemistry of pyroclastic ash

The XRF analysis was plotted on an alkali silica diagram in order to characterize the geochemical composition. The result showed that the sample is rhyolitic in composition (**Table 7.1 and 7.2**). Moreover, XRD analysis was carried out on the raw, fine and coarse grain fraction of the ash to identify the mineral phases and compare the different grain sizes. Both the raw (unsieved) and coarse ash fractions contain glassy particles and subordinate crystals of quartz, sanidine, aegirina pyroxene and extremely rare F-rich apatite crystals which are nearly absent in the fine fraction that is dominated by the glassy grains (**Figure 7.3 and 7.4**). This suggested the dominant role of the vitric phase in providing the soluble components in the leachate during the column experiments.

TW39 (wt %)	Raw	Coarse grained (63mm-2mm)	Fine grained (<63mm)
SiO_2	71.25	71.11	71.70
TiO_2	0.40	0.39	0.36
Al_2O_3	9.40	9.17	9.09
Fe_2O_3	6.53	7.06	7.05
MnO	0.25	0.26	0.28
MgO	0.13	0.16	0.16
CaO	0.33	0.31	0.35
Na_2O	2.66	2.62	2.03
K_2O	4.29	4.27	4.33
P_2O_5	0.01	0.01	0.01
LOI	4.76	4.64	4.64

Table 7.1: Bulk XRF analysis of major oxides (wt%) of the pyroclastic ash.

TW39	SiO_2	TiO_2	Al_2O_3	Fe_2O_3	MnO	MgO	CaO	Na_2O	K_2O	F	Cl
wt %	74.21	0.31	8.30	6.63	0.24	0.00	0.23	2.40	3.27	**0.33**	0.20

Table 7.2: Average (wt%) composition of the glass phase carried out by in-situ SEM microanalysis of glass particles.

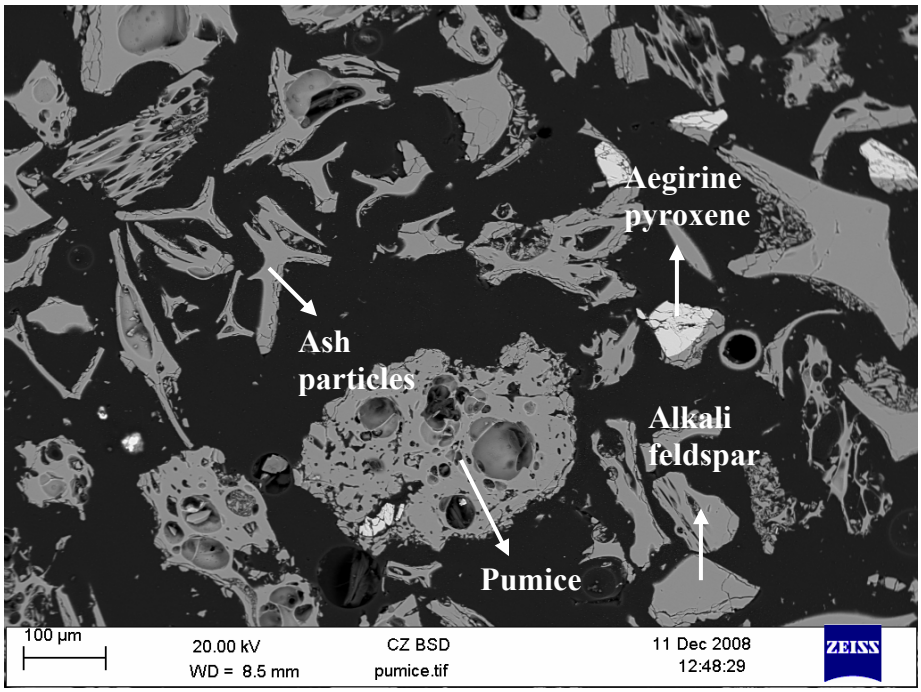

Figure 7.3: Backscattered SEM image of the studied ash. Light grey represents both the glass phase and alkaline feldspar, whereas white grains are aegirina pyroxene crystals. Note the vesicles that characterize the pumice fragments.

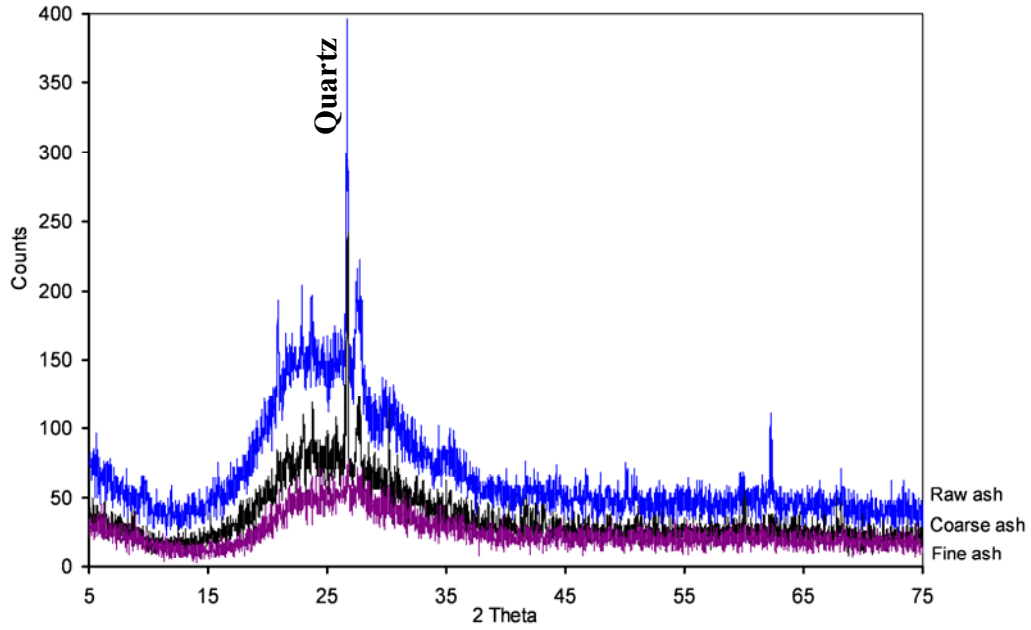

Figure 7.4: XRD analysis results for the three grain fractions (raw, coarse and fine) showing the dominant glassy phase and a few peaks dominated by quartz.

7.5. Geochemical composition of leachates

The composition of the leachates in the column experiments were predominantly controlled by the dissolution of volcanic glass and surface coatings on the glass particles. The reaction kinetics in the column is characterized by a rapid increase of pH (5.5 to alkaline) at the very beginning of the experiment. The consumption of H^+ ions is accompanied by the release of major ions. This suggests the rapid dissolution of volcanic glass and possible occurrence of cation-exchange processes.

Petrographic, XRD and SEM investigation revealed that the studied material mainly consist of glass particles (>90%) and that the subordinate crystals consist of quartz, sanidine, pyroxene and very rare apatite. Therefore, the dissolution of volcanic galss (that is also more reactive) is more important than the dissolution of minerals in controlling leachate composition. Generally, high levels of Na^+, Ca^{2+}, Mg^{2+}, SO_4^{2-}, NO_3^-, Cl^-, F^- are released during the leaching experiments whereas Li^+, K^+, NH_4^+ and Sr^{2+} are leached at very low level (**Table 7.3**). Also acetate and formate, typical intermediate product of organic matter degradation (Christensen et al. 2000), are released at the beginning of the elution; the presence of these oxianions indicates that hydrolization processes of the labile organic matter is taking place.

a)	Raw-volcanic ash leachate major ions composition											
Time (minutes)	Acetate	Formate	Na^+	NH_4^+	K^+	Mg^{2+}	Ca^{2+}	F^-	Cl^-	NO_2^-	NO_3^-	SO_4^{2-}
1	0.72	1.21	36.2	0.63	6.51	5.02	14.82	2.65	45.12	0.32	60.9	16.8
3	0.81	1.33	22.6	0.47	5.64	0.77	2.56	2.23	36.58	0.02	46.9	14.7
6	0.12	0.04	6.61	0.35	3.17	0.27	1.36	1.22	18.45	–	23.97	9.12
9	0.06	0.02	4.83	0.13	2.39	0.17	1.22	1.12	8.79	–	11.87	4.59
12	–	–	4.08	0.11	2.03	0.17	1.01	0.80	3.76	–	4.96	2.14
15	–	–	4.03	0.36	2.16	1.01	3.52	0.66	2.48	–	3.22	1.43
18	–	–	3.41	–	1.70	0.33	2.40	0.53	1.87	–	2.39	1.09
21	–	–	3.10	0.07	1.56	0.21	2.94	0.46	1.54	–	1.97	0.85
24	–	–	3.72	–	1.60	0.58	3.67	0.44	1.29	0.04	1.65	0.79
27	–	–	2.12	–	1.08	0.42	7.50	0.36	3.08	–	1.38	8.71
30	–	–	2.27	–	1.11	0.67	5.45	0.35	2.98	–	1.08	5.57
60	–	–	1.01	0.09	0.77	5.32	3.64	0.23	6.53	–	0.43	23.3
90	–	–	0.21	0.22	0.27	0.12	0.45	0.19	0.43	–	0.18	0.24
120	–	–	0.20	–	0.23	0.09	0.74	0.08	–	–	–	–
150	–	–	0.48	–	0.38	0.17	0.25	0.01	–	–	–	–
180	–	–	0.23	–	0.22	0.12	0.24	0.01	–	–	–	–
210	–	–	0.20	–	0.13	0.02	0.13	0.01	–	–	–	–
240	–	–	0.11	–	0.09	–	–	0.01	–	–	–	–
270	–	–	–	–	–	–	–	–	–	–	–	–
300	–	–	–	–	–	–	–	–	–	–	–	–
330	–	–	–	–	–	–	–	–	–	–	–	–
360	–	–	–	–	–	–	–	–	–	–	–	–
390	–	–	–	–	–	–	–	–	–	–	–	–

b)	Coarse-volcanic ash leachate major ions composition											
Time (minutes)	Acetate	Formate	Na^+	NH_4^+	K^+	Mg^{2+}	Ca^{2+}	F^-	Cl^-	NO_2^-	NO_3^-	SO_4^{2-}
1	0.21	0.36	65.0	3.50	1.20	7.00	23.0	2.31	65.0	–	101.0	45.0
3	0.12	0.12	64.0	3.47	1.19	7.32	21.5	2.31	66.4	–	105.5	45.8
6	0.08	0.35	31.8	1.24	0.46	2.71	5.17	2.14	33.3	0.03	38.1	21.3
9	–	0.31	9.79	0.68	0.21	1.74	2.58	1.66	10.9	–	8.64	7.26
12	–	0.21	6.27	0.48	0.12	1.17	4.28	1.20	5.41	–	7.91	21.6
15	–	0.13	5.37	0.31	0.10	7.76	16.2	0.95	2.69	–	1.58	15.6
18	–	0.12	6.57	0.32	0.08	11.7	19.9	0.75	1.40	–	3.46	13.3
21	–	0.10	3.04	0.08	0.07	10.5	9.19	0.85	3.86	0.02	3.81	4.26
24	–	–	2.16	1.55	0.09	8.69	6.89	0.72	1.79	–	0.04	4.07
27	–	–	3.85	–	0.05	6.79	5.44	0.40	8.68	0.14	1.72	6.24
30	–	–	2.20	–	0.04	4.55	3.87	0.34	1.56	–	7.94	8.18
60	–	–	2.57	–	0.04	2.90	2.41	0.26	1.47	–	2.83	6.50
90	–	–	1.80	–	0.03	1.84	2.82	0.47	0.60	–	0.21	2.48
120	–	–	1.88	–	0.03	1.85	3.42	0.10	0.78	0.13	1.22	7.14
150	–	–	1.53	–	0.05	2.19	4.33	0.11	0.40	–	1.71	6.05
180	–	–	1.55	–	0.03	1.75	2.15	0.10	1.58	–	3.36	4.69
210	–	–	1.02	0.13	0.02	1.17	1.57	0.23	1.67	–	0.81	4.03
240	–	–	0.70	0.05	0.03	0.45	1.70	0.18	1.21	–	1.27	4.21
270	–	–	1.10	–	0.03	1.08	1.09	0.04	1.53	–	0.35	2.78
300	–	–	–	–	–	–	–	–	–	–	–	–

330	–	–	–	–	–	–	–	–	–	–	–	–
360	–	–	–	–	–	–	–	–	–	–	–	–
390	–	–	–	–	–	–	–	–	–	–	–	–

c)	Fine-volcanic ash leachate major ions composition											
Time (minutes)	Acetate	Formate	Na^+	NH_4^+	K^+	Mg^{2+}	Ca^{2+}	F^-	Cl^-	NO_2^-	NO_3^-	SO_4^{2-}
1	1.30	1.50	53.0	1.37	0.43	9.00	24.2	9.02	33.0	–	62.0	69.0
3	0.50	0.20	50.9	1.36	0.43	9.92	23.0	9.18	33.1	–	58.7	67.9
6	0.70	0.10	22.8	0.61	0.19	4.73	11.3	4.45	20.2	–	21.9	33.0
9	0.10	0.50	10.6	0.31	0.09	3.73	3.68	2.44	10.7	–	5.62	16.1
12	–	2.10	6.50	0.19	0.06	2.50	2.61	1.07	4.12	–	0.11	7.31
15	–	0.30	4.88	0.15	0.04	2.20	2.32	0.51	2.20	–	0.02	3.67
18	–	0.30	4.54	0.13	0.04	1.59	1.78	0.37	1.65	–	0.10	3.34
21	–	0.20	3.86	0.13	0.03	0.80	1.66	0.30	1.65	–	0.53	6.33
24	–	–	2.93	0.16	0.03	0.54	1.64	0.29	2.49	–	0.67	9.08
27	–	–	2.71	0.17	0.03	1.04	2.22	0.27	2.76	–	7.64	11.9
30	–	–	3.89	0.21	0.03	3.91	3.37	0.49	1.86	–	6.16	15.4
60	–	–	3.75	0.26	0.02	4.20	5.01	0.23	0.96	–	0.73	15.8
90	–	–	4.64	0.29	0.02	6.70	12.3	0.10	1.55	–	2.12	18.7
120	–	–	6.46	0.36	0.04	7.80	26.2	0.09	1.30	–	3.06	20.9
150	–	–	1.61	0.28	0.05	7.77	18.6	0.07	1.33	–	9.48	20.2
180	–	–	1.26	0.32	0.01	8.60	9.45	0.04	1.67	–	6.36	13.3
210	–	–	2.97	0.25	0.02	7.87	8.72	0.08	1.56	–	0.79	4.70
240	–	–	1.99	0.29	0.04	4.28	4.20	0.04	1.60	–	0.81	1.92
270	–	–	1.68	0.15	0.01	2.01	3.58	0.12	3.27	–	4.64	1.57
300	–	–	1.00	0.10	0.00	1.04	1.02	0.03	1.49	–	0.14	0.44
330	–	–	–	–	–	–	–	–	–	–	–	–
360	–	–	–	–	–	–	–	–	–	–	–	–
390	–	–	–	–	–	–	–	–	–	–	–	–

Table 7.3: Major ions compositions from the column experiment for a) raw ash b) coarse ash and c) fine ash. Note that: concentration is expressed in mg/L, (−) = below detection limits

The chemical analysis of leachates from the three grain size fractions (fine, coarse and raw) showed that the ions Na^+, K^+, F^-, Cl^-, and NO_3^- were consistently decreased with increased flushing time, whereas Ca^{2+}, Mg^{2+} and SO_4^{2-} decreased at the beginning of the experiments and increased after a certain time, and finally decreased gradually (**Figure 7.5**). The geochemical behaviour of Ca^{2+} and Mg^{2+} mimics that of SO_4^{2-} along with time series, particularly for the fine grained ash column (**Figure 7.6).** This probably suggests that the concentration of Ca^{2+}, Mg^{2+} and SO_4^{2-} on the leachates, to a certain extent, have possibly resulted from dissolution of gypsum coatings on tephra particle surfaces. The occurrences of

halogens (F^-, Cl^-) are controlled by the available volcanic gases HF, HCl, adsorbed to the surface of tephra. SO_2 gas adsorbed on the tephra can also be another possible source of SO_4^{2-}.

The leaching experiments showed a pronounced effect of volcanic ash in controlling chemical composition of the leachates which can mirror the leaching behaviour of the rift volcanic ash during rainfall and surface runoff.

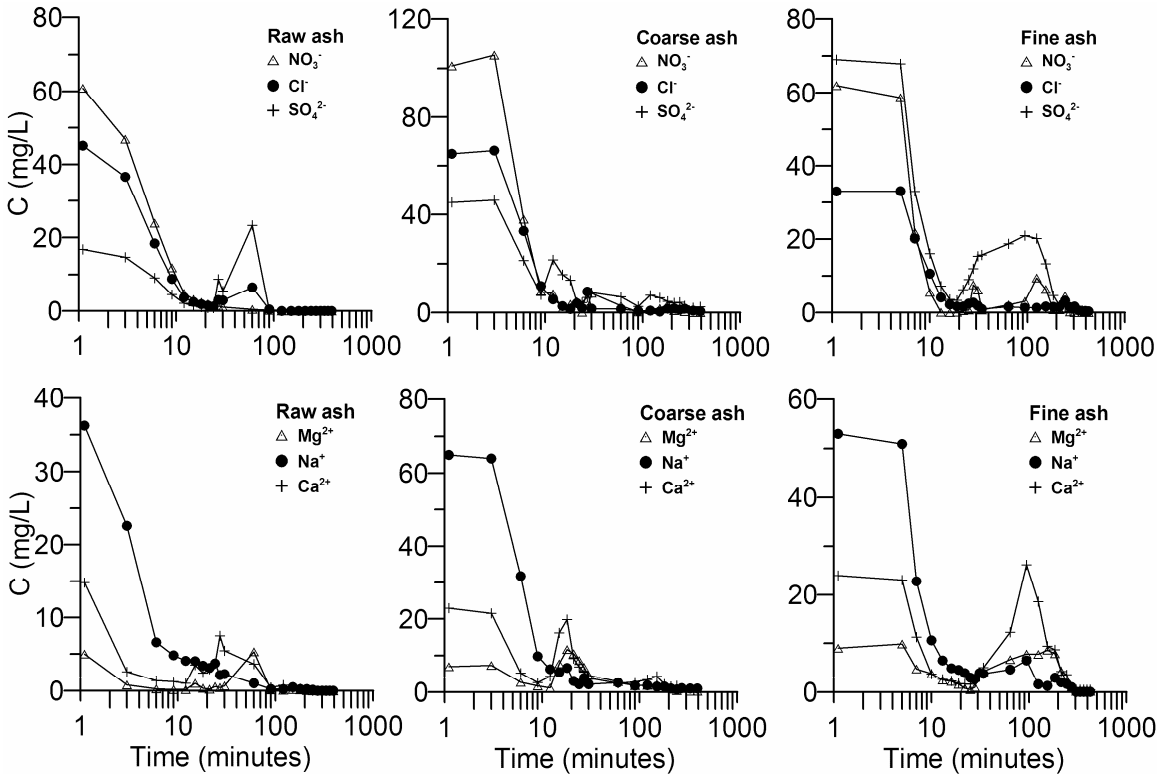

Figure 7.5: Plots of major ions concentration variation versus time series for the raw ash, coarse ash and fine ash leachates.

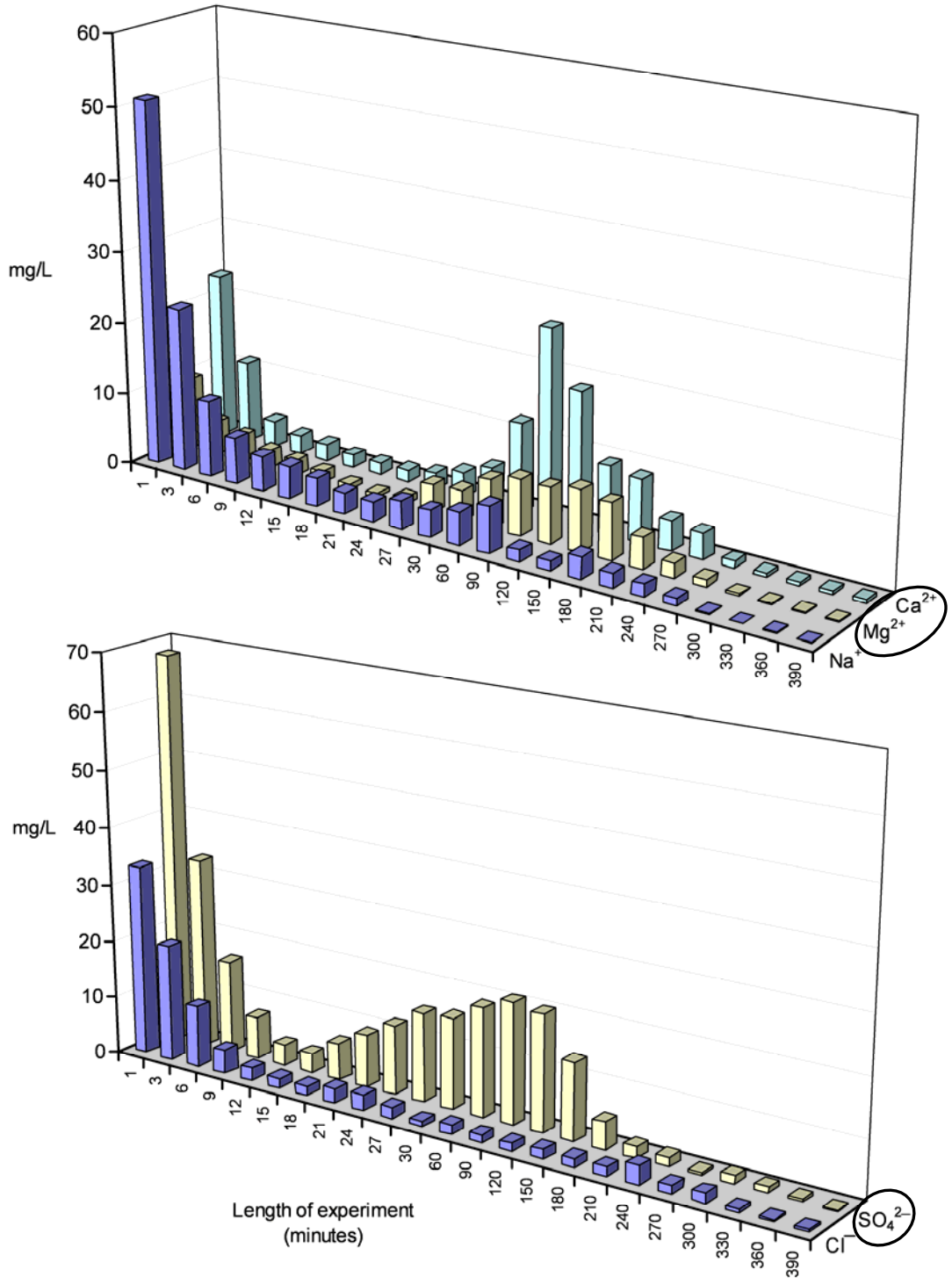

Figure 7.6: 3D-Column diagram showing Ca^{2+} and Mg^{2+} versus SO_4^{2-} concentration variation along the time series.

Considering that F^- is the most problematic water quality issue in the Ethiopian rift system, the performed column experiments puts particular emphasis on the origin and the leaching behaviour of F^- during water-rock interaction processes. The maximum concentration levels at the beginning of the experiment for the fine, coarse and raw grain fractions are 9.2±0.6, 2.3±0.1 and 2.7±0.1 mg/L respectively and consistently decreased along the time series (**Figure 7.7**). During the experiment on the fine ash fraction, the column was filled with 6.6 g (¼th) fine ash and 20 g (3/4th) inert sand in order to increase the column permeability for two main reasons (i) the experimental apparatus here used was not able to produce a flow with elevated counter pressure and (ii) water percolation at field conditions in very fine sediments is normally negligible with respect to coarse sediments (Fetter 2004). Even at 1:4 ratios, the fine fraction released 9.2 mg/L which is higher than the other fractions. This suggested that much of the fluoride is concentrated and released from the finer fractions.

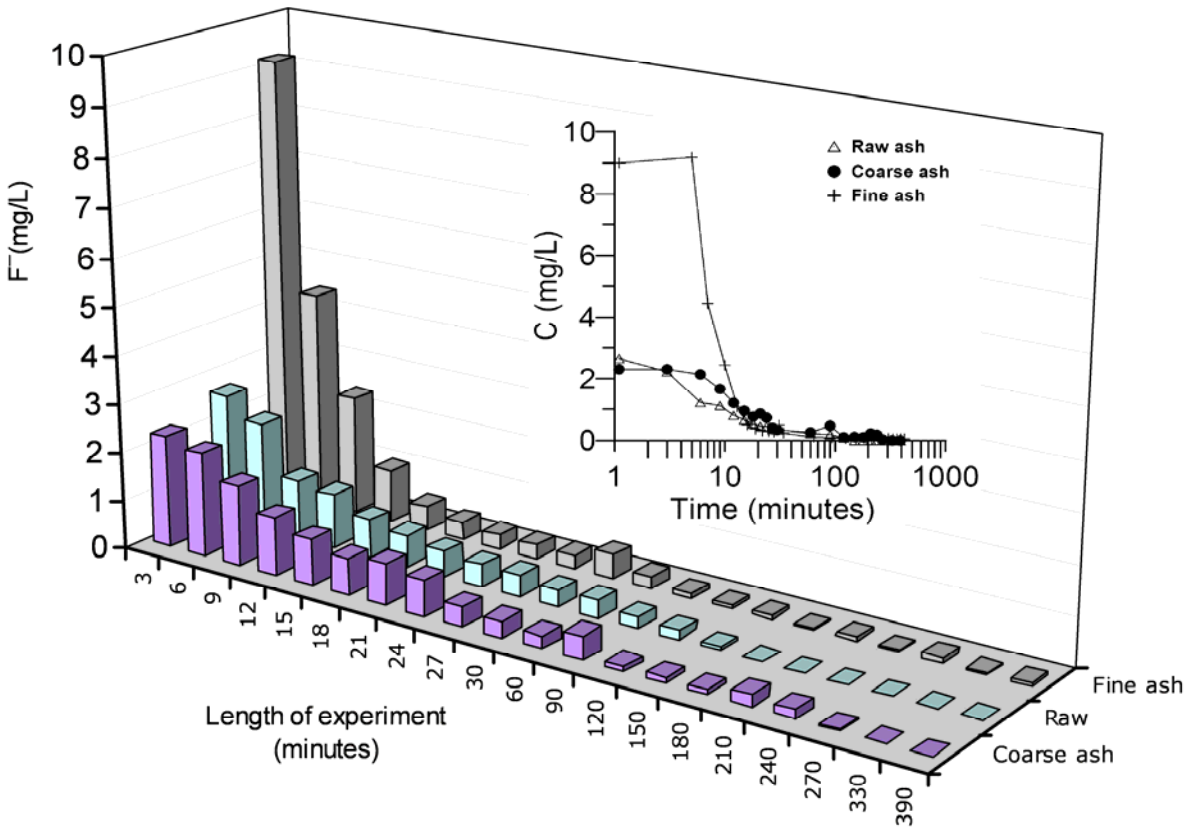

Figure 7.7: Diagrams showing the behaviour of F^- leaching with time for the fine, coarse and raw ash leachates.

7.6. Tracer tests and model results

The main objectives of these tests were to determine if the physical equilibrium approach described by the classical advection dispersion equation can be assumed, or if non equilibrium processes (preferential flows) were relevant for the column experiments. Once this issue was resolved, the main target was to quantify the physical parameters which deterministically describe the flow and transport process.

The mass recovery was near 100% for all tracer tests, and the centre of the mass was recovered after approximately 1 pore volume confirming the assumption of conservative transport for KCl. Instead, the spreading around the centre of mass and the skewness were quite different. For instance, μ_2 and S of the fine ash column were very low as the predominant grain size was the inert sand used to increase the column permeability; while μ_2 and S of the other two columns were comparable. Overall, the moment analysis confirmed the conservative behaviour of the saline tracer used in the tests and the higher spreading and tailing in the raw and coarse columns could suggest possible preferential flow and diffusive mass transfer between mobile and immobile water zones. To quantify this possible mechanism, on every column an additional tracer test with flow interruption (not shown) was performed. The absence of concentration increase, after 30 minutes of flow interruption, lead to exclude the substantial contribution of physical non equilibrium processes in solute transport within the columns. Moreover, the total porosity measured gravimetrically and the effective porosity determined by means of tracer testing gave similar results, thus their ratio approached unity. This implies that there is no considerable partition between mobile and immobile water within the column and there are no indications of preferential flow and corresponding immobile water zones (Eriksson et al., 1997).

	Parameter					
	μ_0	μ_1	μ_2	S	λ_L (cm)	θ
Raw ash column	99.7	1.01	0.09	0.97	2.5	0.40
Coarse ash column	99.8	1.01	0.12	0.99	3.0	0.49
Fine ash column	100.2	0.99	0.03	0.69	0.6	0.45

Table 7.4: Moment analysis results for the three columns.

Parameter	Raw ash	Coarse ash (63µm-2mm)	Fine ash (<63 µm)
Grain size (%)	-	67	28
Hydraulic conductivity (m/s)	1.90E-05	1.10E-04	1.10E-06
Bulk density (Kg/m^3)	1.18	1.68	1.61
Total porosity	0.40	0.51	0.46

Table 7.5: Lists of volcanic ash grain size distribution, hydraulic conductivity, bulk density and effective porosity.

The simulated and observed breakthrough curves of the non reactive tracer (KCl) injected in each of the three columns after the elution experiments are showed in **Figure 7.8.**

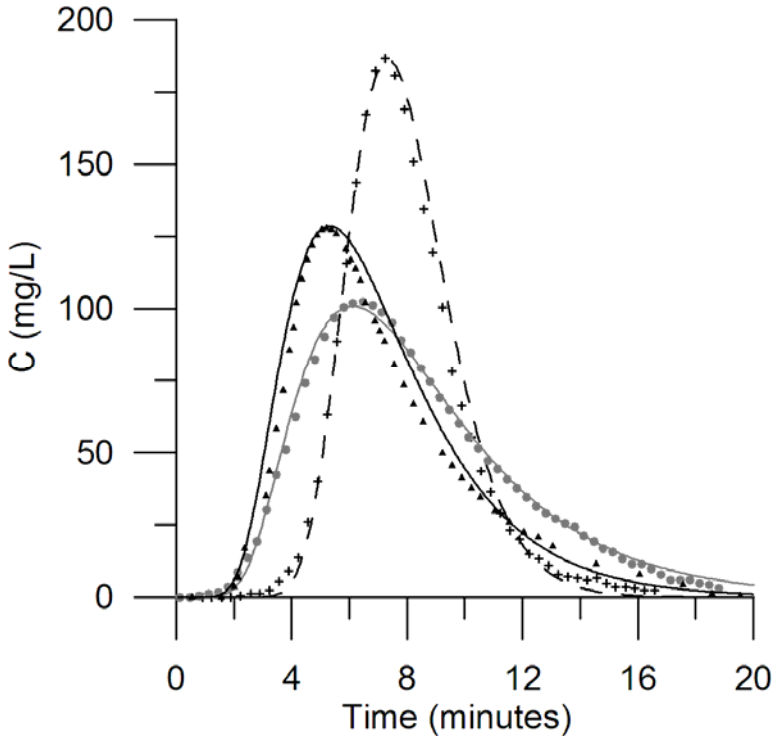

Figure 7.8: Calculated and observed tracer concentration breakthrough curves for the raw column (black line and triangles); for the coarse ash column (light dark line and circles) and for the fine ash column (black dashed line and crosses).

The only parameter adjusted during model calibration process was longitudinal dispersivity (λ_L), as hydraulic conductivity was determined with constant head test and effective porosity (θ) was derived from:

$$\theta = \frac{vQ}{A}$$

Where Q is the flow rate, A is the cross sectional area of the column and v is the measured velocity of the tracer, calculated dividing the length of the column by the time required for the tracer centre of mass to pass through the column. The elevated value for λ_L of raw and coarse ash column is due to the high tortuosity pathway that tracer particles encompass through the ash, while for the fine ash column, the low value is representative of a homogeneous porous media, given by the inert quartz employed. The model fit was satisfactory for all the columns with a correlation coefficient (R^2) of 0.998, 0.996 and 0.997 for the raw, coarse and fine ash column respectively.

With the calibrated model, it is possible to verify the amount of F^- adsorbed onto different grain size constituent of the ash, by integrating the area of the observed elution of F^- and subtracting it to the integrated area of F^- calculated conservative elution. From **Figure 7.9** is evident that the Cl^-, usually not retained by sediments (Griffioen 1992), shows a conservative behaviour and is released rapidly from the matrix, whereas F^- is released more slowly.

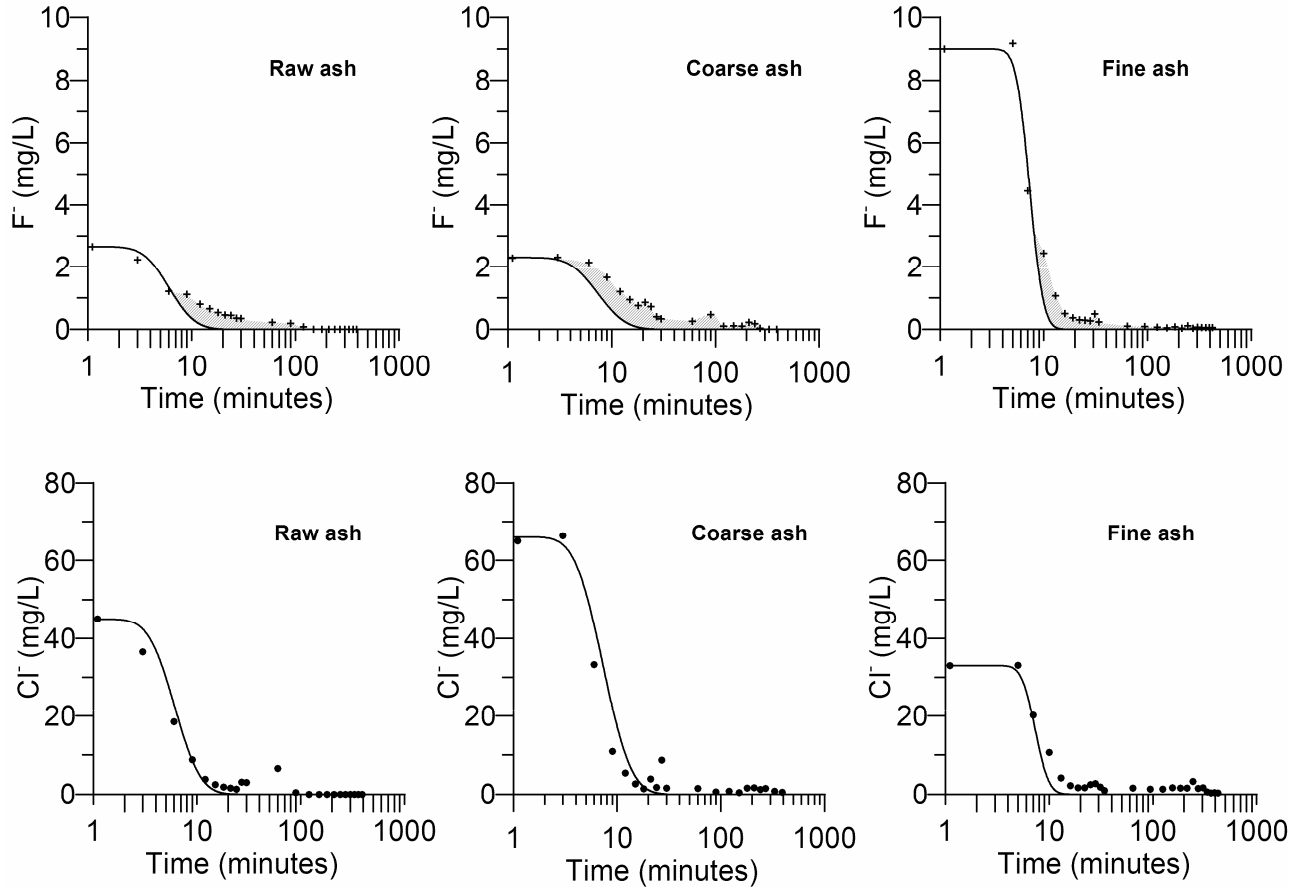

Figure 7.9: Calculated and observed tracer concentration breakthrough curve for the raw, coarse and fine ash column, drawn for F^- and Cl^-.

The result of the study has demonstrated that the pyroclastic deposits are an important reservoir and the ultimate source of fluoride in the water resource of the region. Leaching of fluoride was significant, particularly at start of the column experiments. The highest measured concentration of fluoride from the fine, coarse and raw grain fractions columns were 9.2±0.6, 2.3±0.1 and 2.7±0.1 mg/L respectively and gradually decreased over the duration of the experiment. The recorded behaviour suggests that availability controlled mechanism for the release of fluoride in water, rather than solubility controlled mechanism; the latter is characterized by constant concentrations reached after an equilibration time and is typical of mineral weathering processes. The column experiment on the volcanic ash using synthetic rain water has simulated the leaching behaviour of fluoride during water-rock interaction processes. The total mass of leachable fluoride is resulted from F concentrated in the fine fraction of the pyroclastic ash, which is released in major quantity from amorphous vitric phase. The result has brought an important

implication in the understanding of the source and geochemical behaviour of fluoride in the natural waters of the rift. Here, we propose that the finer fraction of volcanic ash is directly correlated to elevated leachable fluoride, for this reason in case of new exploitations of groundwater resources we recommend to characterize at least the grain size distribution at the field site scale, and to avoid locations with elevated fine (<63 μm) grain size content.

8. Isotope geochemistry of MER waters and rocks

8.1. Introduction

Applications of isotope geochemistry are widely proven techniques that are used as tracers in various environmental problems related to hydrology. They provide important insights into the origin of waters, recharge conditions, water-rock interactions and water flow paths (Clark and Fritz, 1997; Cook and Herczeg, 2000).

Stable isotope fractionation during evaporation of water from the oceans and open water surfaces as well as the reverse process (condensation and rain formation) is responsible for the most notable changes in the water isotopic pattern. These processes cause the depletion of meteoric water and enrichment within lakes, plants, and soil water of heavy isotopic species of H and O relative to the ocean (Clark and Fritz, 1997). The stable isotope composition of groundwater relates these waters to the site of precipitation, infiltration or to their origin from surface water or fossil ground water (Gat and Dansgaard, 1972).

The basis for the interpretation of variations in stable isotope in the hydrologic system is based on the vapour pressure of $H_2{}^{16}O$ which is higher than that of $H_2{}^{18}O$. Due to this variability in isotopic vapour pressures, evaporation produces residual water enriched in the heavier isotopes relative to the initial isotopic composition. Comparison of the stable isotope data for surface water and groundwater samples relative to the global or local meteoric water lines can provide information on these processes. Therefore water that has undergone evaporation lies to the right of the local meteoric water line due to this enrichment (Coplen, 1993). Groundwater can be isotopically fractionated during water-rock interaction processes.

On the other hand, $^{87}Sr/^{86}Sr$ isotopic fingerprint of water is depends on the weathering and a subsequent interaction of water with rock and to attain a specific Sr isotopic value of the parent rock. The ratio varies depending on the type, and age of the weathered rock (Faure, 1986).
Groundwater acquires dissolved Sr: (i) in its recharge area, through infiltration and percolation processes; and (ii) along its flow path, through dissolution of or ion exchange with minerals. Hence, $^{87}Sr/^{86}Sr$ isotope ratios give insight into water-rock interaction processes. Dissolved strontium isotope is

a useful tracer because it undergoes negligible isotopic fractionation and it can be considered representative of the ratio of the source (Goldstein and Jacobsen, 1987; Drever, 1997; Stettler and Allegre, 1978). Once strontium released in the hydrosphere, it retains its isotopic composition without significant fractionation by geologic and hydrologic processes. Any change in the measured $^{87}Sr/^{86}Sr$ value can only be described by the interaction with multiple rocks and by mixing with different fluids having different isotope ratios (Frape et al., 2003; Pande et al., 1994; Ben Othman et al., 1997).

The purpose of this section is to investigate the application of isotope geochemistry on the origin of waters, water-rock interactions and mixings processes (among surface waters and groundwaters) using stable isotopes of O, H and radiogenic Sr isotopes. $^{87}Sr/^{86}Sr$, δD and $\delta^{18}O$ isotopes, in combination with major (Na^+, K^+, Ca^{2+}, Mg^{2+}, F^-, Cl^-, NO_3^-, SO_4^{2-} and HCO_3^-) and trace elements (Li, B, Sr, and Rb) were utilized.

8.2. Sampling and analysis of δD, $\delta^{18}O$ and $^{87}Sr/^{86}Sr$ isotopes.

Stable isotopes of oxygen and hydrogen were analysed on 31 water samples (5 lakes, 12 groundwater wells, 2 geothermal wells, 10 hot springs and 2 rivers), and strontium isotopes for 13 water samples (9 hot springs, 2 geothermal and 1 groundwater well and 1 river) were analysed.

Two separate samples were collected for oxygen, hydrogen, and strontium isotopic analysis. The samples were stored in 100ml polyethylene bottles on the site after filtration using 0.45 μm membrane filters. For O, H, and Sr isotope filtered and none acidified water samples were used.

The determination of O and H isotope composition was carried out using the well established technique of CO_2/H_2 water equilibration by means of an automatic equilibration device on line with a Delta Plus Mass Spectrometer Flow (Epstein and Mayeda, 1953; Horita et al., 1989). The results are reported as delta units (δ) per mil (‰) with respect to the V-SMOW isotopic standard. The analytical precision of $\delta^{18}O$ and δD measurements are better than ±0.05‰ and ±0.7‰ respectively. The $\delta^{18}O$ and δD measurements were performed on the same water aliquot.

Sr isotopic analysis was performed on a sub-set of samples consisting mainly water from the hot springs and geothermal wells. The preliminary preparation of samples was done starting from 100ml of filtered water progressively dried at 40 °C in cleaned vials. About 1 ml of 2.5N ultrapure HCl was added to

dissolve the remaining precipitate. Strontium was separated by ion-exchange chromatography using AGW50 X-8 200-400 mesh Bio-Rad resins in H^+ form.

As concerns rocks (an ignimbrite and a basalt), the labile Sr was extracted using CH_3COONH_4 at the proper concentration to extract most cations by adding 100 ml of solution to 25 g of crushed rock. The Sr isotopic composition was obtained by using a VG Micromass 54E single-collector mass spectrometer equipped with a TAU box and the software "Analyst" (Ludwig, 1994) for data acquisition and reduction. The measured $^{87}Sr/^{86}Sr$ ratio was fractionation-corrected to $^{86}Sr/^{88}Sr=0.1194$; repeated analysis of the NBS 987 standard gave averaged $^{87}Sr/^{86}Sr$ ratio of 0.71025+/-0.00002 (n=12), and no correction was applied to the measured isotopic ratio for instrumental bias.

8.3. Delta Notation of Stable Isotope Data

An isotopic ratio in a sample is measured with respect to a common standard. Ocean water is used as the standard for all H isotope analyses and for most O isotope analyses. It is reported as the deviation (δ) of the isotopic ratio of the sample (e.g. $^{18}O/^{16}O$) from $^{18}O/^{16}O$ of a standard:

$\delta^{18}O$ = (Rsample/Rstandard - 1) x 1000

Where: **Rsample** = $^{18}O/^{16}O$ in the sample

Rstandard = $^{18}O/^{16}O$ in the standard, and

$\delta^{18}O$ = relative difference in concentration, in units of parts per thousand (per mil).

Delta ^{18}O ($\delta^{18}O$) is referred to as delta notation and is the value reported by isotopic laboratories for stable isotope analysis. Delta ^{2}H ($\delta^{2}H$) can be derived by analogy to $\delta^{18}O$ where the ratio $^{2}H/^{1}H$ replaces $^{18}O/^{16}O$ in Rsample and Rstandard. The standard used for determining $\delta^{18}O$ and $\delta^{2}H$ in water originally was standard mean ocean water (SMOW) as defined by (Craig, 1961). The standard used in this work is Vienna standard mean ocean water (VSMOW). If $\delta^{18}O$ and $\delta^{2}H$ samples contain more of the heavier isotopes (^{18}O or ^{2}H) than the reference material, the samples have positive per mil values and are referred to as heavier than the reference material or as being enriched in the heavier isotope. Conversely,

if the samples contain more of the lighter isotopes (^{16}O or H) than the reference material, the samples have negative per mil values and are referred to as lighter than the reference material or as being depleted in the heavier isotope.

8.4. Defining the local meteoric water line (LMWL)

As a result of kinetic and equilibrium processes during evaporation from the ocean and subsequent condensation, the ratios of the stable isotopes of hydrogen (^{1}H and ^{2}H or deuterium) and oxygen (^{16}O and ^{18}O) in water within a particular air mass vary with temperature during condensation and with relative humidity during evaporation (Clark and Fritz, 1997). The stable isotope ratios of water vapor in an air mass reflect the origin of the air mass, and the ratios in the precipitation that evolves from the air mass reflect both the origin of the air mass and the conditions under which condensation occurs. As an air mass travels away from the ocean (or other source areas for water vapor) and precipitation occurs, precipitation that is enriched in the heavier isotopes leaves the air mass first. The remaining water vapor then is composed of lighter isotopes. Subsequent precipitation has an increasingly lighter stable isotope composition.

This depletion effect has been called the "continental effect" and results in lighter stable isotope ratios farther away from the ocean. Furthermore, a strong linear correlation exists between mean annual isotopic composition of precipitation and mean annual surface air temperature. As a result, precipitation at higher latitudes has a lighter stable isotope composition than precipitation closer to the equator. This temperature effect also is seen as a result of elevation; cooler temperatures at higher elevations result in $\delta^{18}O$ depletion that varies between -0.15 and -0.5 permil per 100 m rise in elevation (Clark and Fritz, 1997). The relation between $\delta^{2}H$ and $\delta^{18}O$ in precipitation is described by the Global Meteoric Water Line (GMWL) developed by (Craig, 1961) and expressed by the equation:

$$\delta^{2}H = 8\,\delta^{18}O + 10$$

This relation was developed as an average of many local water lines that differ from the GMWL as a result of climatic and geographic factors. Differential fractionation of $\delta^{2}H$ and $\delta^{18}O$ occurs as a function of humidity during primary evaporation of water vapor from the ocean and as a function of temperature

during secondary evaporation as rain falls from a cloud. These two factors affect the slope and intercept of the Local Meteoric Water Line (LMWL) and produce a different LMWL at different locations.

In the study area the local meteoric water line (LMWL) is defined based on the interpretation of isotopic data ($\delta^{18}O$, δD) of rain in the basin (at Asela, Ziway, Silte, Butagera, and Awasa towns) that were collected by (Chernet, 1998) in the period of June-August 1994 and 1995 with precipitation varying from 2.5 to 75 mm. Generally, it appears that a variation in the isotopic values of the rain occur according to the quantity of rainfall. At higher precipitation quantity, the isotopic values are depleted as compared to at lower rainfall quantity.

Considering all the data collected in the 5 towns the LMWL is defined as:

$\delta D = 6.08\ \delta^{18}O + 8.67$ ($R^2 = 0.88$) (**Figure 8.1**)

All the data used to generate the LMWL are shown in **Appendix 8.1.**

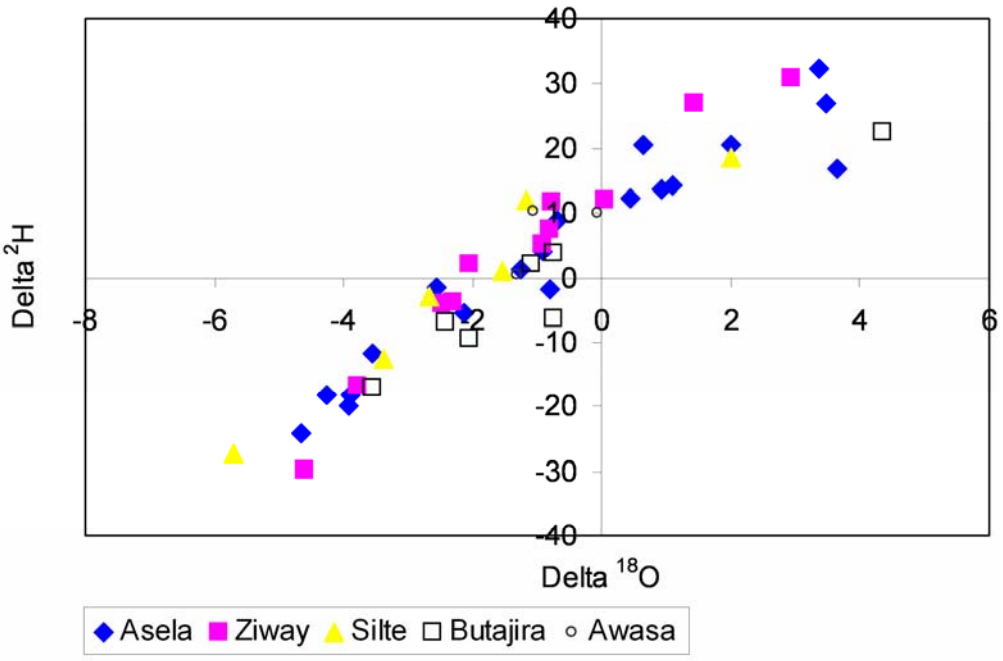

Figure 8.1: LMWL in Ziway-Shala basin, defined using all precipitation data (**Appendix 8.1**)

The evaluation of the samples to determine whether they were affected by secondary processes of evaporation during collection and/or storage, deuterium-excess (δD-8 $\delta^{18}O$) values defined by

(Dansgaard, 1964) were used as an indicator of potential sample evaporation. D-excess remains unchanged during the air masses move across the continent and losses moisture by rainout. If evaporation exists from open surface bodies that return moisture to the air masses, the inherited d-excess values of the air masses can be altered (Gat et al., 1994; Machavaram and Krishnamurthy, 1995). D-excess value of precipitation can also be changed when evaporation from rain drops passing through the air and/or from collector (Gat, 1996). Moisture exchange model of (Merlivat and Jouzel, 1979) showed that for reasonable ranges of temperature (20 to 30°C) and relative humidity (70 to 95 percent) over the ocean, the initial d-excess value of transported moisture should be between 3 and 15 per mil. Any sample with d-excess values less than 3 per mil has to be avoided since they may be affected by evaporation. Based on the above theory, d-excess values below 3 and above 15 per mil have been eliminated. This brings a better correlation (R^2=0.97) with the equation of the:

LMWL: $\delta D = 7.02\ \delta^{18}O + 9.1$ (**Figure 8.2**)

This equation (LMWL) is used in the basin to determine sources of ground-water recharge, to evaluate surface-water and groundwater interaction, and to analyze other geochemical and hydrologic problems.

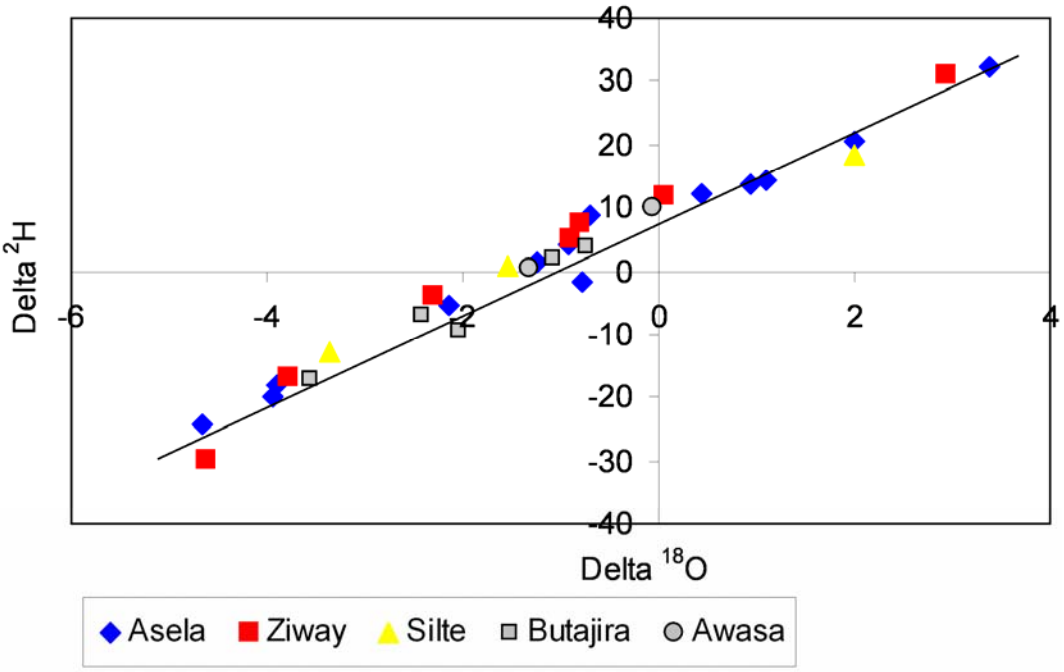

Figure 8.2: LMWL in Ziway-Shala basin defined after excluding samples affected by evaporation. Excluded samples are indicated in Appendix 8.1.

8.5. Stable $\delta^{18}O$, δD and radiogenic $^{87}Sr/^{86}Sr$ isotope composition of waters and rocks

Table 8.1 displays major ions and Table 8.2 displays isotopic ratios of ($\delta^{18}O$ and δD, N=31) and ($^{87}Sr/^{86}Sr$, N=13) and selected trace elements (Sr, Rb, Li and B) of waters including $^{87}Sr/^{86}Sr$ values of 2 representative volcanic rocks (ignimbrite and basalt). Different ranges of isotopic values are recorded for different water groups: for 10 hot spring samples show $\delta^{18}O$ (-3.36‰ − 3.69‰) and δD (-15.85‰ − 24.23‰) (VSMOW), 12 groundwater wells $\delta^{18}O$ (-3.99‰ − 5.14‰) and δD (-19.69‰ − 32.27‰) in contrast to the 5 Lakes $\delta^{18}O$ (3.98‰ − 7.92‰) and δD (26.19‰ − 45.71‰). The 2 deep geothermal wells and 1 out of 2 river samples are depleted in stable isotopic values.

Type	T (°C)	EC	TDS	pH	Na^+	K^+	Mg^{2+}	Ca^{2+}	F^-	Cl^-	HCO_3^-	$SO4^{2-}$
HS1	96	4530	1830	8.36	170	39.1	0.0	0.9	23.5	429	915	253.0
HS2	78	2040	1728	6.79	398	29.4	3.3	11.1	13.1	128	1110	35.0
HS3	93.4	14440	7919	8.16	2288	24.6	0.0	0.3	97.3	1462	3434	612.1
HS4	57.3	10570	7501	7.81	2416	25.9	0.0	1.4	63.9	1324	3642	28.3
HS5	91.4	13190	6589	8	2109	1.5	0.0	1.9	55.0	1148	3251	22.3
HS6	52.6	1780	958	8.15	346	26.4	0.0	3.2	4.5	17	561	0.0
HS7	59.3	4630	3600	7.3	969	66.0	8.0	8.8	17.5	321	2141	68.8
HS8	51.8	4870	3896	8.16	1122	64.1	0.6	1.7	17.6	356	2267	66.2
HS9	38.8	630	499	7.33	105	11.5	5.5	22.1	1.9	27	293	32.6
HS10	62	3900	2766	6.96	802	60.0	0.7	13.9	23.4	435	1407	23.1
GW11	82	2160	1297	7.44	306	109.9	0.0	0.0	13.6	162	653	52.9
GW12	85.6	4600	3051	8.17	771	152.2	0.0	0.8	40.2	207	1842	37.7
WL13	28.3	3360	3564	8.16	858	31.2	4.2	3.7	13.6	106	2547	7.0
WL14	24.6	350	871	7.48	61	9.4	2.3	27.7	3.1	145	226	397.7
WL15	22.5	220	211	8.25	33	2.3	1.1	24.7	1.5	1	146	0.8
WL16	24	220	266	7.31	30	3.6	2.6	25.0	2.0	1	201	0.5
WL17	23.2	1320	1252	8.14	307	12.1	5.6	17.0	13.1	17	872	7.8
WL18	25.2	490	489	7.82	55	2.5	11.2	68.0	0.9	4	342	5.8
WL19	23.7	1770	12797	8.7	443	21.1	1.9	7.2	10.1	19	1229	3.7
WL20	36.4	730	668	7.89	140	14.7	3.2	18.9	3.1	7	475	6.4
WL21	32.3	2260	1952	7.64	480	27.6	30.5	30.7	7.1	266	1077	33.5
WL22	36	2390	1949	8.08	557	25.9	0.1	28.7	14.3	153	1092	107.2
WL23	25.1	2750	2227	7.81	565	25.1	6.7	20.8	20.0	176	958	456.0
WL24	25.3	300	267	7.83	50	5.2	2.7	10.2	1.8	2	195	0.0
LW25	24.2	1730	1377	9.03	387	21.0	0.5	9.7	12.5	131	769	46.5
LW26	22.1	800	715	8.78	161	26.8	6.0	13.5	7.4	24	476	0.6
LW27	25.8	20000	11563	9.6	3426	125.3	0.6	4.5	89.7	1326	6497	95.1
LW28	27.6	20000	52725	9.67	15212	618.9	0.0	0.2	384.1	5361	29646	552.5
LW29	25.2	420	379	8.6	61	10.9	7.6	27.3	1.5	10	253	6.6
RI30	23.3	530	583	8.66	56	12.0	20.9	42.1	1.5	16	409	25.0
RI31	21.5	180	174	7.83	15	4.8	5.2	16.8	1.6	4	125	1.0

Table 8.1: Major ions hydrochemical compositions (in mg/L) of the central MER waters from hot springs, geothermal wells, groundwater wells, lakes and rivers, in the Ziway-Shala basin. HS=Hot springs, WL=Groundwater wells, GW=Geothermal wells, LW= Lakes, RI= Rivers (ID: RI30=Meki, RI31=Ketar).

Type	T (°C)	EC	TDS	pH	Sr	Rb	Li	B	$\delta^{18}O$	δD	d=δD - 8*$\delta^{18}O$	$^{87}Sr/^{86}Sr$
HS1	96	4530	1830	8.36	0.445	0.203	0.506	2.890	-0.41	-0.95	2.33	0.7054
HS2	78	2040	1728	6.79	0.267	0.146	0.451	1.253	-3.03	-15.65	8.59	0.7048
HS3	93.4	14440	7919	8.16	0.179	0.107	0.388	4.635	2.49	20.65	0.73	0.7047
HS4	57.3	10570	7501	7.81	0.201	0.115	0.416	4.975	3.69	24.23	-5.29	0.7065
HS5	91.4	13190	6589	8	0.254	0.101	0.365	4.356	2.26	20.12	2.04	nm
HS6	52.6	1780	958	8.15	0.044	0.014	0.073	0.614	-0.40	2.84	6.04	0.7076
HS7	59.3	4630	3600	7.3	0.124	0.058	0.006	0.762	1.41	12.34	1.06	0.7046
HS8	51.8	4870	3896	8.16	0.055	0.038	0.060	0.930	1.18	12.92	3.48	0.7045
HS9	38.8	630	499	7.33	0.072	0.021	0.024	0.200	-3.36	-15.85	11.03	0.7058
HS10	62	3900	2766	6.96	0.066	0.053	0.427	2.099	-1.15	-3.36	5.84	0.7065
GW11	82	2160	1297	7.44	0.024	0.264	0.084	3.084	-4.65	-12.39	24.81	0.7054
GW12	85.6	4600	3051	8.17	0.032	0.382	0.716	3.391	-1.24	-9.31	0.61	0.7043
WL13	28.3	3360	3564	8.16	0.033	0.074	0.001	5.408	5.14	32.27	-8.85	nm
WL14	24.6	350	871	7.48	0.014	0.008	0.021	0.009	-3.35	-13.7	13.10	nm
WL15	22.5	220	211	8.25	0.046	0.001	0.013	0.007	-2.64	-9.13	11.99	nm
WL16	24	220	266	7.31	0.038	0.002	0.006	0.005	-2.49	-8.11	11.81	nm
WL17	23.2	1320	1252	8.14	0.020	0.002	0.028	0.029	3.21	23.1	-2.58	nm
WL18	25.2	490	489	7.82	0.188	0.001	0.015	0.027	-2.68	-10.99	10.45	nm
WL19	23.7	1770	12797	8.7	0.101	0.009	0.032	0.359	5.02	31.65	-8.51	nm
WL20	36.4	730	668	7.89	0.064	0.010	0.034	0.058	-3.54	-19.69	8.63	nm
WL21	32.3	2260	1952	7.64	0.122	0.012	0.056	0.664	-2.39	-12.01	7.11	nm
WL22	36	2390	1949	8.08	0.057	0.005	0.058	0.492	1.45	6.92	-4.68	nm
WL23	25.1	2750	2227	7.81	0.149	0.027	0.049	0.423	-2.1	-5.19	11.61	nm
WL24	25.3	300	267	7.83	0.054	0.007	0.013	0.000	-3.99	-19.03	12.89	0.7062
LW25	24.2	1730	1377	9.03	0.036	0.006	0.004	0.560	7.03	43.57	-12.67	nm
LW26	22.1	800	715	8.78	0.079	0.030	0.081	0.107	6.99	42.78	-13.14	nm
LW27	25.8	>20000	11563	9.6	0.057	0.054	0.014	3.861	3.98	26.19	-5.65	nm
LW28	27.6	>20000	52725	9.67	0.140	0.063	0.073	0.513	7.92	45.71	-17.65	nm
LW29	25.2	420	379	8.6	0.123	0.003	0.000	0.045	4.88	33.82	-5.22	nm
RI30	23.3	530	583	8.66	0.210	0.009	0.005	0.011	1.67	6.14	-7.22	nm
RI31	21.5	180	174	7.83	0.086	0.006	0.004	0.000	-2.76	-11.31	10.77	0.7063
Basalt												0.7063
Ignimbrite												0.7071

Table 8.2: $\delta^{18}O$, δD, $^{87}Sr/^{86}Sr$ isotopic signatures and trace elements (Sr, Rb, Li, and B) hydrochemical composition (in mg/L) of the central MER waters from hot springs, geothermal wells, groundwater wells, lakes and rivers, in Ziway-Shala basin. HS=Hot springs, WL=Groundwater wells, GW=Geothermal wells, LW= Lakes (LW25=Langano, LW26=Awasa, LW27=Shala, LW28=Abijata, LW29=Ziway), RI= Rivers (ID: RI30=Meki, RI31=Ketar), d is deuterium-excess= (δD -8*$\delta^{18}O$), nm=not measured.

The isotopic values of all water types are drown together with GMWL and LMWL (**Figure 8.3**).

It can be noted that all lake water samples lie below the LMWL. Abijata, Langano, and Awasa show extreme values, as a result of substantial evaporation enrichments relative to the present day precipitation. The lakes plot along the line with the equation ($\delta D = 4.9\delta^{18}O+8.3$).

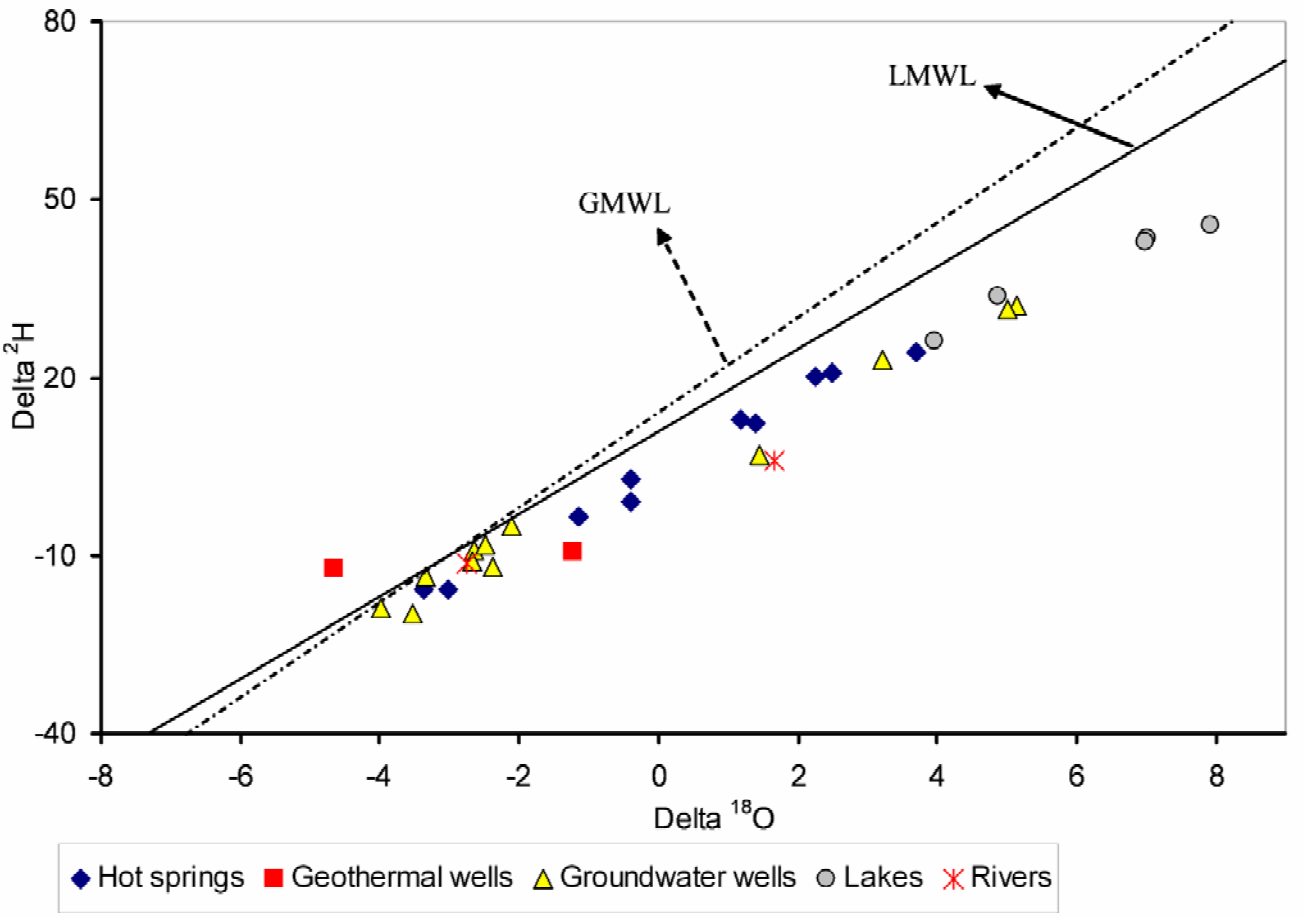

Figure 8.3: δD and $\delta^{18}O$ of the various water types compared with GMWL and LMWL

The two main rivers feeding Lake Ziway from the west side (Meki River; RI30) and east side (Ketar River; RI31) have compositions of $\delta^{18}O$ 1.67‰ and -2.76‰, and δD is 6.14‰ and -11.13‰ (VSMOW) respectively. The relative depletion of $\delta^{18}O$ and δD on Ketar River is most probably caused by the low evaporation effect of shorter drainage path relative to that of the Meki River.

Sample HS1, the hottest spring emerging from a geyser at Edo Laki Island of Northern Bay of Lake Langano, is relatively less depleted in stable isotopes, and likely suggests a possible mixing with the lake water.

On the contrary, hot spring HS2 at the shore of the Tulu Gudu island of Lake Ziway is depleted in δD and $\delta^{18}O$, showing a significant contribution of highlands meteoric water, although mixing of Lake Ziway is certainly expected. The island is a few kilometers away from the active Wenji Fault Belt

(WFB) fault system, at the eastern shore of the lake. This is the recharge zone for meteoric water coming from eastern plateau and the escarpment. The hot spring also shows high concentration of Ca^{2+} (11 mg/L) and Mg^{2+} (3.3 mg/L), which is typical characteristic of basaltic aquifer hosted groundwater from the highlands.

Groundwater wells WL14, WL15, WL16, WL18, WL20, WL23, and WL24, Ketar River (RI31), hot springs HS9 and HS2 lie on the LMWL suggesting that they are mainly recharged by meteoric waters coming from the highlands. Other groundwater wells and hot springs are deviated to the right side of LMWL. The δD and $\delta^{18}O$ enrichments on WL13, WL19, and WL22 suggest a significant subsurface outflow and mixing with Lake Ziway water. Coherently, WL13, WL19, and WL22 are groundwater wells with almost the same (δD, $\delta^{18}O$) value as Lake Ziway (LW29). The positive isotopic values of WL17 show that there exists a possible northward subsurface migration of Lake Awasa. Enrichments of HS3, HS4 and HS5 also show a significant contribution from Lake Shala.

Note that WL18, WL14, WL23 and WL24, are wells found at the north and northeastern side of Lake Ziway respectively. However depletion of WL14, WL18 and WL23 show no evidence of interaction with the lake water. WL24 (northeast of Lake Ziway) and WL21 (northeast of Aluto-Langano geothermal sites) are plausibly influenced by a fault zone where recharging and fast circulation of groundwater occur which in turn are reflected in the depleted isotopic signature of the wells.

The regional groundwater, flows from the flanks of the rift to the rift floor and subsequently towards discharge areas at the alkaline Lake Shala (Ayenew, 1998). The elevation difference between Lake Ziway (~1636 m) and Langano (~1582m) creates potential groundwater flows between the two lakes. However, δD and $\delta^{18}O$ signatures revealed that the Aluto volcanic complex seems to act as a barrier for Lake Ziway recharging into the geothermal system. Deep geothermal wells (GW11 and GW12) have δD and $\delta^{18}O$ similar to the wells in the eastern side of Lake Ziway. The depletion of the geothermal wells indicates that the contribution of highly evaporated (isotopically enriched) water from Lake Ziway in recharging the geothermal system is negligible.

On the other hand, HS10 is the hot spring north of Lake Langano is relatively enriched and it can be due to flow of Lake Ziway around the western rim of the Aluto volcanics. WL21 which is at southern side of Lake Ziway has depleted δD and $\delta^{18}O$, further confirms the unlikely southward flow of the lake.

Cl^- is used as a tracer in the hydrologic system due to its conservative geochemical behavior in natural waters (Feth, 1981). Its concentration and variation is entirely source related. δD (also tend to be conservative) and δD and/or $\delta^{18}O$ versus Cl^- (Cl^-/B) ratio plot discriminate waters having similar

behavior with their distinct geographic area (**Figure 8.4, 8.5, 8.6**). The asymmetrical grouping suggests different fluid reservoirs located at different spatial zone with a noticeable mixing with the lakes. K vs B (**Figure 8.7**) and Li vs F (figure not shown) used similarly to discriminate the different groups of waters. The lithium content of the hot springs is controlled by the character of the adjacent rocks. Thermal springs emerging from basaltic environment are poor in Li (e.g at the Shore of Chitu (HS7; 6.4 µg/L)), whereas hot springs in contact with acidic rocks are enriched in Li, (from the northern shore of Lake Langano (HS1; 506 µg/L).

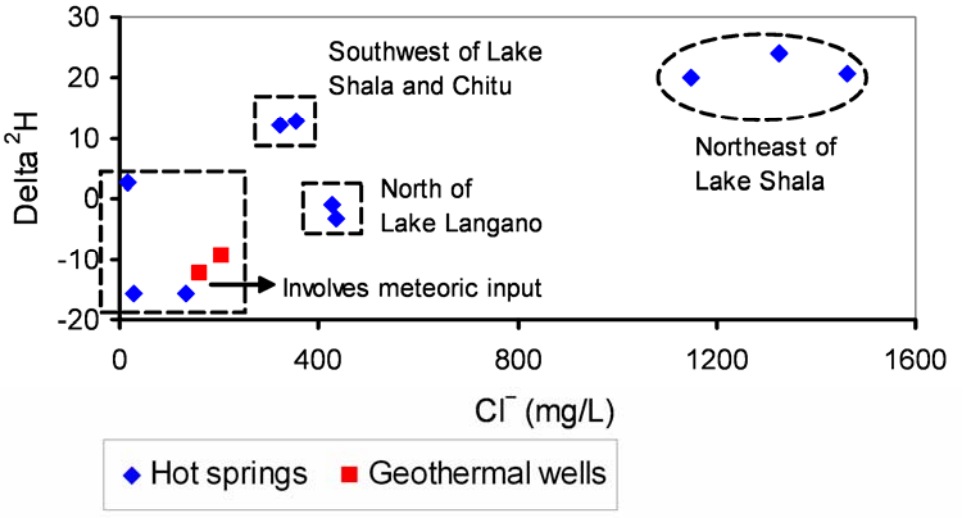

Figure 8.4: Delta ^{2}H versus Cl^- ratio in the hydrothermal waters of the central MER

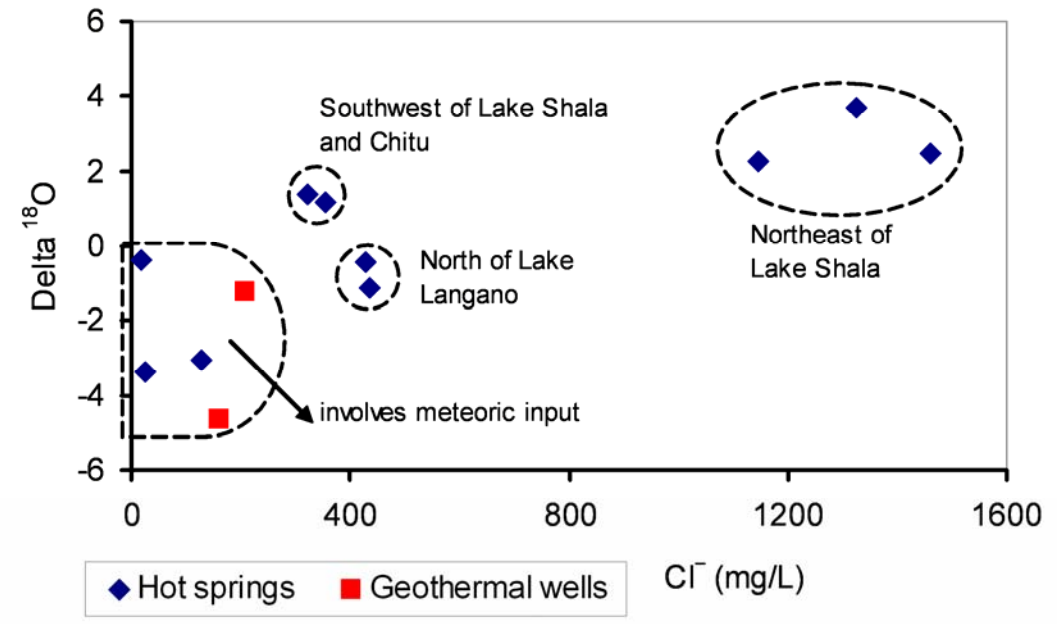

Figure 8.5: Delta ^{18}O versus Cl^- in the hydrothermal waters of the central MER

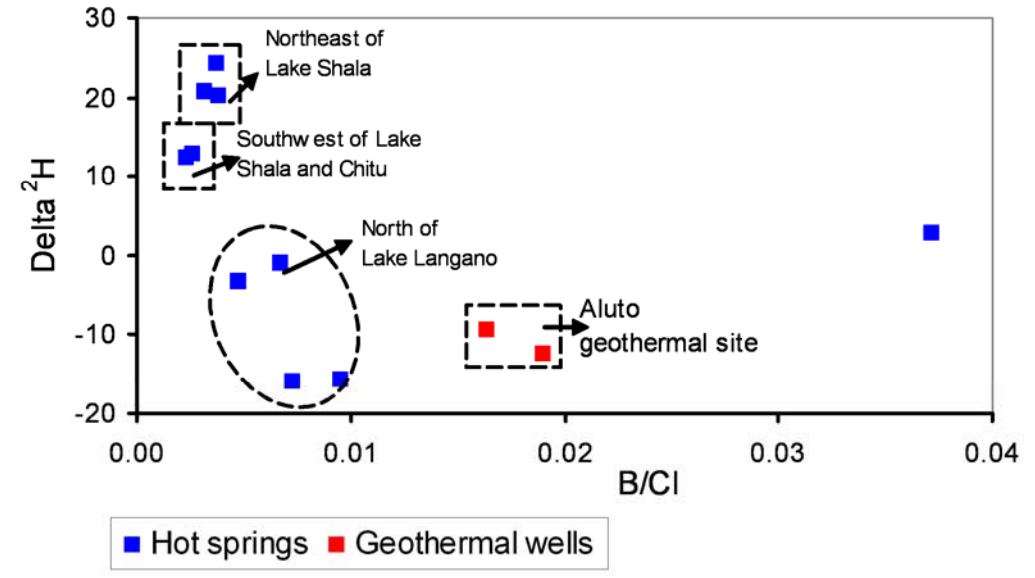

Figure 8.6: Delta ^{2}H versus B/Cl ratio of hydrothermal waters of the central MER

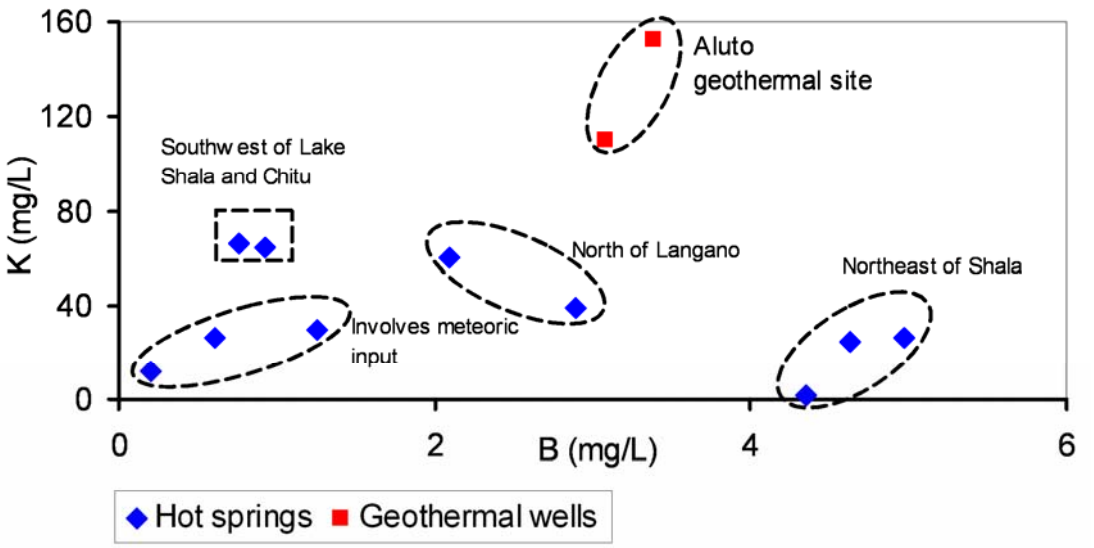

Figure 8.7: K versus B in the hydrothermal waters of the central MER

Dissolved strontium isotopic ratios ($^{87}Sr/^{86}Sr$) ranges from 0.7045 to 0.7076 in the hot springs, and the two deep geothermal wells have 0.7043 and 0.7054. These data are compared with the $^{87}Sr/^{86}Sr$ values of 2 representative volcanic rocks of an ignimbrite and a basalt that are 0.7071 and 0.7063 respectively. The latter integrate a data set provided by (Trua, 1999) that reported Sr isotopic values of some basalt samples from the rift floor and escarpments (0.7039-0.7051) and from the highland (Chilalo volcanics; 0.7044-0.7047).

The diversity in strontium isotopic ratios in waters is probably caused by complex mixings, interactions with multiple lithotypes and different degree of water-rock/sediment interactions.

It can be summarized that the Sr isotopic signatures of MER lithotypes, basalts and rhyolites, are overlapped to each other. This suggests that they are genetically linked as it is described by (Peccerillo et al. 2007), resulting from differentiation processes of mantle-melts progressively affected by crustal contamination.

The isotopic ratios of the dissolved strontium of natural MER waters lie in the ranges of basaltic rocks from the highlands and basaltic and rhyolitic rocks from the rift, showing interaction either with basalt or rhyolites or both, as well as complex mixing processes.

In this light, the less radiogenic Sr isotope ratio probably offers evidence of quick recharge from highland groundwater.

For example HS9 that among hot springs that has the lowest temperature (39 ^{o}C), TDS and fluoride, and highest $Ca^{2+}$and Mg^{2+}, is characterized by $^{87}Sr/^{86}Sr < 0.706$ which indicates a significant contribution of meteoric water recharged through tectonic structures of the WFB. This hot spring has similar ionic characteristics and isotopic signatures of some shallow wells northeast (e.g. WL24; 35m) and southeast (e.g. WL21; 54m) of Lake Ziway. Hot spring HS2 have very similar δD and $\delta^{18}O$ and a very low $^{87}Sr/^{86}Sr$ (0.7048) further indicating the influence of tectonic discontinuities (WFB) in promoting fast water circulations that are feeding hot springs, groundwater and geothermal wells of this sector.

North Langano hot spring HS10, has more radiogenic Sr isotopic signature (0.7065), is most probably indicating slow circulation and a higher interaction with the MER rhyolitic rocks and their derived sediments.

HS7 (hot spring near Lake Chitu) and HS8 (hot spring near SW of Lake Shala), both have similar δD, $\delta^{18}O$, and Sr isotope, suggesting that they are emerging out from the same aquifer with some level of mixing with the highly evaporated Chitu and Shala Lake. Both also show similar major anions and cations with the exception of different Ca^{2+} and Mg^{2+}. The higher Ca^{2+} and Mg^{2+} of hot spring of the Chitu is likely caused by an interaction with the near by basaltic lava flow. The interaction with the basalt is probably responsible for the less radiogenic Sr isotopic value (0.7046).

GW11 and GW12 were drilled along NNE-SSW trending WFB (Wenji Fault Belts). The depleted δD and $\delta^{18}O$ values on the geothermal wells are similar to those wells at eastern escarpment and highland that are of meteoric in origin. The lesser Sr isotope value of well GW12 (0.7043) and GW11 (0.7054) is probably controlled by the lesser radiogenic recharging water infiltrated from WFB.

The K and Rb content of geothermal waters (GW11 and GW12) are significantly higher than the rest of the hot springs. It is probably caused by cation exchange processes where K is released in the fluids at higher temperature. The high K content is expected to be accompanied by the release of Rb due to similar chemical behaviour. **Figure 8.8** shows Sr isotopes of hot springs and geothermal wells versus Rb/Sr ratio.

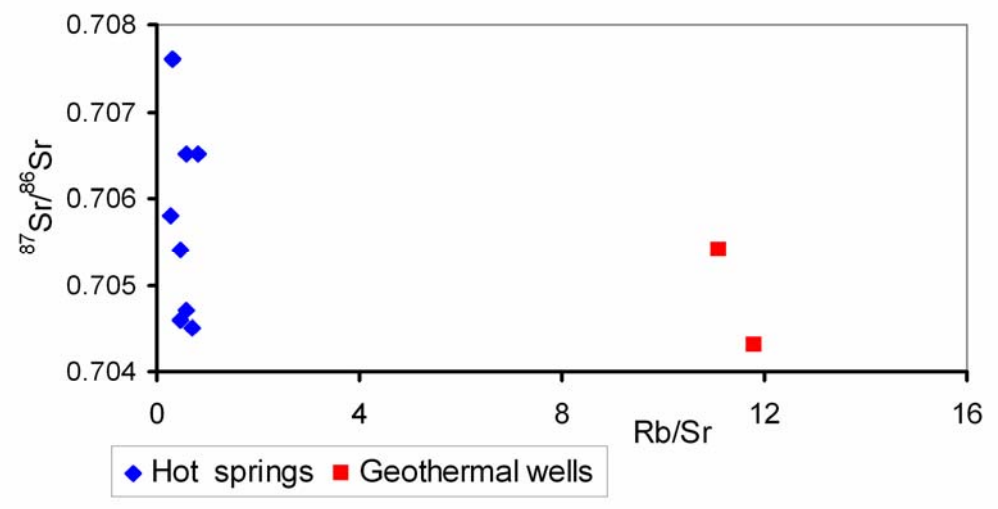

Figure 8.8: Sr isotope versus Rb/Sr ratio in the hydrothermal waters of the central MER

These results are summarized in **Figure 8.9 and 8.10** reporting the direction of the general groundwater flow.

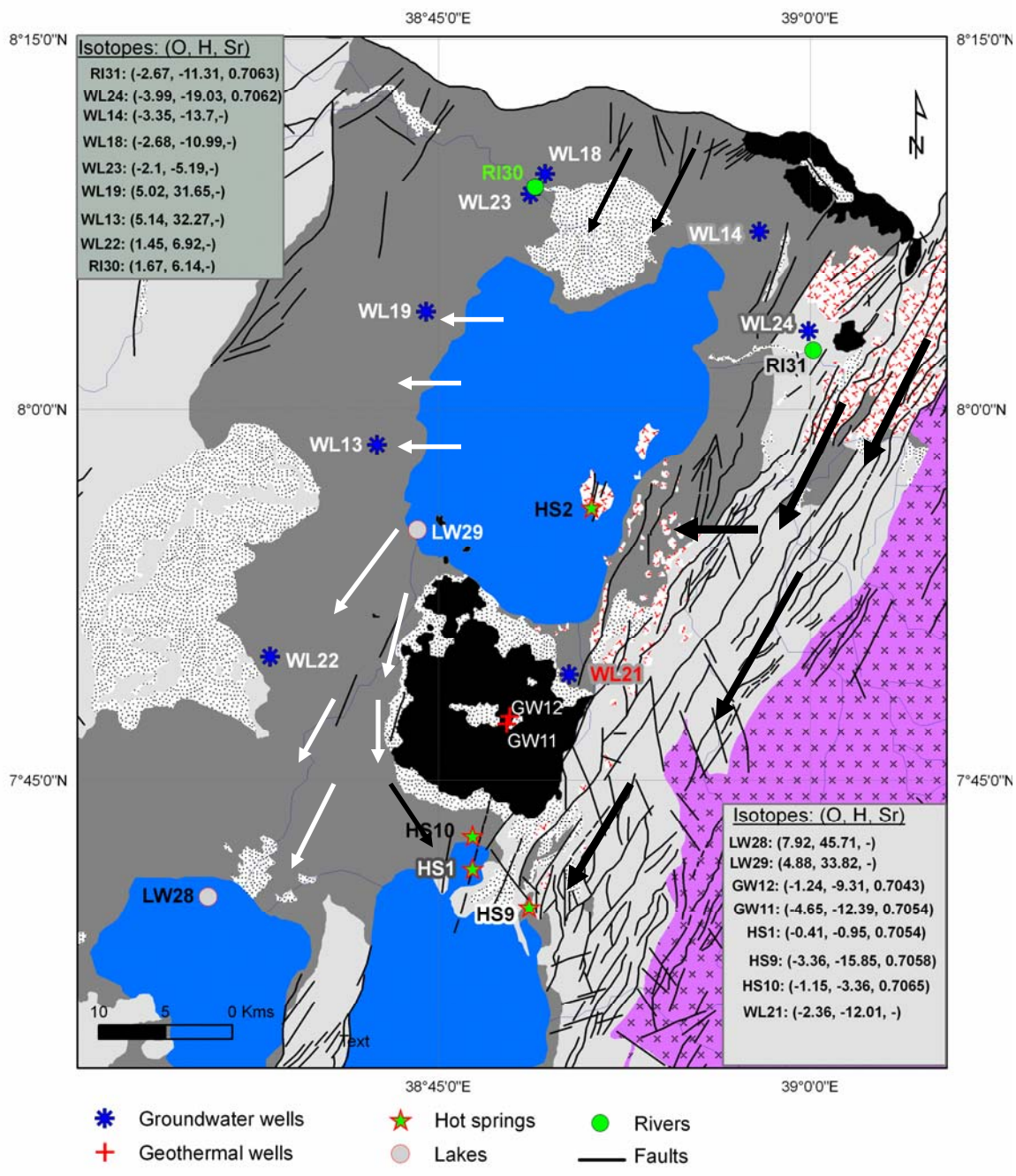

Figure 8.9: Regional groundwater flow directions at the upper part of central MER in Ziway-Shala basin.

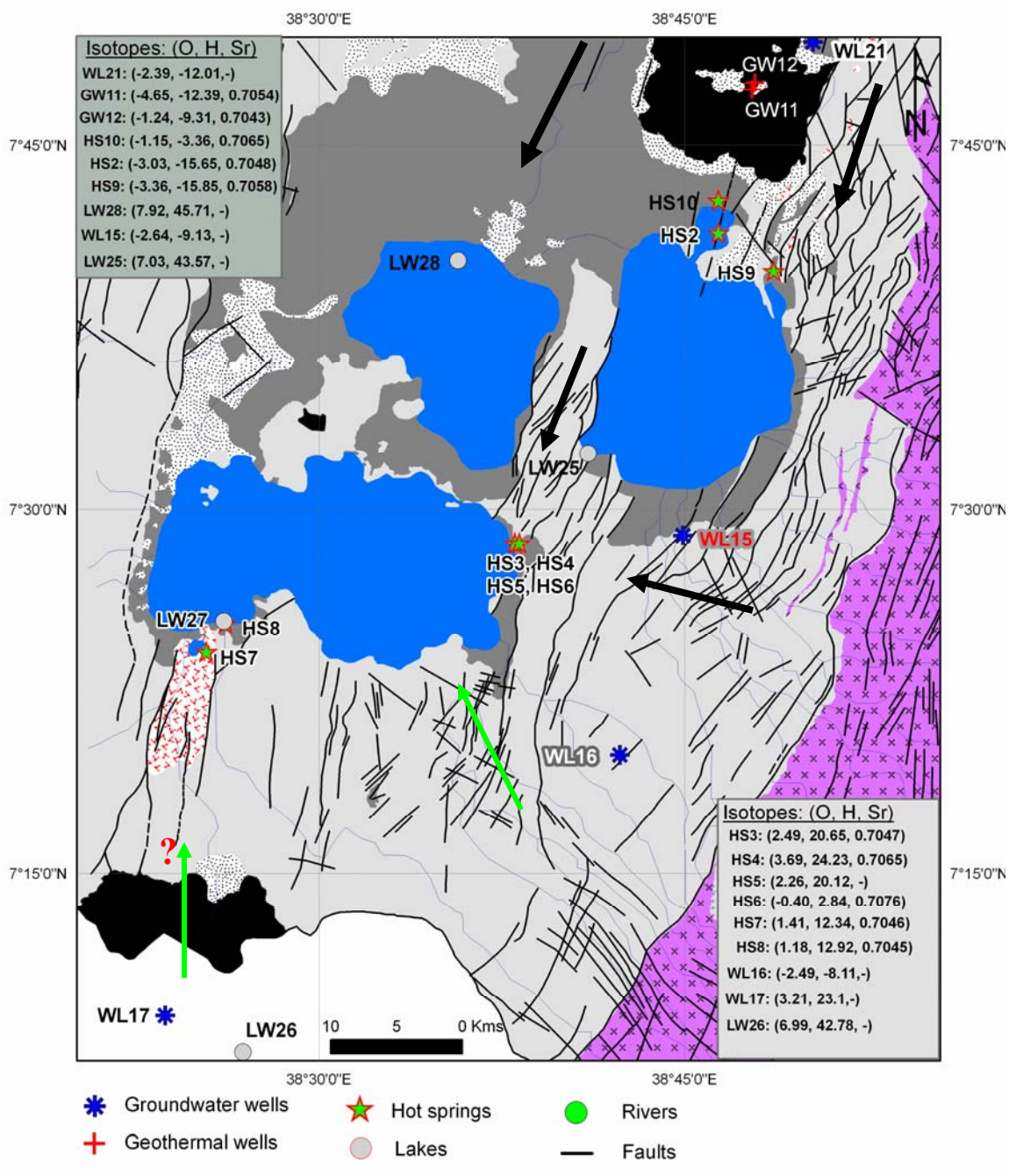

Figure 8.10: Regional groundwater flow directions at the lower part of the central MER in Ziway-Shala basin.

Generally, it can be summarized that the general geochemical evolution of rift waters begins from eastern and western highlands following the regional groundwater flow direction; the pristine waters coming from the highlands should display isotopic compositions characterized by less radiogenic $^{87}Sr/^{86}Sr$ (and more depleted δD, $\delta^{18}O$). This isotopic signature subsequently evolves toward higher $^{87}Sr/^{86}Sr$ for an interaction with the more radiogenic rhyolites of the rift and their weathered and redeposited products.

As future developments, in order to further understand the complex hydrogeochemical system with respect to water-rock interactions, groundwater geochemistry, mechanisms of groundwater recharge and flow pattern, we suggest a multidisciplinary approach, using geochemical (major, trace and rare earth elements) and isotopic data (^{3}H, $^{3}H/^{3}He$, ^{14}C, ^{2}H, ^{18}O, $^{87}Sr/^{86}Sr$).

Conclusions and recommendations

The geochemical composition on natural waters of the central MER in Ziway-Shala basin has been investigated in order to understand the source, genesis and distribution of chemical elements with particular emphases to fluoride.

In this framework we performed an integrated study of both waters and coexisting representative solid aquifer matrixes in the Ziway-Shala lakes basin of the Ethiopian rift valley, in order to unravel the water-rock/sediment interactions that ultimately lead to the peculiar geochemical features of the Ethiopian rift waters. Therefore, the hydrochemical investigation was coupled with the mineralogical/geochemical characterization of the lithologies outcropping in the area. Moreover, laboratory leaching tests (batch and column) were also carried out to evaluate the potential release of fluoride from the various rock/sediment types. These approaches serve to understand the lithologic sources and the enrichment mechanisms controlling the anomalous fluoride content in the water.

The geochemical anomalies in the studied natural waters are predominantly linked to the mode of emplacement of volcanism in the Ethiopian Rift system. The general hydrochemical evolution, in which $Ca^{2+}(Mg^{2+})$-HCO_3^- waters, typical of the highlands, are transformed along the flow path into alkaline pH and Na^+-HCO_3^- waters (typical of the rift area), is clearly related to water-rock/sediment interactions, is probably triggered/favoured by the high geothermal gradient and the high activity of CO_2 that characterize the rift valley. In these interactions, the matrixes are mainly rhyolites consisting of volcanic glass (usually more than 95% in proportion). This glassy material is extremely reactive, and its weathering products (i.e. the fluvio-volcano lacustrine sediments) can further concentrate geochemical elements. Therefore, the interaction of these "reworked" volcanic products with water and carbon dioxide (juvenile?) progressively lead to a "secondary" clay-bearing mineral assemblage that and under high pH conditions can release some chemical species (e.g. F^-, As) into the interacting water.

A comparison of major and trace element concentrations of MER natural waters with standards set by three authorities (WHO, EU directives, USEPA), indicated significant quality problems (in all water groups at different percent proportions). F^-

Likewise, the comparison was extended to the experimental leachates (from batch experiments on rocks and sediments), showing that the concentration of elements potentially affecting health such as F, As, Fe, Al, Mo, and U are often beyond the admissible limits. These comparisons simply define the higher relative vulnerability of natural waters to the above mentioned elements in the region.

Together with the renowned F^- problem, the possible presence of geochemical anomalies in As, B, Mo, V, U, Al, Fe, and Mn have to be taken into consideration in water quality issues. Furthermore, future work has to be done to investigate their possible health impact on the population of MER and other sectors of the east African rift.

Column experiments were also conducted on volcanic ash (vitric ash) materials after separating into different grain size fractions (fine ash, coarse ash and raw ash) to characterize the behaviour of fluoride under flushing of synthetic rain water. The result showed that high concentrations of fluoride were leached out particularly from the fine ash fraction which in turn suggests pyroclastic materials are the ultimate reservoir of fluoride.

Understanding the distribution and geochemistry of fluorine, arsenic and related elements along with their tolerance thresholds is essential in identifying high-risk areas and for the development of adequate remediation technologies, particularly where people live in scattered villages across the basin. However, considering that water treatments are expensive and barely efficient, we suggest avoiding (as far as possible) the drilling of new wells especially a) in those areas characterized by the presence of fluvio-lacustrine sediments b) close to the outpouring of hot springs. In any case activation of new wells should be preceded by chemical analysis including the above mentioned critical elements.

Moreover, we suggest starting to plan new strategies for water exploitation in the highlands (where elemental concentrations (such as F^- and As are typically low). This is mainly important for water supply of towns. These aqueduct infrastructures would imply an initial investment, but would be cost-effective in the long-term.

The stable $\delta^{18}O$, δD and radiogenic ($^{87}Sr/^{86}Sr$) isotopic composition indicate different ranges of stable isotopic values were recorded for different water groups. The Sr isotope signatures are typical of water interacted with the main lithotypes covering the study area. Generally, the result shows that there exists a complex surface water and groundwater interactions that is reflected on a diversity of the stable and Sr isotopic signature in waters.

The general geochemical evolution of rift waters begins from eastern and western highlands following the regional groundwater flow direction; the pristine waters coming from the highlands should display isotopic compositions characterized by less radiogenic $^{87}Sr/^{86}Sr$ (and more depleted δD, $\delta^{18}O$). This isotopic signature subsequently evolves toward higher $^{87}Sr/^{86}Sr$ for an interaction with the more radiogenic rhyolites of the rift and their weathered and redeposited products.

The preliminary results of this study has showed that there is a need for future extended works on the geochemistry of solid samples (rocks, sediments and soils) as well as in waters. These studies should investigate a wide spectrum of chemical elements including all the components that are potentially detrimental to human health and environment, in order to establish baseline geochemical atlases of the region.

Furthermore, from a water resource point of view, the following work must focus on a comprehensive study of various isotopes and geochemical data to constrain groundwater age dating, water-rock interaction and flow path and thus help to model and systematize the hydrologic cycles in the basin.

References

Adriano DC. Trace Elements in Terrestrial Ecosystems, Springer Verlag, New York 1986. pp. 533.

AG Consult, Consulting Hydrogeologists and Engineers Plc. Butajera-Ziway area development study, report, Addis Ababa, Ethiopia 2006; pp. 100.

Allard P, Aiuppa A, Loyer H, Carrot F, Gaudry A, Pinte G, Michel A, Dongarra G. Acid gas and metal emission rates during long-lived basalt degassing at Stromboli volcano. Geophysical Research Letters 2000; 27 (8):1207−1210.

Allison JD, Brown DS, and Novo-Gradac KJ. MINTEQA2/PRODEFA2, A geochemical assessment model for environmental systems, version 3.0 user's manual: Environmental Research Laboratory, Office of Research and Development, U.S. Environmental Protection Agency, Athens, Georgia 1990, pp.106.

Anawar HM, Akai J, Komaki K, Terao H, Yoshioka T, Ishizuka T, Safiullah S, Kato K. Geochemical occurrence of arsenic in groundwater of Bangladesh: sources and mobilization processes. J. Geochem. Explorat. 2003;77:109−131.

Anawar HM, Akai J, Sakugawa H. Mobilization of arsenic from subsurface sediments by effect of bicarbonate ions in groundwater. Chemosphere 2004; 54:753−762.

Appelo, C.A.J., Willemsen, A., Beekman, H. E. And Griffioen, J. Geochemical calculations and observations on salt water intrusions. II validation of a geochemical transport model with column experiments. J. of Hydrology 1990; 120, 225-250.

Appelo CAJ, Van der Weiden MJJ, Tournasst C, Charlet L, Surface Complexation of ferrous iron and carbonate on ferrihydrite and the mobilization of arsenic. Environ Sci Technol 2002;36:3096−103.

Appelo CAJ, Postma D. Geochemistry, groundwater and pollution, 2nd Edition, Balkema, Rotterdam, The Netherlands, 2005; pp. 649.

Armienta MA, Martin-Del-Pozzo AL, Espinasa R, Cruz O, Ceniceros N, Aguayo A, Butron MA. Geochemistry of ash leachates during the 1994−1996 activity of Popocatepetl volcano. Appl. Geochem. 1998; 13:841−850.

Armienta MA, De la Cruz-Reyna S, Morton O, Cruz O, Ceniceros N. Chemical variations of tephra-fall deposit leachates for three eruptions from Popocatepetl volcano. Journal of Volcanology and Geothermal Research 2002;113: 61-80.

Ashely PP, Burley MJ. Control on the occurrence of fluoride in groundwater in the rift valley of Ethiopia. In Nash H, McCall GJH, (eds) "Groundwater Quality", Chapman and Hall, 1994; pp. 45-54

Ayenew T. The hydrogeological system of the Lake District Basin, Central Main Ethiopian Rift. PhD Thesis, Free University of Amsterdam, The Netherlands, 1998.

Ayenew T. Major ions composition of the groundwater and surface water systems and their geological and geochemical controls in the Ethiopian volcanic terrain. SINET, Ethiopian Journal of Science 2005; 28(2):171-188.

Ayenew T. The distribution and hydrogeological controls of fluoride in the groundwater of central Ethiopian rift and adjacent highlands. Environmental Geology 2008; 54: 1313-1324.

Ball JW and Nordstrom DK. WATEQ4F-User's manual with revised thermodynamic data base and test cases for calculating speciation of major, trace and redox elements in natural waters: U.S. Geological Survey Open-File Report 1991; 90−129, pp.185.

Barberi F, Ferrara G, Santacroce R and Varet J, Structural evolution of the Afar triple junction. West Germany, Scwheizerbart 1975; pp 38-54.

Berhe SM, Desta B, Nicoletti M and Teferra M. Geology, geochronology and geodynamic implications of the Cenozoic magmatic province in western and southeast Ethiopia. Geologic society of London Journal 1987; 144:213-226.

Benvenuti M, Carnicelli S, Belluomini G, Dainelli N, Di Grazia S, Ferrari GA, Iasio C, Sagri M, Ventra D, Balemwald Atnafu, Seifu Kebede. The Ziway-Shala basin (Main Ethiopian Rift, Ethiopia): a revision of basin evolution with special reference to the late quaternary. Journal of African Earth Sciences 2002; 35:247-269.

Ben Othman D, Luck JM, Tournoud MG. Geochemistryand water dynamics: application to short time-scale flood phenomena in a small Mediterranean catchment: I. alkalis, alkali−earths and Sr isotopes. Chem. Geol. 1997; 140:9−28.

Bhattacharya P, Claesson M, Bundschuh J, Sracek O, Fagerberg J, Jacks G, Martin RA, Storniolo A, Thir JM. Distribution and mobility of arsenic in the Rio Dulce alluvial aquifers in Santiago del Estero Province, Argentina. Sci. Total Environ. 2006; 358:97−120.

Brusseau ML, Rao PSC, Jessup RE and Davidson JM. Flow interruption: a method for investigating sorption non-equilibrium. Journal of Contaminant Hydrology 1989; 4:223−240.

Brusseau ML, Hu Q, Srivastava R. Using flow interruption to identify factors causing non-ideal contaminant transport. J. Contam. Hydrol 1997; 24:205−219.

Bundschuh J, Farias B, Martin R, Storniolo A, Bhattacharya P, Cortes J, Bonorino G, Albouy, R. Groundwater arsenic in the Chaco-Pampean Plain, Argentina: Case study from Robles County, Santiago del Estero Province. Appl. Geochem. 2004; 19(2): 231-243.

Calderoni G, Masi U, Petrone V. Chemical features of spring waters from the East African Rift. A reconnaissance study. In: Abbate E, Sagri M, Sassi PP (eds) Geology, mineral resources of Somalia and surrounding regions. Istituto Agronomico Oltremare, Firenze 1993; pp. 699-710.

Castro E, Schulz C, Mariño E. El agua potable en la provincia de La Pampa. Consecuencias por la presencia de flúor y arsénico. 2da Reunión Geología Ambiental. Actas, San Salvador de Jujuy, Argentina 1998; pp. 43−55 (in Spanish).

Chalié F, and Gasse F. Late Glacial-Holocene diatom record of water chemistry and lake level change from the tropical East African Rift Lake Abiyata (Ethiopia).Paleo, Paleo, Paleo, 2002; 187:259-283.

Chernet T. Hydrogeology of the lakes region, Ethiopia (Lakes Ziway, Langano, Abitata, Shalla and Awassa). In: The Provisional Military Government of Socialist Ethiopia-Ministry of Mines and Energy, Ethiopian Institute of Geological Surveys, Addis Ababa 1982 pp. 97.

Chernet T, Travi Y. Preliminary observations concerning the genesis of high flouride contents in the Ethiopian Rift. In: Thorweiche U, Schandlmeier H (eds) Geoscientific research in Northeast Africa, Balkema, Rotterdam 1993; 8:651−654.

Chernet T. Etude des me´ canismes de mine´ ralisation en fluorure et e´ le´ ments associe´ s de la re´ gion des lacs du rift Ethiopien, The` se Doctorat, Universite´ d'Avignon 1998; pp. 210.

Chernet T, Travi Y, Valles V. Mechanism of degradation of the quality of natural water in the lakes region of the Ethiopian rift valley. Water Res 2001; 35(12):2819−2832.

Christensen, T.H., Bjerg, P.L., Banwart, S. A., Jakobsen, R., Heron, G., Albrechtsen, H.,. Characterization of redox conditions in groundwater contaminant plumes. J. Contam.Hydrol., 2000; 45: 165-241.

Clark ID, and Fritz P. Environmental isotopes in hydrogeology, pp 328, CRC Press/Lewis Publishers, Boca Raton FL 1997.

Claesson M, Fagerberg J. Arsenic in groundwater of Santiago del Estero. Argentina. Sources, mobilization, controls and remediation with natural materials. Minor Field Studies Scholarship Programme MFS, Royal Institute of Technology (KTH), Stockholm 2003; pp. 62.

Coplen TB. Uses of environmental isotopes. In Regional groundwater quality, ed. W.M.Alley, pp 227-254. Van Nostrand Reinhold, New York 1993.

Costigan M, Cary R, Dobson S. Vanadium Pentoxide and other Inorganic Vanadium Compounds. Concise International Chemical Assessment Document 29. World Health Organization 2001; pp.1−69.

Cook P, Herczeg AL. Environmental tracers in subsystem hydrology. New York: Kluwer Academic Publishers; 2000.

Craig H. Isotopic variations in meteoric waters. Science 1961; 123, 1702−1703.

Cullen WR, Reimer KJ. Arsenic speciation in the environment. Chem. Rev. 1989; 89:pp. 713−764.

Dainelli N, Benvenuti M, Sagri M. Geological map of the Ziway-Shala lakes basin (Ethiopia). 1:250000, Italian Ministry for university and scientific and technological Research (MURST) 2001.

Darling G, Gizaw B, Arusei M. Lake-groundwater relationships and fluid-rock interaction in the East African Rift Valley: isotopic evidence. Journal of African Earth Sciences 1996; 22:423-430.

Dansgaard, W. Stable Isotopes in Precipitation. Tellus 1964; XVI(4):436-468.

Di Paola GM. The Ethiopian Rift Valley (between 7°00' and 8°40' lat. north). Bulletin Volcanology 1972; 36:517-560

Dissanayaka CB The fluoride problem in the groundwater of Sri Lanka. Environmental Management and Health. Int J of Environ Stud 1991; 38:137-156.

Davidson A, Rex D. Age of volcanism and rifting in southwestern Ethiopia. Nature 1980; 283:657−658.

Deer WA, Howie RA, Zussman J. An introduction to the rock-forming minerals. Wiley, New York 1992; 2 edn. p. 720.

Drever IJ. The Geochemistry of Natural Waters: Surface and Groundwater Environments, 3rd ed. Prentice Hall, New Jersey 1997.

Ebinger CJ, Yemane T, WoldeGabriel G, Aronson JL and Walter RC. Late Eocene-Recent volcanism and Faulting in the southern Main Ethiopian Rift. Journal of the Geological Society, London 1993; 150:99-108.

Edenborn HM, Belzile N, Mucci A, Lebel J, Silverberg N. Observations on the Diagenetic Behavior of Arsenic in a Deep Coastal Sediment, Biogeochemistry, 1986; Vol. 2, No. 4, pp. 359−376.

Edmunds M, Smedley P. Fluoride in natural waters. In Selinus O. et al. (eds) "Essentials of Medical geology: the Impacts of Natural Environment on Public Health". Elsevier Academic Press 2005; pp. 301-329.

Eriksson Nils, Archana Gupta, Georgia Destouni. Comparative analysis of laboratory and field tracer tests for investigating preferential flow and transport in mining waste rock. Journal of Hydrology 1997;194, 143−163

Epstein S, and Mayeda T. Variation of ^{18}O content of waters from natural sources, Geochim. Cosmochim. Acta 4 1953; pp. 213−224.

Ethiopian Mapping Authority. National Atlas of Ethiopia. EMA, Addis Abeba 1988.

European Union. Council Directive 98/83/EC of 3 November 1998 on the quality of water intended for human consumption. Official Journal of the European Community 1998; pp. L330/32-L330/54.

Faure G. Principles of isotope geology. Wiley, New York 1986; 589 pp.

FAO/UNESCO. Soil Map of the World. Vol. VI, Africa. UNESCO, Parix 1977; xiv, 299pp.

Feth JH. Chloride in natural continental water: U.S. Geological Survey Water Supply Paper 2176, 1981; 36 pp.

Fetter, C. W. Applied Hydrogeology, 4rd Edition. Macmillan College, New York, 2004; 691 pp.

Frape SK, Blyth A, Blomqvist R, Mcnutt RH and Gascoyne M. Deep fluids in continents: II Crystalline rocks, In surface and groundwater, weathering, and Soils (ed. J.I. Drever) Vol. 5. Treatise on Geochemistry (eds. H.D. Holland and K.K. Turekian), Elsevier-Pergamon, Oxford 2003; pp. 541-580.

Foster AL. Spectroscopic investigation of arsenic species in solid phases. In: Welch AH, Stollenwerk KG, editors. Arsenic in ground water: geochemistry and occurrence. Kluwer Academic Publishers, Boston, 2003; pp.27−65.

Gat JR and Dansgaard W. Stable isotopes survey of the fresh water occurrence in Israel and the northern Jordan Rift Valley. Journal of Hydrology 1972; 16:117-212.

Gat JR, Bowser CJ and Kendall C. The Contribution of Evaporation From the Great Lakes to the Continental Atmosphere: Estimate Based on Stable Isotope Data. Geophys Res Letters 1994; 21:557-560.

Gashaw H. Hydrogeochemistry of waters in Lake Ziway area, Integrated Development for Water Supply and Sanitation, 25th WEDC Conference, Ethiopia 1999.

Gat JR. Oxygen and Hydrogen Isotopes in the Hydrologic Cycle. Annu. Rev. Earth Planet Sci. 1996; 24:225-262.

Giggenback WF. Chemical composition of volcanic gases. In: Scarpa RW, Tilling R.I. (eds.), Monitoring and Mitigation of Volcanic Hazards. Springer, Berlin 1996; pp. 221-256.

Gizaw B. The origin of high bicarbonate and fluoride concentrations in waters of the Main Ethiopian Rift Valley, East African Rift System. Journal of African Earth Sciences 1996; 22(4):391-402.

Gianelli, G., Teklemariam, M. Water-rock interaction processes in the Alutu-Langano Geothermal Field (Ethiopia). Journal Volcanism and Geothermal Research 1993; 56, 429−445.

Goldberg S, Glaubig RA. Anion sorption on a calcareous, montmorillonitic soil−arsenic. Soil Sci. Soc. Am. J. 1988; 52:1297−1300.

Goldstein SJ, Jacobsen SB. The Nd and Sr Isotopic systematics of river water dissolved material: implications for the sources of Nd and Sr in seawater. Chem. Geol. 1987; 66:245−272.

Gregory N. Toxicity hazards arising from volcanic activity. Surveillance 1996; 23(2): 14-15.

Grech P. Fluorosis in young persons: further survey in northern Tanganyika, Tanzania. Brit J Radiol 1966; 39:761−764.

Griffioen, J. Cation-exchange and carbonate chemistry in aquifers following groundwater flow. Ph. D. thesis, Free University, Amsterdam, 1992; 182 pp.

Guo Q, Wang Y, Ma T, Ma R. Geochemical processes controlling the elevated fluoride concentrations in groundwaters of the Taiyuan Basin, Northern China. Journal of Geochemical Exploration 2007; 93:1-12.

Haynes V, Haas H. Southern Methodist University radiocarbon date list. Radiocarbon 1974;16:368−380.

Hart W K, WoldeGabriel G, Walter RC and Mertzman SA. Basaltic volcanism in Ethiopia: Constraints on continenetal rifting and mantle interaction. Journal Geophys. Res. 1989; 94:7731-7748,.

Harbaugh AW, Banta ER, Hill MC and McDonald MG. MODFLOW-2000, The U.S. G. S. modular ground-water model User guide to modularization concepts and the ground-water flow process, U. S. G. S., Open-file report 2000; 00-92.

Hidalgo MC, Cruz-Sanjulian J. Groundwaters composition, hydrochemical evolution and mass transfer in a regional detrital aquifer (Baza basin, southern Spain). Applied Geochemistry 2001; 16:745-758.

Hinkle SR, Polette DJ. Arsenic in ground water of the Willamette Basin, Oregon. Water-Resources Investigations Report 98−4205, Water Resources Dept., Geological Survey (U.S.) 1999.

Horita J, Ueda A, Mizukami K and Takatori I. Automatic δD and δ18O analyses of multi-water samples using H2− and CO2−water equilibration methods with a common equilibration set-up, Appl. Radiat. Isot. 1989; 40, pp. 801−805.

Hofmann C, Courtillot V, Fe´raud G, Rochette P, Yirgu G, Ketefo E, Pik R. Timing of the Ethiopian flood basalts event and implications for plume birth and global change. Nature 1997; 389:838−841.

Kazmin V, Seife MB, Nicoletti N, Petruccini C. Evolution of the Northern Part of the Ethiopian Rift. In: Geodynamic Evolution of the Afro-Arabic Rift System, Accad. Naz. Lincei, Roma, Atti Convegni 1980; 47, pp. 275−292.

Kilham P, Hecky RE. Fluoride: Geochemical and Ecological significance in East African Waters and Sediments. Liminology and Oceanography 1973; 18(6):932-945

Kim MJ, Nriagu J, Haack S. Carbonate ions and arsenic dissolution by groundwater. Environ. Sci. Technol. 2000; 34:3094−3100.

Kim MJ, Nriagu J, Haack S. Arsenic behaviour in newly drilled wells. Chemosphere 2003; 52:623−633.

King RB, Birchall CJ. Land systems and soils of the southern Rift Valley, Ethiopia. Land Resource Report No. 5. LRD, Ministry of Overseas Development, Surbiton 1975; 37pp.

Kloos H, Tekle-Haimanot R. Distribution of fluoride and fluorosis in Ethiopia and prospects for control. Tropical Medicine and International Health 1999; 4:355-364.

Korme T, Chorowicz J, Collet B, Bonavia FF. Volcanic vents rooted on extension fractures and their geodynamic implications in the Ethiopian Rift, J. of Volcanology and Geothermal Research 1997; 79, pp. 205-222.

Ladeira AC, Ciminelli VS. Adsorption and desorption of arsenic on an oxisol and its constituents. Water Reso 2004; 38(8), 2087−2094.

Langelier WF, Ludwig HF. Graphical methods for indicating the mineral character of natural waters. J. Am. Water Work Assoc. 1942; 34:335−352.

Laury RL, Albritton CC. Geology of the Middle Stone Age archaeological sites in the Main Ethiopian Rift Valley. Geological Society of America Bulletin 1975; 86:999−1011.

Le Turdu C, Tiercelin JJ, Gibert E, Travi Y, Lezzar KE, Richert JP, Massault M, Gasse F, Bonnefille R, Decobert M, Gensous B, Jeudy V, Tamrat E, Umer M, Martens K, Atnafu B. The Ziway-Shala lake basin system, Main Ethiopian Rift: Influence of volcanism, tectonics, and climatic forcing on basin formation and sedimentation. Palaeogeography, Palaeoclimatology, Palaeoecology 1999; 150:135-177.

Lester F. Fluoride myelopathy, with a review of literature. Ethiop Med J 1974; 12:39−49.

Ludwig, KR. User's manual for 'Analyst', a computer program for control a thermal-ionization. Single-collector mas spectrometer. USGS Open File Report 1994; 92-543.

Machavaram MV and Krishnamurthy RV. Earth Surface Evaporative Process: A Case Study From the Great Lakes Region of the United States Based on Deuterium Excess in Precipitation. Geochimica et Cosmochimica Acta 1995; 59(20):4279-4283.

Martyn CN, Barker DJP, Osmond C, Harris EC, Edwardson JA, Lacey RF. Geophysical relations between Alzheimer's disease and aluminium in drinking water. Lancet 1 1989; 59-62.

Makin MJ, Kingham TJ, Waddams AE, Birchall CJ, Teffera T. Development prospects in the southern Rift Valley, Ethiopia. Land Resource Study, 21. LRD, Ministry of Overseas Development, Surbiton1975; xiv, pp. 270.

Merla G, Abbate E, Azzaroli A, Bruni P, Canuti P, Fazzuoli M, Sagri M, Sacconi P. A Geological map of Ethiopia and Somalia, 1:2,000000, CNR, Firenze 1979.

Merlivat L, and Jouzel J. Global Climate Interpretation of the Deuterium-Oxygen 18 Relationship for Precipitation. Journal of Geophysical Research 1979; 84(C8):5029-5033.

Mohapatra D, Mishra D, Chaudhury GR, Das RP. Arsenic (V) adsorption mechanism using kaolinite, montmorillonite and illite from aqueous medium. Journal of Environmental Science and Health, Part A, 2007;42: pp. 463−469.

Mohr PA. The Ethiopian Rift System. Bull. Geophysics Obs. Addis Ababa 1962; 5:33−62.

Mohr PA. The Ethiopian rift system, bulletin of the Geophys. Obs. Addis Ababa University 1967; No. 11.

Mohr PA and Wood CA. Volcano spacing and lithospheric attenuation in the eastern rift of Africa. Earth planet. Sci. Lett. 1976; 33:27-37.

Mohr PA, Mitchell JC, Raynolds RGH. Quaternary volcanism and faulting at O_A Caldera, Central Ethiopian Rift. Bulletin of Volcanology 1980; 43:173−189.

Mohr PA. Ethiopian flood basalt province. Nature 1983; 303:577−584.

Moller IJ, Pindborg JJ, Gedalia I, Roed-Peterson B. The prevalence of dental fluorosis in the people of Uganda. Arch Oral Biol 1970; 15:213−225.

Morse JW, Luther GW. Chemical influences on trace metal-sulfide interactions in anoxic sediments. Geochim. Cosmochim. Acta 1999; 63: pp. 3373−3378.

Nicholson SE. A review of climate dynamics and climate variability in eastern Africa. In: Johnson, T.C., Odada, E.O. (Eds.), The Limnology, Climatology and Paleoclimatology of the East African Lakes. Gordon and Breach, Amsterdam 1996; pp. 25−56.

Nicolli HB, Suriano J, Gomez Peral M, Ferpozzi LH, Baleani O. Groundwater contamination with arsenic and other elements in an area of the Pampa, province of Cordoba, Argentina. Environ. Geol. Water Sci. 1989; 14: pp. 3−16.

Nicolli HB, Tineo A, Garcia JW, Falcon CM, Merino MH. Trace-element quality problems in groundwater from Tucuman, Argentina. In: Cidu R (ed) Proc of the 10th International Symposium on Water-Rock Interaction WRI-10, Villasimius, Italy, 10−15 July 2001; pp 993−996.

Nilsson E. Ancient changes of climate in British East Africa and Abyssinia. A study of ancient lakes and glaciers. Geogr. Ann. 1940; 22:1-78.

Nordstrom DK, Jenne EA. Fluoride solubility in selected geothermal waters. Geochimica et Cosmochimica Acta 1977; 41: 175-88.

Oskarsson N. The interaction between volcanic gases and tephra: fluorine adhering to tephra of the 1970 Hekla eruption. Journal of Volcanology and Geothermal Research 1980; 8:251-266.

Ocherse T. Chronic endemic fluorosis in Kenya, East Africa. Br Dent J 1953; 95:57−61.

Olsson B. Dental findings in high-fluoride areas in Ethiopia. Community Dent Oral Epidemiol 1979; 7:51−56.

Pande K, Sarin MM, Trivedi JR, Krishnaswami S, Sharma KK. The Induce river system (India−Pakistan): majorion chemistry, uranium and strontium isotopes. Chem. Geol. 1994; 116:245−259.

Parkhurst DL, & Appelo CAJ. User's guide to PHREEQC (Version 2) A computer program for speciation, batch-reaction, one-dimensional transport, and inverse geochemical calculations. U.S. Geological Survey Water-Resources Investigations Report 1999; 99-4259, pp. 310.

Ptak T, Piepenbrink M, Martac E. Tracer tests for the investigation of heterogeneous porous media and stochastic modelling of flow and transport-a review of some recent developments. Jour. of Hydrol. 2004; 294:122−163.

Peccerillo A, Donati C, Santo AP, Orlando A, Yirgu G, Ayalew D. Petrogenesis of silicic peralkaline rocks in the Ethiopian rift: Geochemical evidence and volcanological implications. J Afr Earth Sci 2007; 48(2−3):161−173.

Rango T, Bianchini G, Beccaluva L, Ayenew T, Colombani N. Hydrogeochemical study in the main Ethiopian rift: new insights to source and enrichement mechanism of fluoride, Environ Geol 2008; DOI 10.1007/s00254-008-1498-3.

Rittle KA, Drever JI, Colberg PJS. Precipitation of arsenic during bacterial sulfate reduction. Geomicrobiol. J. 1995; 13:1−11.

Shifera G, Tekle-Haimanot R. A review of the defluoridation program of drinking water supplies of an Ethiopian community. In: Dahl E, Nielsen LM, editors. Proceedings of the second international

workshop on fluorosis and defluoridation of water. Nazareth: International Society for Fluoride Research 1999; pp. 160−167.

Street FA. Late Quaternary lakes in the Ziway−Shala Basin, Southern Ethiopia. Ph.D. Thesis, University of Cambridge 1979; 457 pp.

Smedley PL, Nicolli H, Barros J, Tullio O. Origin and mobility of arsenic in groundwater from the Pampean Plain, Argentina. 9th Internat. Symp. Water-Rock Interactions. Taupo, New Zealand; 1998.

Smedley PL, Nicolli HB, Macdonald DMJ, Barros AJ, Tullio O. Hydrogeochemistry of arsenic and other inorganic constituents in groundwaters from La Pampa, Argentina. Appl Geochem 2002; 17(3):259−284.

Smith DA, Harris HA, Kirk R. Fluorosis in the Butan, Sudan. J Trop Med Hyg 1953; 8:57−58.

Stettler A, and Allegre CJ. ^{87}Rb-^{87}Sr studies of waters in a geothermal area: The Cantal: France Earth and Planetary Science Letters1978; v. 38:364-372.

Sun X, Doner HE. An investigation of arsenate and arsenite bonding structures on goethite by FTIR. Soil Sci 1996;161:865−872.

Taylor PS and Stoiber RE. Soluble material on ash from active Central American volcanoes. Geol. Soc. Am. Bull. 1973; 84:pp.1031−1042.

Tekle-Haimanot R, Fekadu A and Bushra B. Endemic fluorosis in the Ethiopian Rift Valley. Trop Geogr Med 1987; 39: 209-217.

Tekle-Haimanot R. Neurological complication of endemic skeletal fluorosis with special emphasis on rediculo-myelopathy. Paraplegia 1990; 28:244−251.

Thomas E. Varekamp JC, Buseck PR,. Zinc enrichment in the phreatic ashes of Mt. St. Helens, April 1980. J. Volcanol. Geotherm. Res. 1982; 12, 339−350.

Trua T, Deniel C, Mazzuoli R. Crustal control in the genesis of Plio-quaternary bimodal magmatism of the main Ethiopian rift (MER): geochemical and isotopic (Sr Nd, Pb) evidence. Chemical Geology 1999; 155, 201−231.

UNDP. Investigation of Geothermal Resources for Power Development: Geology, Geochemistry and Hydrogeology of Hot Springs of the East African Rift System within Ethiopia. Rec. Rep. DDSF=ON=116, United Nations, New York 1973; 275 pp.

US EPA. National primary drinking water regulations. EPA 816-F-03-016 United States Environmental Protection Agency 2003.

Varekamp JC, Luhr JF. Prestegaard KL. The 1982 eruptions of El Chichon volcano (Chiapas, Mexico): Character of the eruptions, ash-fall deposits and gasphase. J. Volcanol. Geotherm. Res. 1984; 23:39−68.

Vincent A, Benoit P, Pot V, Madrigal I, Delgado-Moreno L & Labat C. Impact of different and uses on the migration of two herbicides in a silt loam soil: unsaturated soil column displacement studies. Europ. J. of Soil Sci. 2007; 58:320-328.

Waychunas GA, Rea BA, Fuller CC, Davis JA. Surface chemistry of ferrihydrite: part 1. EXAFS studies of the geometry of coprecipitated and absorbed arsenate. Geochim Cosmochim Acta 1993; 57:2251−2269.

Welch AH, Lico MS, Hughes JL. Arsenic in ground water of the western United States: Ground Water 1988; 26(3):333-347.

WHO. Guidelines for drinking-water quality. 1st Addendum to vol. 1. Recommendations, 3rd ed. Geneva: World Health Organisation, 2006. pp. 595.

WoldeGabriel G, and Aronson JL. Volcanotectonic History of the Main Ethiopian Rift, Abstracts with Programs, International Volcanological Congress, Auckland, New Zealand 1986, p 325.

WoldeGabriel G, Aronson JL, Walter RC. Geology, geochronology, and rift basin development in the central sector of the Main Ethiopian Rift. Geological Society of America Bulletin 1990; 102: 439−458.

WoldeGabriel G, Yemane T, Suwa G, White T, Asfaw B. Age of volcanism and rifting in the Burji−Soyoma area, southern Main Ethiopian Rift: geo- and biochronologic data. J. Afr. Earth Sci. 1991; 13:437−447.

WoldeGabriel G, Heiken G, White TD, Asfaw B, Hart WK and Renne PR. Volcanism, tectonism, sedimentation, and the paleoanthropological record in the Ethiopian Rift System, in McCoy, F.W. and Heiken, G. (Eds.), Volcanic Hazards and Disasters in Human Antiquity: Geological Society of America Special Paper 2000; 345: 83-99.

WoldeGabriel G. The Main Ethiopian Rift System: an overview on volcanic, tectonic, rifting, and sedimentation processes, pp 13-43. In Ethiopian Rift Valley lakes (ed. C. Tudorancea and W.D. Taylor. Backhuys Publishers, Leiden 2002.

Wood and JF Talling. Chemical and algal relationships in a salinity series of Ethiopian inland waters, Hydrobiologia 1988; 158: pp. 29−67.

Yirgu G, Ayalew D, Peccerillo MR, Barberio C, Donati P, Donato. Fluorine and chlorine distribution in the volcanics rocks from the Gedemsa volcano, Ethiopian Rift Valley. Acta Vulcanol 1999; 11(1):169−176.

Zanettin B, Nicoletti M and Petrucciani C. The evolution of Checha escarpment and the Ganjuli graben (Lake Abaya) in the southern ethipian rift. Neues Jahrbuch fur Geologie und Palaonotologie 1978; 8: 473-490.

Zheng C¸ Bennett GD. Applied Contaminant Transport Modelling, 2nd Edition, John Wiley & Sons, New York 2002; 621 pp.

Zheng C; Wang PP. MT3DMS: A modular three-dimensional multispecies model for simulation of advection, dispersion and chemical reactions of contaminants in groundwater systems; Documentation and User's Guide, Contract Report SERDP-99- 1; U.S. Army Engineer Research and Development

Centre: Vicksburg, MS, 1999.

APPENDICES

Appendix 4.1: PHREEQC calculations of saturation indices for various water types (groundwater wells, hot springs, geothermal wells, rivers and lakes) in the central MER.

TYPE	RIVER							
Label	1	2	3	4	5	6	7	8
EC	500	530	180	90	60	40	150	150
TDS	425	583	174	98	73	53	118	156
Temp	22.2	23.3	21.5	18.7	10.6	11.5	16.9	14
pH	8.42	8.66	7.83	8.3	7.89	7.76	7.89	7.86
Na^+	64.2	56.3	15.2	5	4.8	3.4	12.9	15.8
K^+	15.1	12	4.8	2.1	3.4	2	5.1	7.3
Mg^{2+}	9.4	20.9	5.2	2.7	1.4	1.2	2.3	2.2
Ca^{2+}	25.9	42.1	16.8	18.5	10.7	8.4	17.9	40.7
SO_4^{2-}	7	25	1	0.8	1.5	0.2	2.3	4.1
Cl^-	15	16	4	1.4	2.2	1	3.4	6.8
F^-	2.2	1.5	1.6	0.2	0.1	0.1	0.5	0.3
NO_3^-	3.8	1.97	2.6	2	6.2	1.8	11.9	10.2
Alkalinity as HCO_3^-	286.7	408.7	125.1	67.1	48.8	36.6	73.2	79.3
Calcite	**0.77**	**1.3**	**-0.3**	**0**	**-0.95**	**-1.47**	**-0.48**	**-0.2**
Fluorite	**-0.7**	**-0.92**	**-1.06**	**-2.76**	**-3.46**	**-3.56**	**-1.96**	**-2.04**

Type	HOT SPRINGS													
label	9	10	11	12	13	14	15	16	17	18	19	20	21	22
EC	2750	14440	10570	13190	1780	4630	4870	630	3900	4530	4665	2040	2160	4600
TDS	1600	7919	7501	6589	958	3600	3896	499	2766	1830	3679	1728	1297	3051
Temp	**48.5**	**93.4**	**57.3**	**91.4**	**52.6**	**59.3**	**51.8**	**38.8**	**62**	**96**	**45**	**78**	82	85.6
pH	8.88	8.16	7.81	8	8.15	7.3	8.16	7.33	6.96	8.36	9.11	6.79	7.44	8.17
Na^+	593.1	2288.1	2415.5	2108.8	346.3	969.4	1122.3	105	802.2	169.9	944.9	397.7	305.9	770.9
K^+	17.6	24.6	25.9	1.5	26.4	66	64.1	11.5	60	39.1	47.2	29.4	109.9	152.2
Mg^{2+}	0	0	0	0	0	8	0.6	5.5	0.7	0	0.2	3.3	0	0
Ca^{2+}	0.9	0.3	1.4	1.9	3.2	8.8	1.7	22.1	13.9	0.9	0.9	11.1	0	0.8
SO_4^{2-}	3.3	612.1	28.3	22.3	0	68.8	66.2	32.6	23.1	253	54	35	52.9	37.7
Cl^-	279	1462.2	1324.1	1147.8	16.5	320.9	356.2	27.3	435.3	429	488	128	162.3	207.4
F^-	19.6	97.3	63.9	55	4.5	17.5	17.6	1.9	23.4	23.5	45.9	13.1	13.6	40.2
NO_3^-	0	43	0	0	0	0	0	0.3	0	34.37	0	0	0	0
Alkalinity as HCO_3^-	988.2	3434.3	3641.7	3251.3	561.2	2141.1	2267.2	292.8	1407	915	2098.4	1110.2	652.7	1842.2
Calcite	**0.16**	**-0.39**	**-0.09**	**0.37**	**0.16**	**0.22**	**0.17**	**-0.14**	**0.01**	**0.11**	**0.32**	**-0.1**	**-2.66**	**0.03**
Fluorite	**-0.97**	**-0.73**	**0**	**-0.3**	**-1.41**	**-0.11**	**-86**	**-1.09**	**0.42**	**-1.16**	**-0.5**	**-0.18**	**-3.17**	**-0.74**

Type	Groundwater wells													
Label	28	29	30	31	32	33	34	35	36	37	38	39	40	41
EC	840	1160	210	340	1020	640	2750	300	3360	2180	470	350	200	220
TDS	876	1164	188	323	1013	623	2227	267	3564	1884	367	871	204	211
Temp	24.6	26	24.5	21.5	28.2	24.4	25.1	25.3	28.3	27.3	25.6	24.6	22.6	22.5
pH	8.09	8.29	8.3	7.57	8.27	7.69	7.81	7.83	8.16	8.78	7.64	7.48	7.56	8.25
Na^+	180	241.3	31.2	17.6	231.5	90.1	564.8	49.8	858.2	466.9	81.4	60.9	30.4	32.7
K^+	67.3	33	5.2	5.5	17.7	10.6	25.1	5.2	31.2	16.7	7.8	9.4	14.1	2.3
Mg^{2+}	5.7	4.9	0.8	7.7	3.1	11.5	6.7	2.7	4.2	0	2.4	2.3	1.9	1.1
Ca^{2+}	7.8	4.4	7.3	45.7	6.7	33.4	20.8	10.2	3.7	1.6	22.5	27.7	13.5	24.7
SO_4^{2-}	4	5	1	0	2	6	456	0	7	186	63.5	397.7	2	0.8
Cl^-	9	16	1	2	12	20	176	2	106	167	4.4	144.6	1.3	1
F^-	4.2	2.8	1.2	0.4	2.1	3.6	20	1.8	7.3	21.4	2.4	3.1	0.8	1.5
NO_3^-	0.42	1.6	0.22	0.47	1.3	4.3	104	1	0	29.5	6.4	15.2	1.6	0.4
Alkalinity as HCO_3^-	597.8	857.1	140.3	244	738.1	448.4	957.7	195.2	2546.8	1024.8	183	225.7	140.3	146.4
Calcite	0.29	0.35	0	0.22	0.5	0.44	0.44	-0.2	0.45	0.21	-0.2	-0.35	-0.58	0.37
Fluorite	-0.78	-1.47	-1.71	-1.9	-1.54	-0.24	0.75	-1.25	-1	-0.033	-0.7	-0.58	-1.77	-0.97

Type	**Lakes**				
Label	23	24	25	26	27
EC	1730	>20000	>20000	>20000	420
TDS	1377	27228	11563	52725	379
Temp	24.2	24.6	25.8	27.6	25.2
pH	9.03	10.1	9.6	9.67	8.6
Na^+	387	17724.8	3426.1	15211.5	61.2
K^+	21	1108.8	125.3	618.9	10.9
Mg^{2+}	0.5	0	0.6	0	7.6
Ca^{2+}	9.7	0	4.5	0.2	27.3
SO_4^{2-}	46.5	287.8	95.1	552.5	6.6
Cl^-	130.9	6329.9	1325.6	5361.4	10.5
F^-	12.5	233.4	89.7	384.1	1.5
NO_3^-	4.7	0	0	0	2.4
Alkalinity as HCO_3^-	768.6	38583	6496.5	30596	253.2
Calcite	1.1	-2	1.2	-0.07	0.95
Fluorite	0.08	-1.03	0.57	0	-1.05

Groundwater wells									Cold springs	
42	43	44	45	46	47	48	49	50	51	52
220	1320	520	2260	2390	460	490	1770	730	180	280
266	1252	501	1952	1949	420	489	12797	668	137	258
24	23.2	30.6	32.3	36	23.6	25.2	23.7	36.4	22.5	27.6
7.31	8.14	7.6	7.64	8.08	7.1	7.82	8.7	7.89	6.6	7.8
29.9	306.8	85.8	480	557.1	69.5	54.9	442.9	139.8	17	40
3.6	12.1	10.2	27.6	25.9	12	2.5	21.1	14.7	5	6
2.6	5.6	10.4	30.5	0.1	4.6	11.2	1.9	3.2	2.1	4.2
25	17	34	30.7	28.6	41	68	7.2	18.9	22.7	22
0.5	7.8	4	33.5	107.2	8.7	5.8	3.7	6.4	4.8	2.2
1.5	16.9	10.8	266.3	152.8	11	4.4	19.4	7.3	5	2
2	13.1	4.1	7.1	14.3	1.7	0.9	10.1	3.1	0.7	1.3
0	0.65	0.24	2.7	0	0.01	0.05	0	0.03	24	0.01
201.3	872.3	341.6	1076.7	1091.9	271	341.6	1229.12	474.8	79	180
-0.41	0.7	0.27	0.61	1.02	-0.32	0.71	1.24	0.49	-1.57	0.03
-0.75	0.52	-0.15	0.02	0.55	-0.72	-1.12	-0.93	-0.74	-1.65	-1.22

Appendix 4.2: PHREEQC calcultions of saturation indices for groundwater wells (1-14) and geothermal wells (15-21) in the Ziway-Shala basin (source: Ayenew, 2008)

										Saturation indices	
Label	TDS	Na^+	K^+	Mg^{2+}	Ca^{2+}	F^-	Cl^-	Alkalinity as HCO_3^-	SO_4^{2-}	**$CaCO_3$**	**CaF_2**
1	259	22	3.7	9.6	16.9	0.1	3.6	203	0	-0.17	-3.4
2	179	15	4.3	8.3	10.8	1.1	5.3	134	0	-0.52	-1.48
3	326	24	5.1	11.3	22.5	1.5	7.1	254	0	0.03	-0.94
4	299	21.5	6	8.3	23	1.2	7.1	232	0	0.01	-1.11
5	164	34	5.4	4.7	23	2.9	7	85.4	1.7	-0.31	-0.31
6	133	10	5	8.5	14.5	0.3	3	89	3	0.48	-2.47
7	209	23	12	12.3	20.5	0.3	3	135	2.5	-0.18	-2.36
8	120	4	5	10.4	9	0.4	5	84.8	1.5	-0.78	-2.42
9	407	45	10	14.2	18	0.2	8	305	6.5	0	-2.81
10	245	12	6	11.4	15.5	0.3	8	189	3	-0.24	-2.48
11	454	38	12	13.2	30.5	0.1	23	334	3.5	0.1	-3.2
12	484	43	14	17	28	0.2	7	366	9	0.25	-2.65
13	297	19.5	6.1	19.8	22.1	1.5	7.1	209	12.5	-0.007	-0.97
14	416	34	6	11.5	36.1	1.5	2.4	323	0.9	0.32	-0.76
15	2225	619	153	0.3	0.3	40.8	253	1006	153	-1.49	-0.23
16	3078	563	50	0.5	1	26	51	2255	132	-0.67	-0.15
17	2686	850	50	0.2	1	67	20	1544	154	-0.75	0.66
18	3567	1015	138	0.4	1.9	27.8	671	1647	65.5	-0.53	0.16
19	2093	725	48	0.9	1.5	23	611	604	80	-0.9	-0.01
20	3016	854	47	0.6	1.3	27	302	1769	15.5	-0.64	0.01
21	2904	820	125	0.2	0.5	48	402	1464	43.8	-1.13	0.1

Appendix 4.3: Na^+, HCO_3^- (in mmoles/L) and Na^+/ HCO_3^- ratios with the corresponding F^- concentration variations in waters from Ziway−Shala basin. Note the different behaviour of samples characterized by Na^+/ HCO_3^- ratio above and below unity. WL=Groundwater wells, HS=Hot springs, GWL=Geothermal wells, HGW=Highland groundwater wells (Source of samples in bold font: Ayenew 2008).

ID	Type	Na^+ (mmoles/L)	HCO_3^- (mmoles/L)	Na^+/HCO_3^-	F^-
1	WL	24.6	15.7	1.56	20.0
2	WL	20.3	16.8	1.21	21.4
3	WL	24.2	17.9	1.35	14.3
4	WL	13.3	14.3	0.93	13.1
5	WL	19.3	20.2	0.96	10.1
6	HS	34.9	23.1	1.51	23.4
7	HS	99.5	56.3	1.77	97.3
8	HS	105	59.7	1.76	63.9
9	HS	41.1	34.4	1.19	45.9
10	HS	91.7	53.3	1.72	55.0
11	HS	42.2	35.1	1.20	17.5
12	HS	48.8	37.2	1.31	17.6
13	HS	25.8	16.2	1.59	19.6
14	HS	15.1	9.20	1.64	4.50
15	GWL	13.3	10.7	1.24	13.6
16	GWL	33.5	30.2	1.11	40.2
17	**GWL**	26.9	16.5	1.63	40.8
18	**GWL**	36.9	25.3	1.46	67.0
19	**GWL**	44.1	27.0	1.63	27.8
20	**GWL**	31.5	9.90	3.18	23.0
21	**GWL**	37.1	29.0	1.28	27.0
22	**GWL**	35.7	24.0	1.49	48.0
23	WL	37.3	41.8	0.89	7.30
24	WL	7.82	9.80	0.80	4.22
25	WL	10.5	14.1	0.75	2.79
26	WL	11.1	17.7	0.63	7.13
27	WL	10.1	12.1	0.83	2.10
28	WL	1.36	2.30	0.59	1.15
29	WL	0.76	4.00	0.19	0.40
30	WL	3.92	7.35	0.53	3.60
31	WL	2.17	3.20	0.68	1.80
32	WL	2.65	3.70	0.72	3.08
33	WL	1.42	2.40	0.59	1.46
34	WL	1.30	3.30	0.39	1.98
35	WL	2.39	5.60	0.43	0.89
36	WL	6.08	7.78	0.78	3.05
37	WL	1.32	2.30	0.57	0.81

38	WL	3.73	5.60	0.67	4.06
39	WL	3.02	8.75	0.35	1.65
40	RI	0.66	2.05	0.32	1.60
41	RI	2.79	4.70	0.59	2.16
42	RI	2.45	6.70	0.37	1.50
43	RI	0.22	1.10	0.20	0.20
44	RI	0.21	0.80	0.26	0.05
45	RI	0.15	0.60	0.24	0.11
46	RI	0.56	1.20	0.47	0.50
47	RI	0.69	1.30	0.53	0.29
48	**HGW**	0.96	3.32	0.29	0.10
49	**HGW**	0.65	2.20	0.30	1.10
50	**HGW**	1.04	4.16	0.25	1.50
51	**HGW**	0.93	3.80	0.25	1.20
52	**HGW**	1.48	1.40	1.06	2.90
53	**HGW**	0.43	1.46	0.30	0.30
54	**HGW**	1.00	2.21	0.45	0.30
55	**HGW**	0.17	1.39	0.13	0.40
56	**HGW**	1.96	5.00	0.39	0.20
57	**HGW**	1.22	4.92	0.25	0.70
58	**HGW**	0.52	3.10	0.17	0.30
59	**HGW**	1.65	5.48	0.30	0.10
60	**HGW**	1.87	6.00	0.31	0.20
61	**HGW**	0.85	2.74	0.31	1.50
62	**HGW**	1.47	4.80	0.31	1.50

Appendix 5.1: International quality standards for drinking water, and number of leachates from volcanic rocks exceeding the minimum threshold defined by the authorities. NG (no guidelines), NM (not mentioned), **Bold** font: (the minimum standard considered).

	VOLCANIC ROCK LEACHATES											
mg/L	**TW9**	**TW11**	**TW29**	**TW30**	**TW31**	**MIN**	**MAX**	**MEDIAN**	**WHO, 2006**	**EU Direc-tives,1998**	**USEPA, 2003**	**Nº of samples exceeding the limit**
Na^+	31.9	31.0	10.6	8.75	14.2	8.75	31.9	14.2	NG	**200 mg/L**	**200 mg/L**	**0**
K^+	1.90	17.34	10.44	4.71	4.40	1.90	17.34	4.7	NM	NM	NM	**-**
Ca^{2+}	13.3	118	9.27	6.42	8.77	6.42	118	9.3	NM	NM	NM	**-**
Mg^{2+}	1.20	3.76	0.28	0.26	0.21	0.21	3.76	0.3	NM	NM	NM	**-**
F^-	2.55	2.47	3.74	2.72	2.44	2.44	3.74	2.6	**1.5 mg/L**	**1.5 mg/L**	4 mg/L	**5**
Cl^-	1.45	69.2	1.72	2.09	1.50	1.45	69.2	1.7	NM	**250 mg/L**	**250 mg/L**	**-**
HCO_3^-	140	67.0	55.0	61.0	79.3	55.0	140	67.0	NM	NM	NM	**-**
NO_3^-	bdl	212.5	5.49	0.15	0.53	bdl	213	0.5	50 mg/L	50 mg/L	**10 mg/L**	**1**
SO_4^{2-}	0.98	16.9	5.60	2.51	1.23	0.98	17.0	2.5	NG	**250 mg/L**	**250 mg/L**	**-**
TDS	53	472	48	28	33	28	472	48.0				
pH	7.5	6.4	6.5	6.5	6.7	6.4	7.5	6.5				
Li	22.4	2.93	27.6	1.76	5.11	1.8	27.6	5.1	NM	NM	NM	**-**
B	24.8	13.6	bdl	bdl	bdl	bdl	24.8	-	**500 µg/L**	NM	NM	**0**
Al	68.3	bdl	192	78.1	1862	bdl	1862	78.1	**200 µg/L**	**200 µg/L**	**50-200 µg/L**	**2**
V	6.50	2.12	15.6	17.2	8.21	2.12	17.2	8.2	NM	NM	NM	**-**
Cr	2.60	3.14	3.42	2.61	3.06	2.60	3.4	3.1	**50 µg/L**	**50 µg/L**	100 µg/L	
Mn	6.62	bdl	8.33	3.33	190	bdl	190.3	6.6	400 µg/L	**50 µg/L**	**50 µg/L**	**1**
Fe	73.3	bdl	378	108	5223	bdl	5223.0	107.6	NG	**200 µg/L**	300 µg/L	**2**
Co	0.59	0.57	0.20	0.39	0.15	0.15	0.59	0.4	NM	NM	NM	**-**
Ni	2.64	2.28	1.68	1.57	1.96	1.68	2.6	2.0	**70 µg/L**	**70 µg/L**	NM	**0**
Cu	1.58	1.56	1.51	0.29	1.12	0.29	1.58	1.5	2000 µg/L	2000 µg/L	**1300 µg/L**	**0**
Zn	3.37	13.6	11.9	12.9	41.1	3.4	41.1	12.9	NG	NM	**5000 µg/L**	**0**
Ga	4.08	0.01	0.31	0.11	2.65	0.01	4.1	0.3	NM	NM	NM	**-**
As	2.21	1.72	2.70	0.25	4.91	0.25	4.9	2.2	**10 µg/L**	**10 µg/L**	**10 µg/L**	**-**
Rb	1.66	13.8	9.55	4.12	5.64	1.66	13.8	5.6	NM	NM	NM	**-**
Sr	bdl	252	4.10	4.61	5.43	bdl	252	4.6	NM	NM	NM	**-**
Mo	9.61	16.3	8.59	10.4	4.44	4.44	16.3	9.6	**70 µg/L**	NM	NM	**0**
Sb	0.19	0.01	0.13	bdl	0.16	bdl	0.2	0.1	**20 µg/L**	**5 µg/L**	**6 µg/L**	**-**
Pb	0.14	0.13	0.17	0.05	3.42	0.05	3.4	0.1	**10 µg/L**	**10 µg/L**	15 µg/L	**0**
U	0.95	0.24	0.05	bdl	0.36	bdl	0.95	0.2	**15 µg/L**	NM	NM	**-**
Be	bdl	bdl	bdl	bdl	bdl	bdl	bdl	bdl	NG	NM	**4 µg/L**	**-**
Bi	bdl	bdl	bdl	bdl	bdl	bdl	bdl	bdl	NM	NM	NM	**-**
Te	bdl	0.13	bdl	bdl	0.19	bdl	0.19	bdl	NM	NM	NM	**-**
Ba	bdl	97.1	bdl	bdl	bdl	bdl	97.1	bdl	**700 µg/L**	NM	2000 µg/L	**0**
Hg	bdl	bdl	bdl	bdl	bdl	bdl	bdl	bdl	6 µg/L	**1 µg/L**	2 µg/L	**-**

Tl	0.49	0.20	bdl	bdl	bdl	bdl	0.49	bdl	NM	NM	**2 µg/L**	**0**
Ag	bdl	bdl	bdl	bdl	0.03	bdl	0.03	bdl	NG	NM	**100 µg/L**	**0**
Cd	bdl	0.17	0.13	0.06	3.25	bdl	3.3	0.1	**3 µg/L**	5 µg/L	5 µg/L	**1**

Appendix 5.2: International quality standards for drinking water, and number of leachates from sediments exceeding the minimum threshold defined by the authorities. NG (no guidelines), NM (not mentioned), **Bold** font: (the minimum standard considered).

	SEDIMENT LEACHATES											
mg/L	**TW14**	**TW15**	**TW22**	**TW34**	**TW39**	**TW43**	**MIN**	**MAX**	**MEDI -AN**	**WHO, 2006**	**EU Direc-tves,1998**	**USEPA, 2003**	**Nº of samples exceeding the limit**
Na^+	33.4	108	88.0	33.5	12.9	60.5	12.9	108	47.0	NG	**200 mg/L**	**200 mg/L**	**-**
K^+	4.22	34.00	25.53	7.24	4.24	9.08	4.24	34.0	8.2	NM	NM	NM	**-**
Ca^{2+}	20.2	9.47	18.0	18.6	5.48	15.6	5.48	20.2	16.8	NM	NM	NM	**-**
Mg^{2+}	1.20	2.02	2.43	3.53	0.14	0.66	0.14	3.53	1.6	NM	NM	NM	**-**
F^-	3.20	6.98	7.03	1.06	2.08	7.63	1.06	7.63	5.1	**1.5 mg/L**	**1.5 mg/L**	**4 mg/L**	**5**
Cl^-	2.28	14.4	13.3	28.9	6.69	1.81	1.81	28.9	10.0	NM	**250 mg/L**	**250 mg/L**	**-**
HCO_3^-	165	634	384	49.0	49.0	244	49.0	634	204	NM	NM	NM	**-**
NO_3^-	8.33	44.7	6.49	64.3	16.7	bdl	bdl	64.3	12.5	**50 mg/L**	**50 mg/L**	**10 mg/L**	**0**
SO_4^{2-}	5.19	21.5	16.2	16.2	2.94	1.45	1.45	21.5	10.7	NG	**250 mg/L**	**250 mg/L**	**0**
TDS	78	244	177	174	51	97	51	244	135				
pH	7	8	8	6.5	6	8.7	6.0	8.7	7.5				
Li	9.41	23.6	165	12.5	1.24	15.1	1.24	165	13.8	NM	NM	NM	**-**
B	15.1	427	220	17.7	bdl	5.75	bdl	427	16.4	**500 µg/L**	NM	NM	**-**
Al	bdl	2.15	8.42	bdl	323	257	bdl	323	5.3	200 µg/L	200 µg/L	**50-200 µg/L**	**2**
V	29.7	26.5	254	5.58	9.74	15.5	5.58	254	21.0	NM	NM	NM	**-**
Cr	4.67	7.29	6.95	3.22	1.91	4.09	1.91	7.29	4.4	**50 µg/L**	**50 µg/L**	100 µg/**L**	**-**
Mn	bdl	bdl	0.11	bdl	5.51	38.9	bdl	38.9	0.1	400 µg/L	**50 µg/L**	**50 µg/L**	**-**
Fe	bdl	bdl	bdl	1.98	624	1154	bdl	1154	1.0	NG	**200 µg/L**	300 µg/L	**2**
Co	0.35	0.45	1.52	1.53	0.07	0.17	0.07	1.53	0.4	NM	NM	NM	**-**
Ni	1.72	2.49	5.57	2.61	1.31	2.37	1.31	5.57	2.4	**70 µg/L**	**70 µg/L**	NM	**-**
Cu	0.83	2.10	4.79	1.52	0.45	1.49	0.45	4.79	1.5	2000 µg/L	2000 µg/L	**1300 µg/L**	**-**
Zn	16.9	8.77	10.5	35.5	6.78	34.8	6.78	35.5	13.7	NG	NM	**5000 µg/L**	**0**
Ga	0.05	0.05	0.02	0.10	0.37	1.14	0.02	1.1	0.1	NM	NM	NM	**-**
As	11.8	17.4	220	1.23	1.96	6.62	1.23	220	9.2	**10 µg/L**	**10 µg/L**	**10 µg/L**	**3**
Rb	2.58	15.3	21.8	5.03	6.83	10.2	2.58	21.8	8.5	NM	NM	NM	**-**
Sr	62.3	107	65.5	58.4	1.92	15.3	1.92	107	60.4	NM	NM	NM	**-**
Mo	7.86	11.3	181	6.09	5.34	2.52	2.52	181	7.0	**70 µg/L**	NM	NM	**1**

Sb	0.10	0.82	5.03	4.62	0.1	0.44	0.10	5.03	0.6	20 µg/L	**5 µg/L**	**6 µg/L**	**1**
Pb	0.18	0.35	0.04	bdl	0.43	0.57	bdl	0.6	0.3	**10 µg/L**	**10 µg/L**	15 µg/L	**-**
U	0.75	5.04	63.6	0.05	0.17	0.83	0.05	63.6	0.8	**15 µg/L**	NM	NM	**1**
Be	bdl	bdl	bdl	bdl	bdl	bdl	bdl	bdl	bdl	NG	NM	**4 µg/L**	**0**
Bi	bdl	bdl	bdl	bdl	bdl	bdl	bdl	bdl	bdl	NM	NM	NM	**-**
Te	bdl	bdl	bdl	bdl	bdl	0.07	bdl	0.07	bdl	NM	NM	NM	**-**
Ba	bdl	bdl	bdl	bdl	bdl	bdl	bdl	bdl	bdl	**700 µg/L**	NM	2000 µg/L	**-**
Hg	bdl	bdl	bdl	bdl	bdl	bdl	bdl	bdl	bdl	6 µg/L	**1 µg/L**	2 µg/L	**-**
Tl	0.02	0.05	bdl	bdl	bdl	bdl	bdl	0.05	bdl	NM	NM	**2 µg/L**	**0**
Ag	bdl	bdl	bdl	bdl	bdl	bdl	bdl	bdl	bdl	NG	NM	**100 µg/L**	**0**
Cd	0.02	bdl	bdl	0.05	0.25	0.49	bdl	0.49	bdl	**3 µg/L**	**5 µg/L**	**5 µg/L**	**-**

Appendix 6.1: Compositions of major ions and SiO_2 in the groundwater wells in Ziway and Meki area (Data collected from Meki and Ziway Catholic Mission offices, January 2007).

ID	X	Y	EC	PH	SiO2	Na^+	K^+	Ca^{2+}	Mg^{2+}	Cl^-	CO_3^{2-}	HCO_3^-	F^-	SO_4^{2-}
1	38.744	8.073	600	8.4	88	54	13	46.5	27.2	22	24	354	0.9	nil
2	38.723	8.023	2162	8.5	84	578	25	4.8	2.9	64	48	1379	4.0	nil
3	38.940	8.296	877	8.5	94	204	13	13.4	2.9	48	43	420	7.7	nil
4	38.749	8.164	805	8.4	52	204	15	6.1	1.2	2	72	415	4.9	nil
5	38.770	8.164	1008	8.1	89	228	14	6.4	5.8	12	nil	634	6.5	7.4
6	38.726	8.060	2542	8.4	86	646	28	9.6	2.9	175	48	1244	6.9	107.8
8	39.071	8.649	600	8.4	88	54	13	46.5	27.2	22	24	354	0.9	nil
10	38.742	8.125	1258	8.4	88	299	17	11.2	1.0	64	24	610	5.6	54.0
11	38.719	7.987	1654	8.6	83	394	18	12.8	10.7	86	24	952	3.9	nil
12	38.714	8.008	1483	8.7	91	374	17	6.4	2.9	16	48	903	7.2	nil
13	38.656	7.991	1550	8.9	45	415	11	3.2	2.0	54	48	805	14.0	77.0
14	38.854	8.184	1688	8.5	76	400	20	9.7		122	108	744	7.7	nil
15	38.752	8.082	1397	8.5	91	347	18	8.0	2.9	16	27	878	9.4	nil
16	38.699	7.926	1127	8.6	91	269	17	6.4	4.9	16	24	683	5.1	nil
17	38.770	8.223	430	8.1	82	65	6	28.9	6.8	4	nil	281	2.8	nil
18	38.712	7.956	1270	8.0	95	179	15	75.4	32.0	70	nil	756	3.1	nil
19	38.722	8.160	578	8.1	87	102	10	25.7	13.6	4	nil	415	3.5	nil
20	38.717	8.043	2697	8.6	81	672	25	4.8	2.9	227	72	1122	6.3	127.6
21	38.716	8.021	1494	8.8	89	388	15	3.2	1.0	34	48	586	7.8	nil
22	38.819	8.167	483	8.6	59	68	3	36.9	1.0	9	12	256	0.5	nil
23	38.680	8.018	2485	8.7	100	646	17	4.8	1.0	142	72	903	12.3	338.0
24	38.813	8.196	464	8.6	78	78	7	20.8	4.9	6	12	268	1.0	nil
25	38.674	7.836	1045	8.8	87	258	11	6.4	1.9	20	48	586	5.3	nil
26	38.887	8.167	1983	8.7	74	485	36	17.6	7.8	69	36	1196	9.0	nil
27	38.722	8.029	1917	8.7	86	496	20	4.8	1.0	60	72	1074	10.3	14.4
28	38.691	7.920	1917	8.2	98	483	25	11.2	5.8	98	nil	1122	14.4	42.0
29	38.639	7.835	2348	8.9	94	595	26	3.2	1.0	188	72	952	19.2	114.4
30	38.887	8.204	716	8.7	78	156	10	9.6	2.0	8	24	390	3.6	nil
31	38.832	8.231	1330	8.7	65	315	12	17.6	4.9	22	24	793	16.0	nil
32	38.700	7.936	1150	8.6	86	269	15	9.6	3.9	20	24	683	4.1	nil
33	38.742	8.067	1696	8.4	97	442	26	6.4	2.9	34	96	964	9.0	nil
34	38.679	8.018	2485	8.7	100	646	17	4.8	1.0	142	72	903	12.3	338.0

Appendix 8.1: $\delta^{18}O$ and $\delta^{2}H$ precipitation data used to produce the LMWL of Ziway-Shala basin. Note that sample numbers 1, 2, 4, 7, 15, 20, 21, 28, 29, 31, 32, 33, 39, 44 are evaporated samples and excluded)

Nº	Date	Area	$\delta^{18}O$	$\delta^{2}H$	Deutrium excess =($\delta^{2}H$ -8 $\delta^{18}O$)
1	06/01/1995	Asela	**3.64**	**16.90**	-12.22
2	06/01/1995	Asela	**0.65**	**20.60**	15.40
3	07/01/1995	Asela	**0.44**	**12.20**	8.68
4	07/01/1995	Asela	**-2.56**	**-1.60**	18.88
5	07/01/1995	Asela	**2.00**	**20.50**	4.50
6	07/01/1995	Asela	**-4.65**	**-24.30**	12.90
7	08/01/1995	Asela	**-3.54**	**-11.70**	16.62
8	08/01/1995	Asela	**1.10**	**14.30**	5.50
9	08/01/1995	Asela	**0.93**	**13.60**	6.16
10	08/01/1995	Asela	**-2.14**	**-5.40**	11.72
11	08/01/1995	Asela	**3.49**	**26.90**	-1.02
12	09/01/1995	Asela	**-1.25**	**1.40**	11.40
13	09/01/1995	Asela	**3.37**	**32.40**	5.44
14	07/01/1994	Asela	**-3.93**	**-19.80**	11.64
15	08/01/1994	Asela	**-4.25**	**-18.30**	15.70
16	08/01/1994	Asela	**-3.90**	**-18.10**	13.10
17	08/01/1994	Asela	**-0.79**	**-1.80**	4.52
18	09/01/1994	Asela	**-0.92**	**4.20**	11.56
19	09/01/1994	Asela	**-0.70**	**8.90**	14.50
20	07/01/1995	Ziway	**-0.77**	**11.80**	17.96
21	07/01/1995	Ziway	**-2.46**	**-4.10**	15.58
22	07/01/1995	Ziway	**-3.78**	**-16.90**	13.34
23	08/01/1995	Ziway	**-4.61**	**-29.70**	7.18
24	08/01/1995	Ziway	**-0.91**	**5.10**	12.38
25	08/01/1995	Ziway	**0.06**	**12.00**	11.52
26	08/01/1995	Ziway	**-2.30**	**-3.90**	14.50
27	09/01/1995	Ziway	**-0.81**	**7.60**	14.08
28	09/01/1995	Ziway	**-2.05**	**2.00**	18.40
29	09/01/1995	Ziway	**1.44**	**27.10**	15.58
30	09/01/1995	Ziway	**2.95**	**31.00**	7.40
31	07/01/1995	Silte	**-2.68**	**-3.10**	18.34
32	08/01/1995	Silte	**-5.71**	**-27.40**	18.28
33	08/01/1995	Silte	**-1.16**	**12.00**	21.28
34	08/01/1995	Silte	**-1.55**	**0.90**	13.30
35	09/01/1995	Silte	**1.99**	**18.40**	2.48
36	09/01/1995	Silte	**-3.37**	**-12.70**	14.26
37	07/01/1995	Butajira	**-2.43**	**-6.80**	12.64
38	07/01/1995	Butajira	**-0.75**	**-6.40**	-0.40
39	07/01/1995	Butajira	**4.35**	**22.50**	-12.30
40	08/01/1995	Butajira	**-2.05**	**-9.50**	6.90
41	08/01/1995	Butajira	**-1.09**	**2.10**	10.82

42	08/01/1995	Butajira	**-3.56**	**-17.10**	11.38
43	08/01/1995	Butajira	**-0.75**	**3.90**	9.90
44	07/01/1995	Awasa	**-1.05**	**10.30**	18.70
45	07/01/1995	Awasa	**-0.06**	**9.90**	10.38
46	08/01/1995	Awasa	**-1.32**	**0.50**	11.06